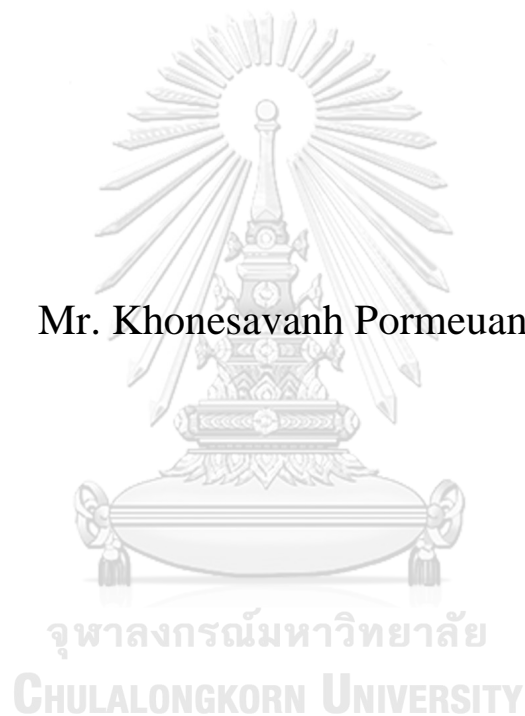


# SHEAR STRENGTH OF REINFORCED CONCRETE BEAM WITH EMBEDDED STEEL TRUSSES

Mr. Khonesavanh Pormeuanpieng



A Thesis Submitted in Partial Fulfillment of the Requirements  
for the Degree of Master of Engineering in Civil Engineering  
Department of Civil Engineering  
Faculty of Engineering  
Chulalongkorn University  
Academic Year 2018  
Copyright of Chulalongkorn University

กำลังรับแรงเหวี่ยงของคานคอนกรีตเสริมเหล็กที่มีโครงถักเหล็กอยู่ภายใน



นายคอนสวรรค์ ปอเมืองเพียง

วิทยานิพนธ์นี้เป็นส่วนหนึ่งของการศึกษาตามหลักสูตรปริญญาวิศวกรรมศาสตรมหาบัณฑิต

สาขาวิชาวิศวกรรมโยธา ภาควิชาวิศวกรรมโยธา

คณะวิศวกรรมศาสตร์ จุฬาลงกรณ์มหาวิทยาลัย

ปีการศึกษา 2561

ลิขสิทธิ์ของจุฬาลงกรณ์มหาวิทยาลัย

Thesis Title                                   SHEAR STRENGTH OF REINFORCED CONCRETE  
BEAM WITH EMBEDDED STEEL TRUSSES  
By   Mr. Khonesavanh Pormeuanpieng  
Field of Study                               Civil Engineering  
Thesis Advisor                               Assistant Professor CHATPAN CHINTANAPAKDEE,  
Ph.D.

---

Accepted by the Faculty of Engineering, Chulalongkorn University in Partial  
Fulfillment of the Requirement for the Master of Engineering

----- Dean of the Faculty of Engineering  
(Associate Professor SUPOT  
TEACHAVORASINSKUN, D.Eng.)

THESIS COMMITTEE

----- Chairman  
(Associate Professor WITHIT PANSUK, Ph.D.)  
----- Thesis Advisor  
(Assistant Professor CHATPAN CHINTANAPAKDEE,  
Ph.D.)  
----- External Examiner  
(Suthipoul Viwathanatapa, Ph.D.)



จุฬาลงกรณ์มหาวิทยาลัย  
CHULALONGKORN UNIVERSITY

คอนกรีตเสริมเหล็ก : กำลังรับแรงเฉือนของคานคอนกรีตเสริมเหล็กที่มีโครงเหล็กฝังไว้ภายใน. ( **SHEAR STRENGTH OF REINFORCED CONCRETE BEAM WITH EM BEDDED STEEL TRUSSES**) อ.ที่ปรึกษาหลัก : ศศ. ดร.ฉัตรพันธ์ จินตนาภักดี

โครงเหล็กสามารถฝังไว้ในคานคอนกรีตเสริมเหล็กเพื่อที่จะเสริมกำลังด้านแรง (strength) และความแข็งคืด (stiffness) ของคานที่ต้องรับแรงที่สูงมากภายใต้พื้นที่จำกัด กำลังรับแรงเฉือนของคานประเภทนี้ยังไม่ได้มีการศึกษาอย่างทั่วถึง งานวิจัยนี้มีเป้าหมายที่จะประมาณกำลังรับแรงเฉือนของคานคอนกรีตเสริมเหล็กที่มีโครงเหล็กฝังไว้ข้างใน วิธีที่ใช้ในการคำนวณมีหลายวิธี 1) สูตรการคำนวณกำลังรับแรงเฉือนด้วยวิธีดั้งเดิม 2) วิธี Strut-and-Tie Model (STM) และ 3) วิธีไฟไนต์เอลิเมนต์ (FE) วิธีดั้งเดิมและ STM จะใช้ตามมาตรฐาน ACI 318 (2014) และ AASHTO LRFD (2012) ผลการคำนวณทั้งสามถูกนำไปเปรียบเทียบกับผลการทดสอบเพื่อหาค่ากำลังรับแรงเฉือนของชิ้นงานตัวอย่าง โดย Zhang และคณะ (2016) คานสี่ตัวถูกพิจารณาในการศึกษานี้ซึ่งเป็น คานคอนกรีตเสริมเหล็กที่ฝังและไม่ฝังโครงเหล็ก และถูกแบ่งตามปริมาณเหล็กปลอกที่ใช้ กำลังรับแรงเฉือนจากคอนกรีต เหล็กปลอก และ โครงเหล็ก ถูกวิเคราะห์ด้วยวิธีไฟไนต์เอลิเมนต์แบบไม่เป็นเชิงเส้น ในแบบจำลอง FE คอนกรีตและเหล็กยังคงถูกสมมติให้ยึดแน่นติดกัน วิธี STM ของ AASHTO ให้ค่าประมาณของกำลังรับแรงเฉือนที่ถูกต้องใกล้เคียงกับผลการทดสอบดีกว่าวิธีที่อื่น เหมาะสมที่จะนำไปใช้ออกแบบคานประเภทนี้ วิธี FE ให้ค่ากำลังรับแรงเฉือนที่มากเกินไปสำหรับคานคอนกรีตเสริมเหล็กที่ฝังด้วยโครงเหล็กเพราะฉะนั้นควรมีการศึกษามากกว่านี้เพื่อให้ได้ค่าการประมาณของกำลังรับแรงเฉือนจากวิธี FE ที่ดีกว่านี้ก่อนที่จะไปใช้ในการปฏิบัติ

จุฬาลงกรณ์มหาวิทยาลัย  
CHULALONGKORN UNIVERSITY

สาขาวิชา           วิศวกรรมโยธา  
ปีการศึกษา        2561

ลายมือชื่อนิสิต .....

ลายมือชื่อ อ.ที่ปรึกษาหลัก .....

# # 5970473921 : MAJOR CIVIL ENGINEERING

KEYWORD RC beam Shear capacity Embedded steel trusses Nonlinear finite  
D: element analysis Strut-and-Tie Model

Khonesavanh Pormeuanpieng :  
SHEAR STRENGTH OF REINFORCED CONCRETE BEAM WITH EM  
BEDDED STEEL TRUSSES. Advisor: Asst. Prof. CHATPAN  
CHINTANAPAKDEE, Ph.D.

A steel truss might be embedded in reinforced concrete (RC) beam to enhance strength and stiffness of the beam under extremely high force demands within limited space. Shear strength of such beam construction has not yet been well investigated. This research aims to predict shear strength of RC beam with embedded steel trusses. Several approaches were considered: 1) conventional shear formula; 2) strut-and-tie model (STM); and 3) finite element (FE) method. Shear strength formula and STM follow ACI 318 (2014) and AASHTO LRFD (2012). These approaches were implemented, and results were compared with reference to shear strength test results of physical specimens by Zhang et al. (2016). Four beam specimens were considered including RC beam with and without embedded truss and variations of stirrup reinforcements. Nonlinear finite element analysis was carried out to study on the shear capacity provided by concrete, stirrups and steel trusses. In FE models, concrete and steels were assumed as perfectly bonded. STM per AASHTO provides a better estimate of shear strength than other approaches and more suitable to be used in design of such beams. FE models over-estimate shear strength of the reinforced concrete beam with embedded steel trusses. More investigation should be conducted to obtain better estimation of shear strength by FEM before it can be used in practice.



Field of Study: Civil Engineering

Student's Signature

Academic Year: 2018

Advisor's Signature

Year:

.....

## ACKNOWLEDGEMENTS

This culmination of my master's research would not have been possible without the continuous support from advisors, family members, and peers.

Firstly, I would like to acknowledge my advisor, Asst. Prof. Dr. Chatpan Chintanapakdee, who has provided me motivation, proper guidance, and close monitoring, throughout my time at Chulalongkorn University. His enthusiasm to work on current research topics and publish my studies in conferences is unmatched and has allowed me to compile the best possible version of my thesis.

Next, I would like to acknowledge my Master's Thesis committee members: Assoc. Prof. Dr. Withit Pansuk whom I have worked with personally and enjoyed, and Dr. Suthipoul Viwathanatepa for his constructive comments, and both for their time and suggestions. In addition, I would like to thank the scholarship program for ASEAN countries from Chulalongkorn university which provided me with financial support throughout my graduate study.

And, last but not least, my parents, for their tremendous financial and moral support, without whom this thesis would not have been completed, and my lab mates, Tosporn Prasertsri, Kimleng Khy, Nattanai Kuangmia, Teerit Wutthisirisart, Pakawats Minchainant and Tek Nath Kararia for their friendship advice, and support.

# TABLE OF CONTENTS

	<b>Page</b>
ABSTRACT (THAI) .....	iii
ABSTRACT (ENGLISH).....	iv
ACKNOWLEDGEMENTS .....	v
TABLE OF CONTENTS.....	vi
LIST OF TABLES .....	x
LIST OF FIGURES .....	xi
CHAPTER 1 INTRODUCTION.....	1
1.1 Background.....	1
1.2 Objectives .....	9
1.3 Scope and assumptions.....	10
1.4 Research methodology .....	10
1.5 Outline of thesis.....	12
CHAPTER 2 LITERATURE REVIEWS.....	13
2.1 Overview .....	13
2.2 Theoretical background and analysis methods.....	13
2.2.1 Fundamental mechanism of shear transfer in RC beam.....	13
2.2.2 Truss analogy mechanism .....	15
2.2.2.1 Internal forces in plastic truss model.....	18
2.2.3 Modified Compression Field Theory (MCFT).....	20
2.2.3.1 Compatibility equations.....	21
2.2.3.2 Equilibrium equations.....	23
2.2.3.3 Material constitutive relationships.....	25
2.3 Recent code provisions.....	29
2.3.1 American Concrete Institute 318 (2014) .....	29
2.3.2 AASHTO LRFD (2012).....	33

2.4 Strut-and-tie model (STM) .....	38
2.4.1 Overview .....	38
2.4.2 Theoretical background .....	39
2.4.3 Code provisions in ACI 318 (2014) .....	40
2.4.3.1 Strength of struts .....	40
2.4.3.2 Strength of nodal zones .....	43
2.4.3.3 Strength of ties .....	43
2.4.3.4 Shear strength requirement for deep beam .....	45
2.4.4 Code provisions in AASHTO LRFD (2012) .....	46
2.4.4.1 Strength of struts .....	46
2.4.4.2 Strength of ties .....	47
2.4.4.3 Strength of nodal zone .....	47
2.4.4.4 Crack control reinforcement .....	48
2.4.5 Procedure of STM .....	50
2.5 Past experimental studies of RC beams with embedded steel trusses .....	51
2.5.1 RC beams with embedded steel trusses .....	51
2.5.2 Steel-truss RC transfer beam in tall buildings .....	61
2.6 Previous works on finite element analysis of RC and composite beams .....	64
2.7 Summary of literature reviews .....	70
<b>CHAPTER 3 CALCULATION BY CODE METHODS .....</b>	<b>71</b>
3.1 Calculation of shear strength by conventional shear strength formulas .....	72
3.1.1 Result of shear strength per ACI 318 and AASHTO LRFD .....	72
3.2 Calculation of shear strength by strut-and-tie model (STM) .....	73
3.2.1 ACI 318 (2014) .....	75
3.2.1.1 SRCB1 beam .....	75
3.2.1.2 SRCB2 beam .....	78
3.2.1.3 SRCB3 beam .....	81
3.2.1.4 SRCB4 beam .....	84
3.2.2 AASHTO LRFD (2012) .....	87



3.2.2.1 SRCB1 beam .....	87
3.2.2.2 SRCB2 beam .....	90
3.2.2.3 SRCB3 beam .....	93
3.2.2.4 SRCB4 beam .....	96
3.2.3 Summary of shear strength by STM.....	98
CHAPTER 4 FINITE ELEMENT ANALYSIS .....	100
4.1 Modeling assumptions .....	100
4.2 Element-type selection in ANSYS 18.2 .....	100
4.2.1 Concrete.....	100
4.2.2 Steel reinforcement.....	101
4.2.3 Steel plate .....	101
4.3 Material models .....	102
4.3.1 Concrete.....	102
4.3.1.1 Finite element input data .....	103
4.3.1.2 Compressive uniaxial stress-strain relationship .....	104
4.3.1.3 Criterion of failure .....	106
4.3.2 Steel reinforcement, steel section, and steel plate .....	107
4.4 Finite element models of the studied beams.....	109
4.4.1 Configuration and dimensions.....	109
4.4.2 Discretization.....	111
4.4.2.1 Concrete.....	111
4.4.2.2 Steel reinforcement.....	112
4.5 Loads and boundary conditions.....	112
4.6 Analysis types.....	113
4.7 Finite element analysis procedure .....	116
CHAPTER 5 RESULTS AND DISCUSSIONS .....	117
5.1 Finite element analysis results.....	117
5.1.1 Cracking and crushing of concrete .....	117
5.1.2 Maximum stress of concrete and steel .....	120

5.1.3 Load-deflection curves .....	122
5.2 FE results and physical test by Zhang et al. (2016).....	123
5.3 Discussion of results of shear strength in current study .....	124
CHAPTER 6 CONCLUSIONS AND RECOMMENDATIONS .....	127
6.1 Conclusions .....	127
6.2 Recommendations .....	128
REFERENCES .....	129
APPENDIX Finite element analysis batch script in ANSYS of SRCB1.....	134
VITA.....	147



## LIST OF TABLES

	<b>Page</b>
Table 2-1 Strut coefficient $\beta_s$ .....	41
Table 2-2 Nodal zone coefficient $\beta_n$ .....	43
Table 2-3 Material properties of steel (Zhang et al., 2016) .....	51
Table 2-4 Material properties of concrete (Zhang et al., 2016) .....	51
Table 2-5 Structural performance of test specimens (Zhang et al., 2016) .....	56
Table 2-6 Comparison of the test results and calculation (Zhang et al., 2016) .....	61
Table 2-7 Details of specimens (Wu et al., 2011) .....	61
Table 2-8 Concrete and steel material (Wu et al., 2011) .....	62
Table 2-9 Summary of material properties for SFRC beam (Özcan et al., 2009) .....	66
Table 2-10 Concrete and steel materials (Vasudevan and Kothandaraman, 2014) .....	67
Table 3-1 The studied beams .....	71
Table 3-2 Steel properties of current studied beams .....	71
Table 3-3 Concrete properties of current studied beams .....	72
Table 3-4 Shear capacity of studied beams by conventional shear formula .....	73
Table 3-5 Summary of internal forces in truss members for STM .....	74
Table 3-6 Shear strength by STM following ACI 318 and AASHTO LRFD .....	99
Table 4-1 Summary of element types for ANSYS models .....	102
Table 4-2 Summary of material properties and parameters of concrete models .....	104
Table 4-3 Summary of material properties and parameters of steel for models .....	108
Table 4-4 Nonlinear analysis control commands in ANSYS .....	114
Table 4-5 Output control commands .....	114
Table 4-6 Nonlinear algorithm and convergence criteria parameters .....	114
Table 4-7 Advance nonlinear control settings .....	115

## LIST OF FIGURES

	<b>Page</b>
Figure 1.1 A building with transfer structure.....	2
Figure 1.2 The concentrated load from column of the upper level to beam .....	3
Figure 1.3 The James Building, New York .....	3
Figure 1.4 The Brunswick Building, Chicago, Illinois .....	4
Figure 1.5 Jardine House, Connaught Place, Hong Kong .....	5
Figure 1.6 Methodology flowchart .....	11
Figure 2.1 Shear transfer mechanisms in RC beams without shear reinforcement (MacGregor et al., 1997).....	14
Figure 2.2 Shear transfer mechanisms in RC beams with shear reinforcement .....	14
Figure 2.3 Distribution of internal shears in a beam with web reinforcement (MacGregor et al., 1997).....	15
Figure 2.4 Internal forces in a cracked beam (MacGregor et al., 1997) .....	16
Figure 2.5 Truss analogy (MacGregor et al., 1997).....	16
Figure 2.6 Statically determinate truss (MacGregor et al., 1997).....	17
Figure 2.7 Variable angle truss model (Nilson et al., 2004) .....	17
Figure 2.8 Forces in stirrups (MacGregor et al., 1997) .....	19
Figure 2.9 Stress in compression diagonals (MacGregor et al., 1997) .....	20
Figure 2.10 Replacement of $V$ with internal forces of $D$ and $N$ (MacGregor et al., 1997) .....	20
Figure 2.11 Stress-strain relation of concrete element (Vecchio and Collins, 1988) .	21
Figure 2.12 Compatibility conditions of the cracked element (Vecchio and Collins, 1988) .....	22
Figure 2.13 The Free body diagram of a part of element (Vecchio and Collins, 1986) .....	24
Figure 2.14 Stress in cracked concrete (Vecchio and Collins, 1986) .....	25
Figure 2.15 Concrete average stress-strain relationship in compression (Vecchio and Collins, 1986).....	26

Figure 2.16 Average concrete stress-strain relationship in tension (Vecchio and Collins, 1986).....	27
Figure 2.17 Transmitted shear stress across crack by aggregate interlocking (Vecchio and Collins, 1986).....	27
Figure 2.18 Stress-strain relationship for steel reinforcement (Vecchio and Collins, 1986) .....	29
Figure 2.19 Shear resisted by vertical stirrups (MacGregor et al., 1997).....	31
Figure 2.20 Shear resisted by inclined stirrups (MacGregor et al., 1997).....	31
Figure 2.21 Calculation flowchart of shear capacity by ACI 318 (2014).....	33
Figure 2.22 Calculation flowchart of shear capacity by AASHTO LRFD (2012) .....	37
Figure 2.23 Stress trajectories in B-regions and near discontinuities (D-regions) (Birrcher et al., 2009).....	39
Figure 2.24 Strut-and-tie model of a simply supported beam under a concentrated load (Birrcher et al., 2009).....	39
Figure 2.25 RC beam approximated as a truss by STM (Birrcher et al., 2009) .....	40
Figure 2.26 Reinforcement crossing a strut .....	42
Figure 2.27 Hydrostatic nodes (ACI 318, 2014).....	45
Figure 2.28 Crack control reinforcement (AASHTO LRFD, 2012).....	49
Figure 2.29 Calculation flowchart of STM.....	50
Figure 2.30 Profile and cross-section detail of SRCB1 and SRCB2 (Zhang et al., 2016) .....	52
Figure 2.31 Profile and cross-section detail of SRCB3 (Zhang et al., 2016) .....	53
Figure 2.32 Profile and cross-section detail of SRCB4 (Zhang et al., 2016) .....	54
Figure 2.33 Profile and cross-section detail of SRCB5 (Zhang et al., 2016) .....	55
Figure 2.34 Load-deflection curve under loading point (Zhang et al., 2016).....	57
Figure 2.35 Analytical model of interior-force on the failure section (Zhang et al., 2016) .....	58
Figure 2.36 Analytical-model of stress in shear compression zone (Zhang et al., 2016).....	59
Figure 2.37 Design configuration of the specimens (mm) (Wu et al., 2011) .....	63
Figure 2.38 Load-deflection curves (Wu et al., 2011).....	64

Figure 2.39 Steel-concrete composite section with studs shear connects (Mahmoud, 2016) .....	64
Figure 2.40 The finite element modeling of steel and contact elements (Mahmoud, 2016) .....	65
Figure 2.41 The specimen configuration (Özcan et al., 2009).....	65
Figure 2.42 Experimental and FEM load-deflection responses (Özcan et al., 2009) ..	66
Figure 2.43 Details of the specimen (Vasudevan and Kothandaraman, 2014).....	67
Figure 2.44 Finite element model with reinforcement (Vasudevan and Kothandaraman, 2014).....	68
Figure 2.45 Comparison of the ultimate bending moment capacity (Vasudevan and Kothandaraman, 2014).....	68
Figure 2.46 Composite truss configuration used for a basic investigation of shear flow at the steel-concrete interface (Machacek and Cudejko, 2009) .....	69
Figure 2.47 Axonometric view of FE modeling (Machacek and Cudejko, 2009).....	69
Figure 2.48 Load-deflection curves (Machacek and Cudejko, 2009).....	70
Figure 3.1 Truss layout of STM calculation .....	73
Figure 3.2 The strut, tie, and nodal zone configuration of STM .....	75
Figure 4.1 Solid65 3-D reinforced concrete solid (ANSYS, 2018).....	101
Figure 4.2 Link180 3-D spar element (ANSYS, 2018) .....	101
Figure 4.3 Solid185 3-D solid element (ANSYS, 2018) .....	102
Figure 4.4 Typical uniaxial compressive and tensile stress-strain curve for concrete (Bangash, 1989) .....	103
Figure 4.5 Simplified compressive uniaxial stress-strain curve for concrete (Kachlakev et al., 2001) .....	105
Figure 4.6 Compressive uniaxial stress-strain curve for ANSYS models .....	106
Figure 4.7 Three dimension failure surface for concrete (ANSYS, 2018) .....	107
Figure 4.8 Stress-strain curve for steel reinforcement .....	108
Figure 4.9 FE model-detail configuration of SRCB1 .....	109
Figure 4.10 FE model-detail configuration of SRCB2 .....	110
Figure 4.11 FE model-detail configuration of SRCB3 .....	110
Figure 4.12 FE model-detail configuration of SRCB4 .....	111

Figure 4.13 Loading and Boundary conditions.....	112
Figure 4.14 Newton-Raphson iterative solution(ANSYS 18.2 Inc., 2018) .....	113
Figure 4.15 Finite element analysis flowchart.....	116
Figure 5.1 First crack of concrete SRCB1 .....	117
Figure 5.2 First crack of concrete SRCB2 .....	118
Figure 5.3 First crack of concrete SRCB3 .....	118
Figure 5.4 First crack of concrete SRCB4 .....	118
Figure 5.5 Multiple crack patterns of concrete SRCB1 .....	119
Figure 5.6 Multiple crack patterns of concrete SRCB2.....	119
Figure 5.7 Multiple crack patterns of concrete SRCB3 .....	119
Figure 5.8 Multiple crack patterns of concrete SRCB4.....	119
Figure 5.9 The maximum von mises stress of concrete SRCB1.....	120
Figure 5.10 The maximum von mises stress of steel reinforcement SRCB1 .....	120
Figure 5.11 The maximum von mises stress of concrete SRCB2.....	120
Figure 5.12 The maximum von mises stress of steel reinforcement SRCB2 .....	121
Figure 5.13 The maximum von mises stress of concrete SRCB3.....	121
Figure 5.14 The maximum von mises stress of steel reinforcement SRCB3 .....	121
Figure 5.15 The maximum von mises stress of concrete SRCB4.....	121
Figure 5.16 The maximum von mises stress of steel reinforcement SRCB4 .....	122
Figure 5.17 Load-deflection of FEM result of the studied beams .....	122
Figure 5.18 Load-deflection of FEM of the studied beams and test results by Zhang et al. (2016).....	123
Figure 5.19 Summary of shear strength of the studied beams .....	124
Figure 5.20 Shear strength ratio of proposed FEM, conventional shear strength formula, and STM to physical test beams by Zhang et al. (2016).....	125

# CHAPTER 1

## INTRODUCTION

### 1.1 Background

Large opening space at the ground/basement or lower levels are essential for shopping malls, public lobbies, parking lots, etc. Also, at the upper floors of high-rise buildings are typically condominiums, apartments, and hotels with the regular column spacing frames. Hence, to meet multi-purpose architectural and functional requirements, the columns these lower floor levels have to be arranged at larger spacing. As a result, an interface in between the closely spaced column of upper floors and the widely spaced columns at the ground/basement floor or lower floors level has to be provided. This interface is usually attained using beams or plate. The beam as mentioned above is called transfer beam, which is specially defined as a beam that transfers large vertical loads collected from all the upper closely spaced columns acting on it to the widely spaced column supporting it. Figure 1.1 and Figure 1.2 show examples of transfer structures and load transfer paths.

Deep transfer beams are horizontal members, which transfer heavy gravity loads predominantly through shearing action (Londhe, 2011). Many researchers have been extensively studied the shear strength of such reinforced concrete beams.

Behavior and ultimate shear capacity of 27 RC transfer beams were investigated by Londhe (2011) with different parameters such as percent of longitudinal steel ratio, percent of horizontal web steel ratio, and compressive strength. Also, the experimental results have been used for calibrating an analytical model for estimating the shear strength of transfer beams in high-rise buildings.

In the last few decades, the strut-and-tie model (STM) has been widely employed in design of reinforced concrete deep beams. Ahmad et al. (2011) have studied on prediction of the shear strength of deep beams. Six deep beams with different shear-span-to-depth ratios have been designed to resist assumed loads and then tested under monotonic loads. The loads carrying capacity of the deep beams were calculated by STM following ACI 318-06 and compared with experimental results and provision of



Eurocode 2. It has been observed that STM based on ACI 318-06 and Eurocode 2 give reasonable prediction.

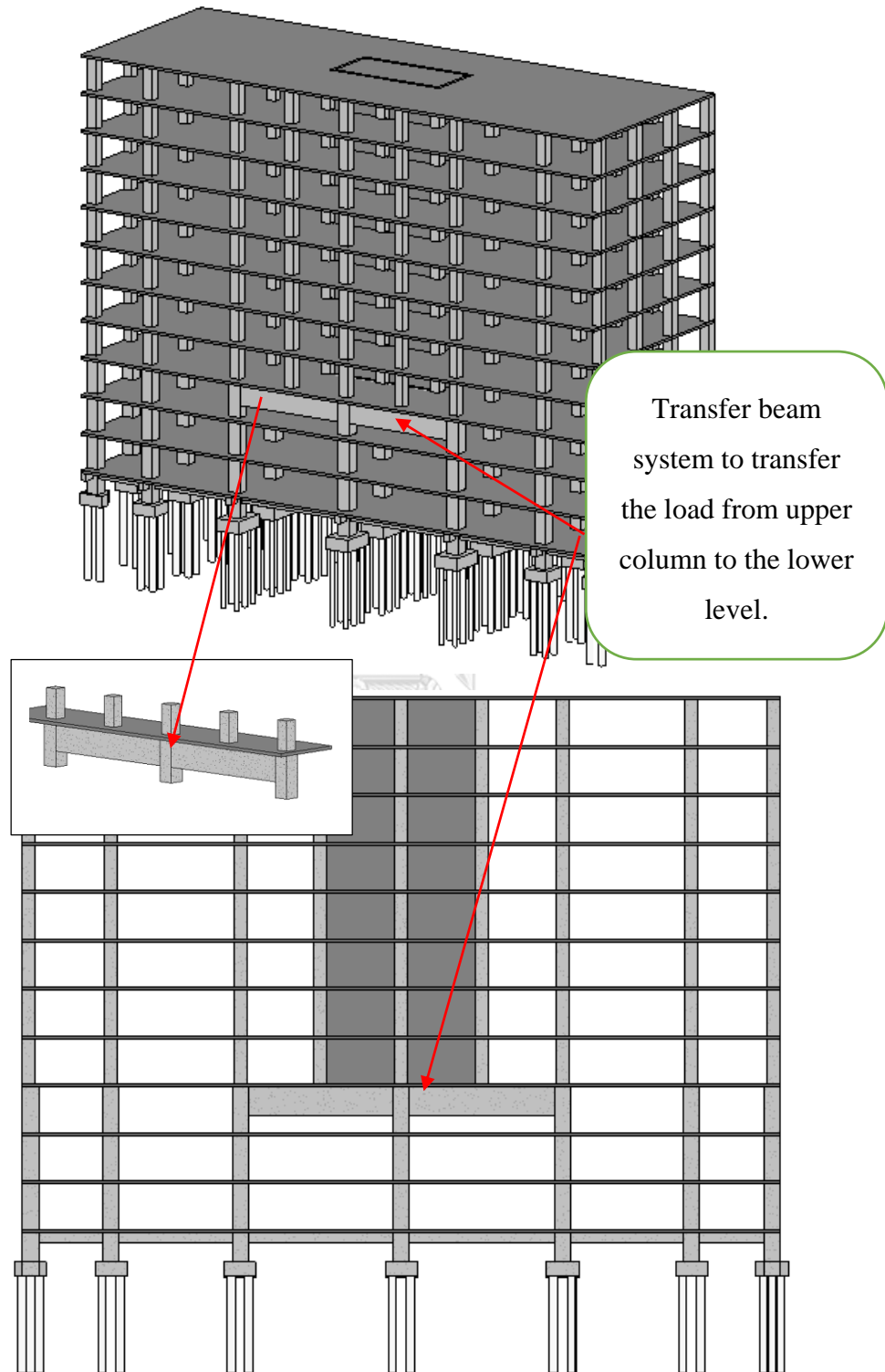


Figure 1.1 A building with transfer structure

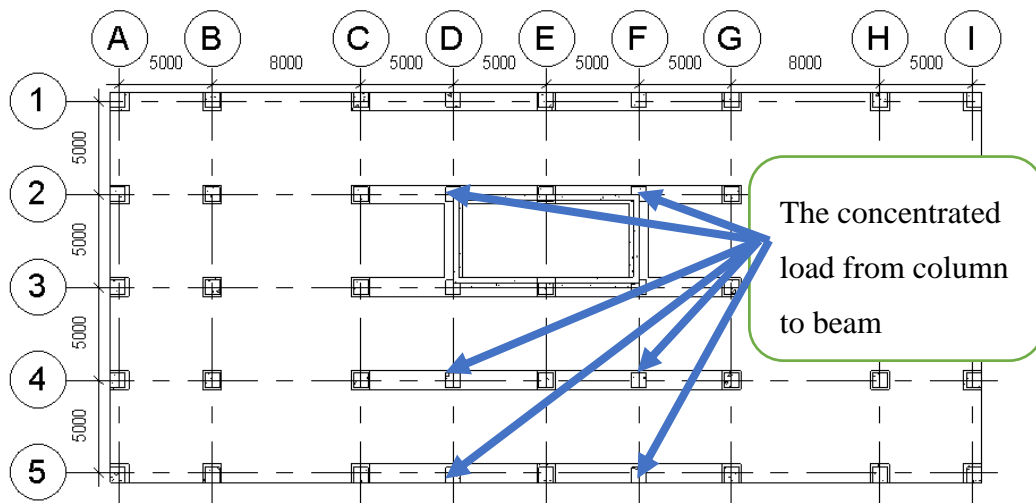


Figure 1.2 The concentrated load from column of the upper level to beam

Some of the high-rise buildings which transfer beams have been used are shown in Figure 1.3 to Figure 1.5.



Figure 1.3 The James Building, New York

(source: <https://www.crsi.org/cfcs/cmsIT/baseComponents/fileManagerProxy.cfc?method=GetFile&fileID=8CB68811-95B5-6FD6-FDB17383B7065BD2>)

The James is a 255-ft 18-story hotel in Manhattan. The principal structural element is located on the 3<sup>rd</sup> floor where east-west beams transfer the hotel columns and span over the lobby below.



Figure 1.4 The Brunswick Building, Chicago, Illinois

(source: <http://khan.princeton.edu/khanBrunswick.html>).

The 474-ft Brunswick Building was constructed in 1961. The main feature of the Brunswick Building is the 24-ft deep transfer wall-beam near the ground level; this shows that the depth of transfer beam has a significant effect on the way in which the forces in the closely spaced columns above the wall-beam are transferred to the widely spaced columns below.



Figure 1.5 Jardine House, Connaught Place, Hong Kong

(source: <https://www.e-architect.co.uk/hong-kong/jardine-house>).

The 178-m Jardine House building was constructed using the tubular system. In this building, closely spaced columns and beams are replaced by perforated walls with circular openings. It incorporates transfer beam 4.2 m deep supporting upper columns with clear span of 7.5m below to transfer the uniform loads from above to the widely spaced massive columns (Subarao, 2006).

Panjehpour et al. (2015) modified the strut effectiveness factor in STM for RC deep beams recommended by ACI 318-11 and AASHTO LRFD (2012) and experimental results. Six RC deep beam specimens with different shear-span-to-depth ratios were tested. Nonlinear finite element modeling (FEM) was developed. The shear strength results obtained from the experiment were compared with the FEM results and STM recommended by ACI 318-11 and AASHTO LRFD (2012).

To investigate the shear behavior of RC deep beams, Ismail et al. (2016) conducted an extensive experimental program examining 24 deep beams. The parameters included concrete compressive strength, shear-to-depth ratio, shear reinforcement, and member depth. Finite element analysis was also performed by the microplane model M4 was carried out in ABAQUS. (2010) to represent the behavior of concrete deep beams more reliably and to validate the model against experiment. Parametric were conducted to further investigate the effect of concrete strength, shear-span-to-depth ratio and shear reinforcement. The concrete strength and shear-span-to-depth-ratio were the two most significant parameters controlling the behavior of RC deep beams based on the experimental and numerical results. The analysis also showed that minimum amount of shear reinforcement increases the shear capacity of RC deep beams by 20% compared with the beam without shear reinforcement and more shear reinforcement does not provide significant additional shear capacity.

The experimental and numerical investigations were carried out to understand the vertical load-carrying behavior and performance of a composite structure with an innovative composite transfer beam by Nie et al. (2017) to overcome the traditional RC transfer beams. The experiment with vertical-monotonic-loading test and lateral-cyclic-loading test were conducted. The numerical simulation with a multiscale modeling scheme was developed to predict the overall structural behavior, the individual story and component behavior. The comparison results with the experiment demonstrated a reasonable level of accuracy. Moreover, both the experimental tests and numerical analysis pointed that the shear deformation mode and the energy dissipation in the composite joint core were also significant mechanical characteristics of the composite transfer frame.

The shear strength of concrete-encased composite structural members has been investigated by using steel shape was entirely encased in concrete. Weng et al. (2001)

The study was to examine the diagonal shear failure and shear bond failure. Through an understanding of those failure modes, a new approach was proposed to predict the shear capacity of composite beams. The proposed method to predict the shear capacities was verified by comparing with previous test results by Zhang and Yamada (1993). The shear strength anticipated from the proposed approach by Weng et al. (2001) were also compared with American and Japanese provisions. The comparison showed that the proposed method yielded acceptable prediction of shear strength and provided a rational expression on the mechanism of shear bond failure. Moreover, Weng et al. (2002) further focused on the experimental study of the shear splitting failure of composite concrete encased steel beams. Nine full-scale specimens with three types were conducted, and the experiments pointed out that the steel flange width ratio had a dominant effect on the shear splitting failure of composite beams. The test results also showed that the application of shear studs had a positive impact on preventing the failure mode of composite beams with large steel flange ratio. A new method proposed by Weng et al. (2002) for predicting the failure mode of composite beams gave an acceptable prediction as compared with the test results.

Leng et al. (2015) examined the failure mechanism and shear strength of steel-concrete-steel (SCS) sandwich deep beams. The investigation was carried out by experiment. Three beams with different shears spans were tested under anti-symmetric point loads, and the failure mode pattern was found to be different from RC members. The steel plates and the shear connectors were strongly dominant the shear capacity of beams, and the membrane action of the outer steel plates produced the beams with excellent strength and ductile performance. A plastic limit analytical model was developed based on tests results of the continuous beams in this paper and simple beams from the previous study to explain the force transfer mechanism and shear strength prediction of the beams.

A new type of steel reinforced concrete transfer beams, the steel truss reinforced concrete STRC transfer beam was developed and utilized in tall building to solve and replace the disadvantage of conventional RC beams. Wu et al. (2011) conducted the experimental studies on the mechanical behavior of the STRC composite transfer beams. Based on the preliminary investigations the result of STRC transfer beam reached to high limit capacity, substantial rigidity, and good ductilities Compared the

STRC transfer beam with standard RC transfer beam, 30-40 % of the limit capacity was increased, and 30-50% of the rigidity can be improved.

Further study has been established to demonstrate the shear capacity of reinforced concrete beams using embedded steel trusses by Zhang et al. (2016). The investigation was carried out on experiment and theoretical research. Five beam specimens with small shear span-depth ratio were tests to inquire their structure performance and ultimate shear strength. According to the test results showed that a steel angle truss adding horizontal reinforcement was the better composition method for an embedded steel truss to improve the shear capacity of a concrete beam. 80.4%, 93.3%, and 495.7% of the ultimate shear strength, elastic deflection stiffness, and elastoplastic deflection stiffness respectively of the reinforced concrete beam using steel angle truss adding horizontal reinforcement was increased compared with conventional RC beams. To predict the ultimate shear strength of reinforced concrete beams with embedded steel trusses Zhang et al. (2016) also considered a flexural-shear strength model and approach. The prediction results were consistent with the test results, and maximum relative error is less than 9%.

Three-dimensional FE model, using a general-purpose finite-element software has been used to investigate the nonlinear analysis of Steel-Concrete Composite plate Girder by Baskar et al. (2002). The fully restrained steel beam to column connection subjected to blast loads was examined using finite element analysis (Dassault Systèmes Simulia Corporation, 2010) by Sabuwala et al. (2005). Models were validated by comparing against experimental data from the previous study.

The general purpose finite element package, ANSYS 8.0 was applied for the numerical analysis to identify the crack in reinforced concrete beams Dahmani et al. (2010) using SOLID65 solid elements. The compressive crushing strength of concrete was simplified using plasticity algorithm while the concrete cracking in tension zone was considered by the nonlinear material model. Smeared reinforcement was used and introduced as a percentage of steel embedded in concrete beams. RC beams with FRP were extensively studied by many researchers using finite element modeling and analysis. Martin and Kuriakose (2016) dealt with the finite element analysis of RC beams with different FRP composite sheet specimens using ANSYS 15. Reinforced concrete beams with FRP laminates was developed using smeared cracking approach

available in ANSYS by Ibrahim and Mahmood (2009). Moreover, Shrivastava et al. (2015) conducted the comparative study of RC beams laminated with and without FRP using FA analysis. The two beams were modeled using ANSYS; one beam was without FRP, another beam was with FRP and the results obtained were compared.

Ismail et al. (2016) introduced numerical investigation of RC deep beams using the microplane M4 material model. The experimental results of 20 deep-beams were verified against the model. To investigate the effect of shear span to depth ratio and concrete compressive strength for RC deep beams with and without shear reinforcement a parametric study was carried out. The critical parameters affected the shear capacity of RC deep beams were the shear span to depth ratio and concrete strength.

Based on the reviews of the background of the mechanical behavior and shear strength of structural members, especially for the deep-transfer beam which is an essential member of the building structure. This section discusses the four factors that encourage the research undertaken in this master study.

The above review showed that the reinforced concrete beam with embedded steel trusses had provided an excellent improvement of the shear capacity comparing conventional RC beams based on the experimental results.

The rational approach to predicting the capacity of the reinforced concrete beam with embedded steel truss has limited source to refer and has not yet been provided in codes.

Few studies have been conducted on experimental investigations steel truss reinforced concrete beams, but numerical modelings have not yet been considered. The numerical investigation of the reinforced concrete beam with embedded steel trusses to investigate the mechanical behavior of the beam is limited and should be investigated further.

## **1.2 Objectives**

The principal objectives of the proposed research are the followings:

1. To conduct the analytical method following the most-relevant code provisions to predict the shear capacity of RC transfer beam with embedded steel trusses.



2. To investigate the shear strength of RC beams with embedded steel trusses by developing finite element modeling of such beam subjected to high shear force demand, e.g., under concentrated load near support.
3. To discuss the comparative study of analytical method, experimental and numerical results

### **1.3 Scope and assumptions**

The limitation of this study is following:

1. The experimental results and proposed approach from Zhang et al. (2016) were used as reference for comparison.
2. Only shear strength is investigated in this study.
3. Only ACI 318-14 and AASHTO LRFD (2012) provisions are adopted in current study.
4. The torsional and flexural effects are neglected in this study.
5. The materials and section properties of the studied beams are based on the experimental study from the previous research.

### **1.4 Research methodology**

Procedure for this study is summarized as follows:

1. The studied beams configuration, dimensions, and material properties in this study are based on such beams mentioned above.
2. The analytical methods provided by ACI 318 (2014) and AASHTO LRFD (2012) (sectional method and strut-and-tie model) are adapted to predict the shear capacity of the RC beam with embedded steel trusses.
3. Finite element models by ANSYS 18.2 of such beams are developed for numerical investigation.
4. The comparative study between the proposed approved, experimental results from Zhang et al. (2016) and ACI 318 (2014), AASHTO (2012), FEM results of the studied beams are carried out.

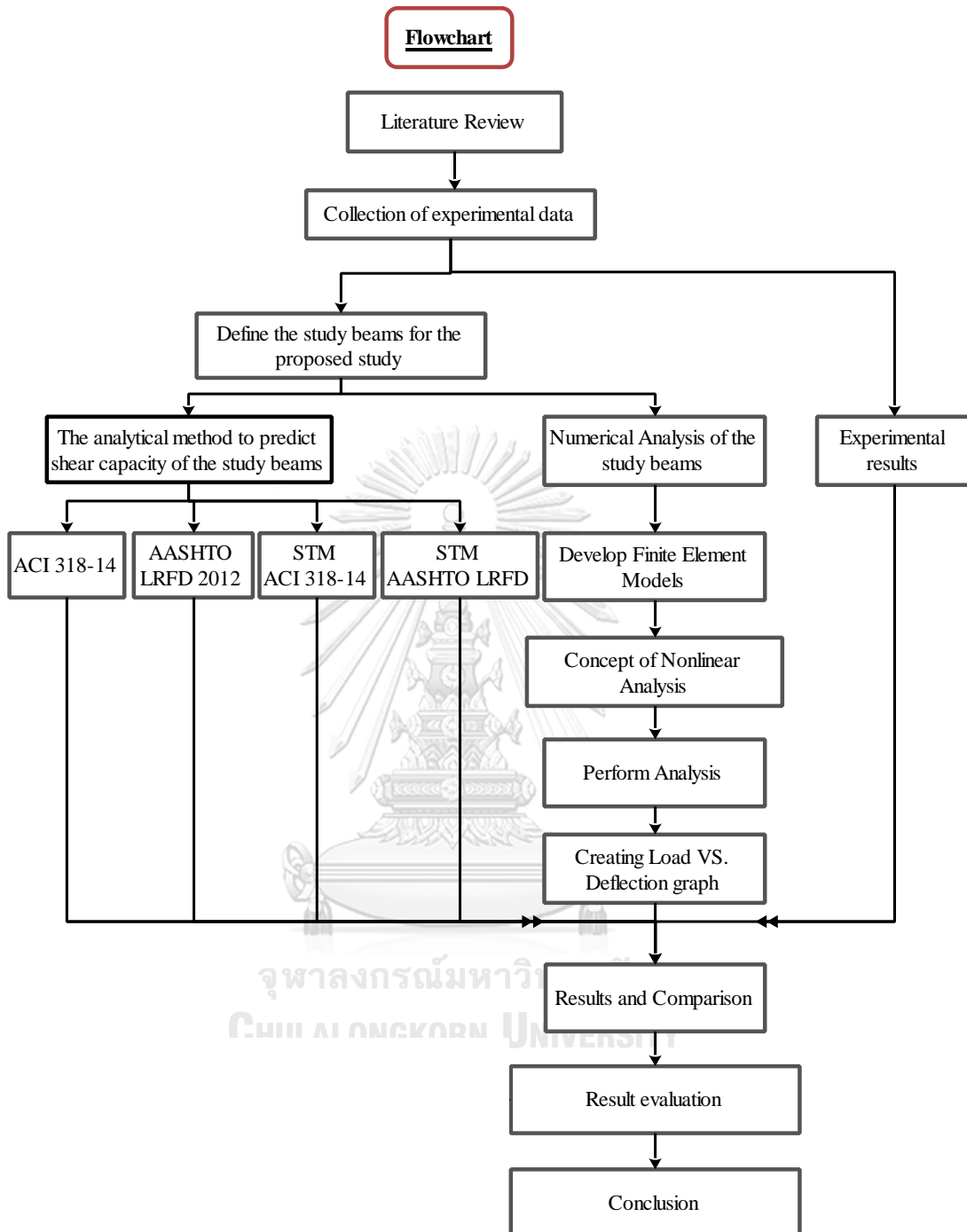


Figure 1.6 Methodology flowchart

## 1.5 Outline of thesis

This thesis work consists of six chapters as briefly described below:

Chapter 1 describes the overview and shear behavior in building structure, motivation, objective, scopes and method of work. Chapter 2 describes the literature review including theoretical background of shear design, code provision for predicting shear capacity, experimental studies of composite RC beams and finite element studied. The calculation of shear strength by analytical methods including conventional shear design formula and Strut-and-Tie Model following ACI 318 (2014) and AASHTO LRFD (2012) are described in Chapter 3. Finite element analysis procedure is presented in Chapter 4. Chapter 5 describes the results and discussion of this study. Finally, conclusion and recommendation for future research are in Chapter 6.



## CHAPTER 2

### LITERATURE REVIEWS

#### 2.1 Overview

Transfer beams are structural members of building that are used to transfer heavy loading of discontinuing columns in the building to the support or lower level of that building. Such concentrated heavy loads cause substantial bending moment and shear.

The shear failure is described by the formation of a single diagonal or series of diagonal cracks occurring at an angle with respect to the beam axis. The diagonal cracks appear due to the presence of diagonal tension in the reinforced concrete beam. Therefore, shear failures are also known as diagonal tension failure. Shear failure is unexpected and brittle behavior compare with flexural failure. Shear failure in reinforced concrete has received much debate due to the complexity of shear resistance mechanism. Over decades, extensive research has been carried out the world to provide analytical shear design models.

This chapter views the current knowledge of the shear behavior of reinforced concrete beams. The review underline the brief design method for determining shear strength, current code provisions for predicting shear capacity of reinforced concrete beams. Literature review also include experimental investigation and rational models which have been proposed by others to describe shear behavior. Moreover, numerical studied of shear strength of reinforced concrete beams are included.

#### 2.2 Theoretical background and analysis methods

##### 2.2.1 Fundamental mechanism of shear transfer in RC beam

The fundamental mechanisms of shear transfer in RC beams illustrated in the free-body diagrams (Figure 2.1 and Figure 2.2) by MacGregor et al. (1997). In the beams without shear reinforcement, the applied shear ( $V$ ) is transferred through a combination which consist of shear in the compression zone ( $V_{cy}$ ), dowel action of the longitudinal reinforcement ( $V_d$ ) and the vertical component of aggregate interlocking over the surface of the inclined crack ( $V_{ay}$ ) Figure 2.1. The concrete contribution

mechanisms were represented by these three components  $V_{cy}$ ,  $V_d$ , and  $V_{ay}$ . The proportions transferred by each of these components have been the topic of research for decades and remain a subject of discussion. The main parameters that affected this proportion of shear transfer by each component influenced by the compression zone depth, shear-span-to-depth ratio, crack width roughness, concrete strength, and other parameters. In the case of RC beams with shear reinforcement, as shown the in free-body diagram in Figure 2.2, there is an extra vertical force ( $V_s$ ) from the presence of stirrups, and this is considered to be the steel contribution to shear resistance.

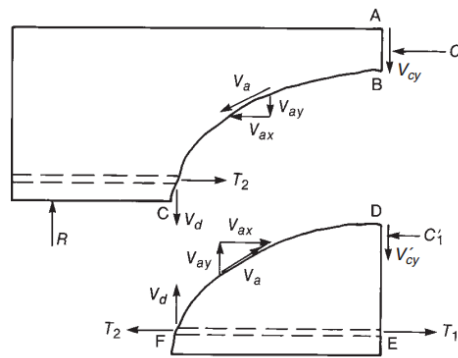


Figure 2.1 Shear transfer mechanisms in RC beams without shear reinforcement  
(MacGregor et al., 1997)

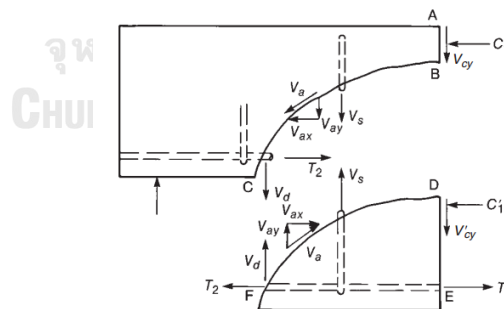


Figure 2.2 Shear transfer mechanisms in RC beams with shear reinforcement  
(MacGregor et al., 1997)

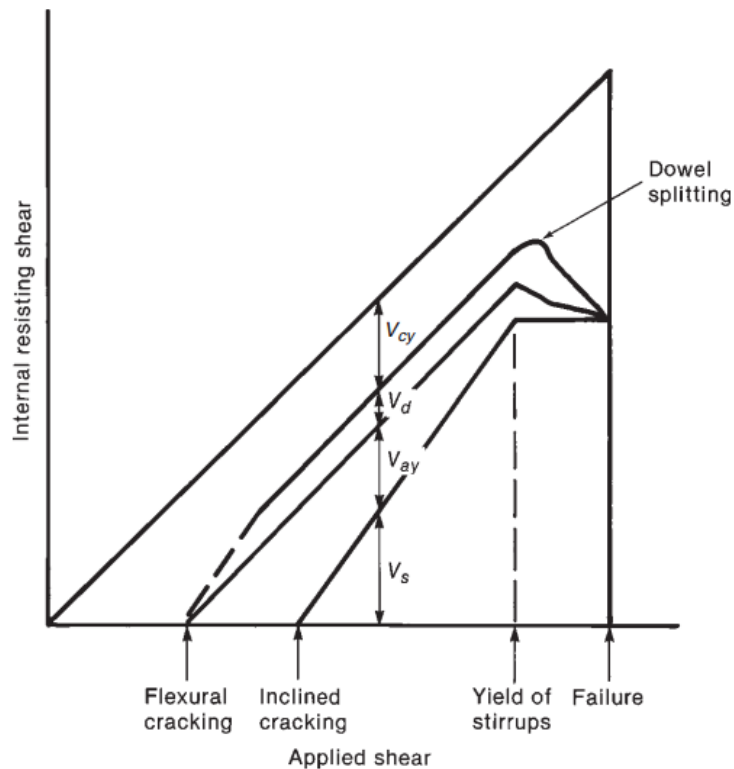


Figure 2.3 Distribution of internal shears in a beam with web reinforcement  
(MacGregor et al., 1997)

Figure 2.3 show that each of the components of this process has a brittle load-deflection response except  $V_s$ . The contributions of  $V_{cy}$ ,  $V_d$ , and  $V_{ay}$  are challenging to measure. In design, these are lumped together as  $V_c$ , the shear carried by the concrete represented by Eq. (2.1). Therefore, the nominal shear strength  $V_n$  is Eq. (2.2)

$$V_c = V_{cy} + V_a + V_d \quad (2.1)$$

$$V_n = V_c + V_s \quad (2.2)$$

### 2.2.2 Truss analogy mechanism

The Swiss engineer Ritter (1899) and the German engineer Mörsh (1902) introduced the 45-degree truss analogy to predicted the shear behavior of concrete

beams. These procedures gave an excellent conceptual model to show the forces that exist in cracked concrete beams.

A beam with inclined cracked as shown in Figure 2.4 develops compressive and tensile forces,  $C$  and  $T$ , in its top and bottom flange, inclined compressive forces in the concrete diagonals between the cracks and vertical tensions in the stirrups. The highly-indeterminate system of forces of Figure 2.4, can be interchanged by an analogous truss. The simplest truss was shown in Figure 2.5.

The analogous truss was derived from several assumptions and simplifications. In Figure 2.5, truss has been constructed by lumping all of the stirrup cut by section A-A into one vertical member b-c and all the diagonal concrete members cut by section B-B into one diagonal member e-f (MacGregor et al., 1997). The shear on section B-B was resisted by the compression stress of the diagonal member. The compression chord along the top of the truss was the force in the concrete and was shown as a truss member. The compression members in the truss were shown with a dashed line, and tensile members were shown with a solid line.

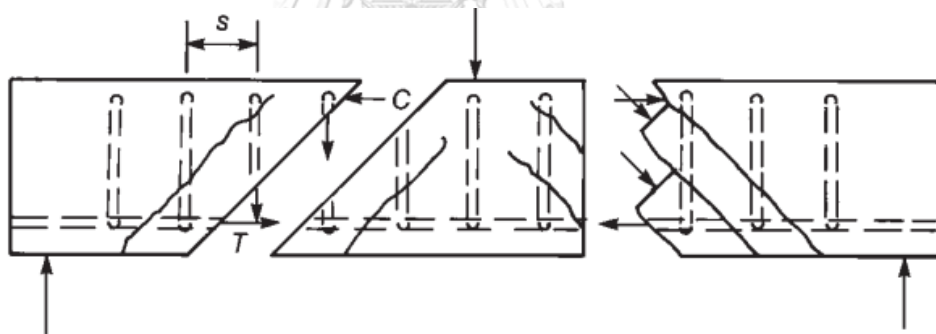


Figure 2.4 Internal forces in a cracked beam (MacGregor et al., 1997)

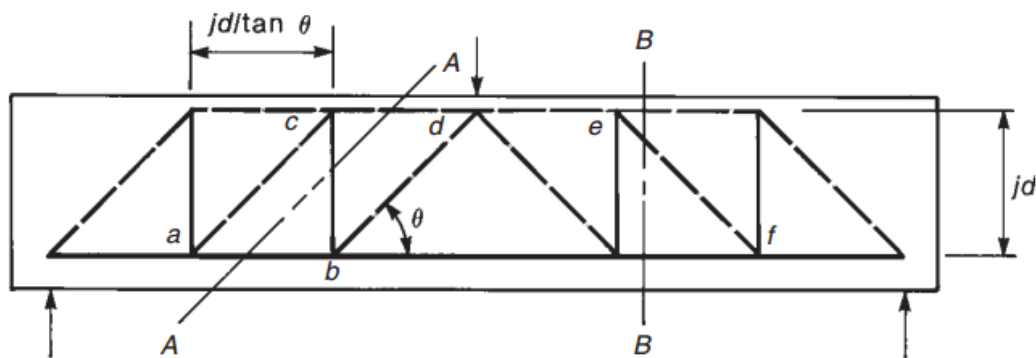


Figure 2.5 Truss analogy (MacGregor et al., 1997)

In design, the ideal distribution of stirrups would correspond to all stirrups reaching yield by the time the failure load is reached. Assume that all stirrups have yield and that each transmits a force of  $A_v f_{yt}$  cross the crack Figure 2.8, where  $A_v$  is the area of the stirrup legs, and  $f_{yt}$  is yield strength of the transverse reinforcement. The truss becomes a statically determinate plastic-truss model; the beam will be proportioned so that the stirrups yield before the concrete crushes (MacGregor et al., 1997), and it will not depend on plastic action in the concrete. The shear components  $V_{cy}$ ,  $V_{ay}$ ,  $V_d$  in Figure 1.2 are ignored in this truss model.

For design, it is easier to stage the truss as shown in Figure 2.6, where the tension force in each vertical member represents the force in all the stirrups within a length  $w(jd \cot \theta)$ . The load has been idealized as concentrated loads of  $w(jd \cot \theta)$  acting at the panel points. The truss in Figure 2.6 is statically determinate.

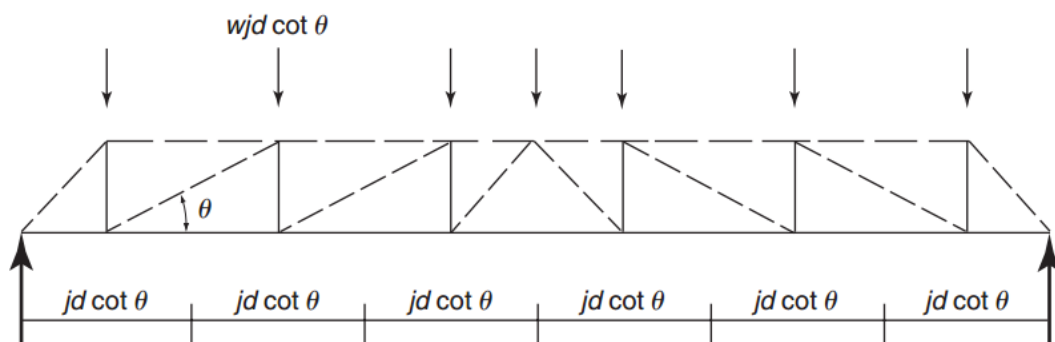


Figure 2.6 Statically determinate truss (MacGregor et al., 1997)

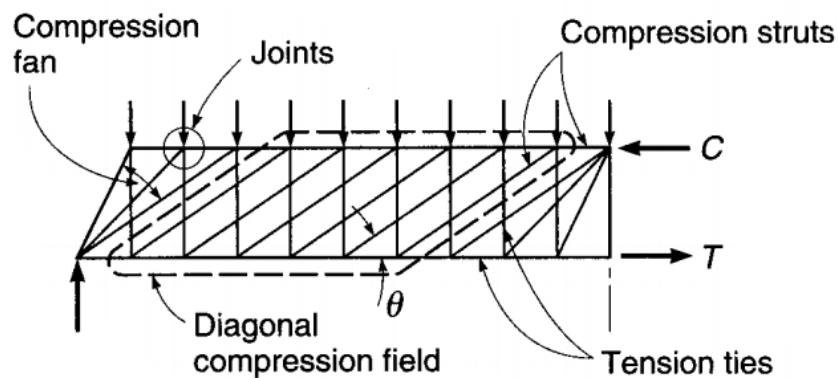


Figure 2.7 Variable angle truss model (Nilson et al., 2004)



### 2.2.2.1 Internal forces in plastic truss model

The free-body diagram cut by section A-A parallel to the diagonals in the compression region, the entire vertical component of the shear force is resisted by tension forces in the stirrups crossing this section. The horizontal projection of section A-A is  $jd \cot \theta$ , and the number of stirrups it cuts is  $jd \cot \theta / s$ . The force in one stirrup is  $A_s f_{yt}$ , which can be calculated from

$$A_s f_{yt} = \frac{Vxs}{jd \cot \theta} \quad (2.3)$$

The free-body diagram Figure 2.9 is cut by a vertical section B-B. The vertical force,  $V$ , acting on the section is resisted by the vertical component of the diagonal compressive force  $D$  (Figure 2.10). The width of the diagonals is  $jd \cot \theta$ , as shown in Figure 2.9, expressing  $D$  as  $V / \sin \theta$ , the average compressive stress in the diagonals is

$$f_2 = \frac{V}{b_w jd \cos \theta \sin \theta} \quad (2.4)$$

With the use of trigonometric identities, this equation becomes

$$f_2 = \frac{V}{b_w jd} \left( \tan \theta + \frac{1}{\tan \theta} \right) \quad (2.5)$$

where  $b_w$  is the thickness of the web. If the web is fragilely thin, the stress may cause web crushing.

The shear  $V$  on section B-B in Figure 2.9 can be replaced by the diagonal compression force and an axial tension force as shown in Figure 2.10, and Eq. (2.6) and (2.7).

$$D = \frac{V}{\sin \theta} \quad (2.6)$$

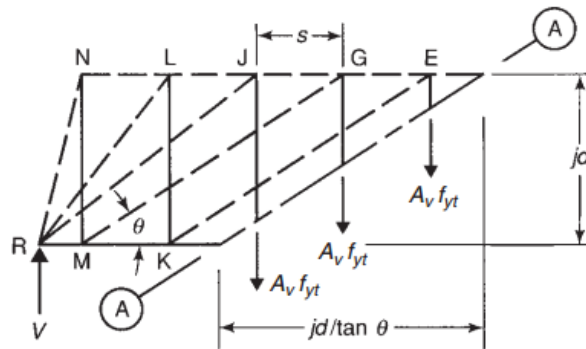


Figure 2.8 Forces in stirrups (MacGregor et al., 1997)

$$N_v = \frac{V}{\tan \theta} \quad (2.7)$$

If it is assumed that the shear stress is constant over the height of the beam, the resultants of  $D$  and  $N_v$  act at midheight. So, a tensile force of  $\frac{N_v}{2}$  acts in each of the top and bottom chords. This reduces the force in the compression chord and increases the force in the tension chord.

Drawing such a truss, it is necessary to choose  $\theta$ . Value of  $\theta$  in compression field region (Figure 2.7), when a reinforced concrete beam with stirrups is loaded to failure, inclined cracks initially develop at an angle of 35 to 45 degree from the horizontal line. With further loading, the angle of compression stress may cross some of the cracks. For this to occur, the aggregate interlock must exist.

In design, the value of  $\theta$  should be in the range of  $25^\circ \leq \theta \leq 65^\circ$ . The choice of a small value of  $\theta$  reduces the number of stirrups required but increases the compression stresses in the web and increases  $N_v$ . The opposite is true for large angles (MacGregor et al., 1997).

In the analysis of the given beam, the angle  $\theta$  is determined by the number of stirrups needed to equilibrate the applied loads and reactions. The angle should be within limits provided, except in compression-fan regions (Figure 2.7) where the angle  $\theta$  varies.

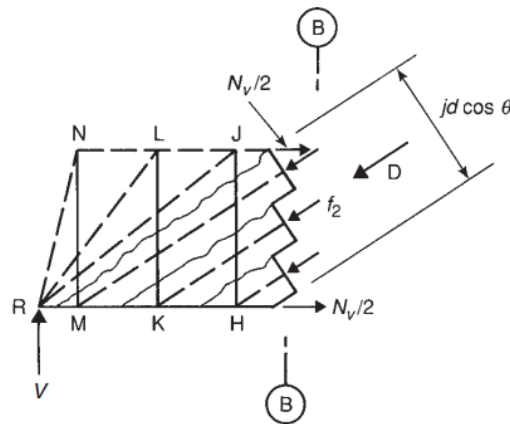


Figure 2.9 Stress in compression diagonals (MacGregor et al., 1997)

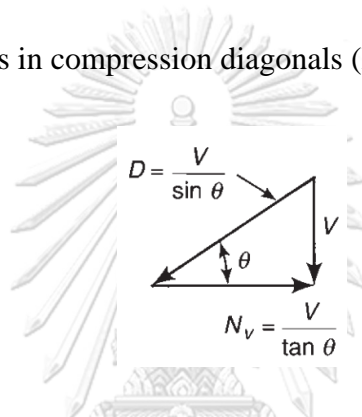


Figure 2.10 Replacement of  $V$  with internal forces of  $D$  and  $N$   
(MacGregor et al., 1997)

### 2.2.3 Modified Compression Field Theory (MCFT)

Modified Compression Field Theory (MCFT) was presented by Vecchio and Collins (1986). Vecchio and Collins (1986) conducted an experimental program on thirty RC panels and developed the MCFT to predict the load-deformation relationship of RC elements subjected to in-plane shear and normal stresses. MCFT treats cracked concrete as a new material with its stress-strain relationship. Furthermore, the formulation in term of equilibrium, compatibility, and the stress-strain relationship is made with regard to average stress and average strain.

MCFT is an improvement of the Compression Field Theory (CFT) that was developed by Mitchell and Collins (1974) as a theory to describe the behavior of RC elements under pure torsion. The main difference between CFT and MCFT is the utilization of the tensile strength of the concrete in MCFT. Dependent upon the measured stress and strain of the tested elements, Vecchio and Collins (1986) observed

that cracked concrete is capable of carrying a significant amount of stress in the principal tensile direction. Thus, the tensile strength of the cracked concrete, which was antecedently neglected, was added to the constitutive material models.

A simplified assumption was made to derive MCFT. The assumption is that average direction of principal compressive stress in the cracked concrete is associated to average direction of principal tensile strain; inclination of critical cracks are parallel to the direction of the principal compressive stress. Also, the theory assumes that for any state of stress there is only one corresponding state of strain, and concrete and reinforcement are perfectly bonded together.

If one considers a small concrete element where the longitudinal (X-axis) and transverse (Y-axis) have co-occurred with the reinforcement directions, then the element will contain the axial stress  $f_x$  and  $f_y$ , and the shear stress  $v_{xy}$ . If the edges remain straight and parallel upon deformation, then the new shape can be defined by normal strains  $\epsilon_x$  and  $\epsilon_y$ , and shear strain  $\gamma_{xy}$  as illustrated in Figure 2.11.

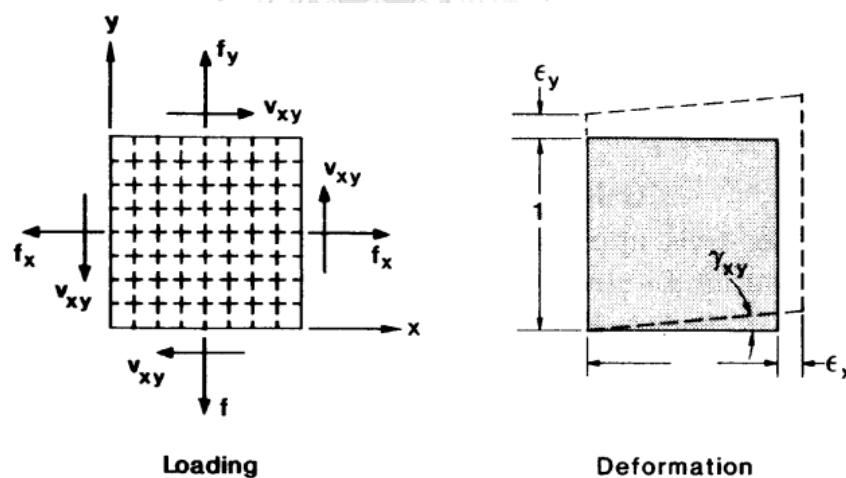


Figure 2.11 Stress-strain relation of concrete element  
(Vecchio and Collins, 1988)

The equilibrium equations, compatibility equations, and material constitutive relationships of the MCFT are summarized as follows.

### 2.2.3.1 Compatibility equations

Due to compatibility conditions strains in concrete should be equal to strains of steel. The strains in concrete and steel are expressed as average strains even though

local conditions may widely vary. Any deformation in the concrete must be matched by an equal deformation in the steel, a change in concrete strain will illustrate an identical change in steel strain. The compatibility of reinforced concrete is demonstrated by Mohr's circle of strain as shown in Figure 2.12. Some essential compatibility equations are:

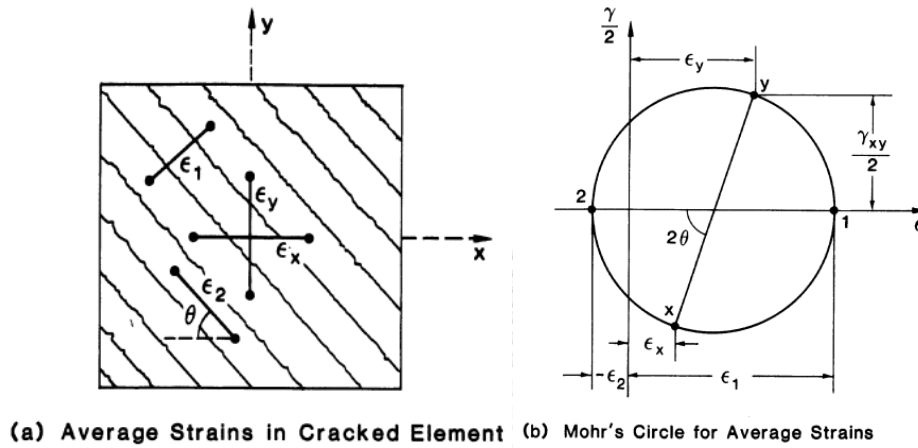


Figure 2.12 Compatibility conditions of the cracked element  
(Vecchio and Collins, 1988)

$$\epsilon_{sx} = \epsilon_{cx} = \epsilon_x \quad (2.8)$$

and

$$\epsilon_{sy} = \epsilon_{cy} = \epsilon_y \quad (2.9)$$

$$\gamma_{xy} = \frac{2(\epsilon_x - \epsilon_2)}{\tan \theta} \quad (2.10)$$

$$\epsilon_x + \epsilon_y = \epsilon_1 + \epsilon_2 \quad (2.11)$$

$$\tan^2 \theta = \frac{\epsilon_x - \epsilon_2}{\epsilon_y - \epsilon_2} = \frac{\epsilon_1 - \epsilon_y}{\epsilon_1 - \epsilon_x} \quad (2.12)$$

where  $\epsilon_{sx}$ ,  $\epsilon_{cx}$ ,  $\epsilon_{sy}$ ,  $\epsilon_{cy}$  are strains of steel and concrete in x and y-directions respectively;  $\epsilon_1$  and  $\epsilon_2$  are strain in principal directions;  $\epsilon_x$  and  $\epsilon_y$  are strains in x and y-directions;  $\gamma_{xy}$  is a shear strain, and  $\theta$  is the angle between principal compression

strain direction and the x-axis. The MCFT assumes that the direction of principal strain coincides with the direction of principal average stress. In other words, MCFT assumes  $\theta_c = \theta$ ;  $\theta_c$  is the angle between concrete principal stress direction and the x-axis.

### 2.2.3.2 Equilibrium equations

The forces applied to the concrete element (Figure 2.13) are resisted by stresses in both concrete and steel reinforcement. For the free body diagram shown in Figure 2.13. The following equations were derived:

$$f_x = f_{cx} + \rho_{sx} \cdot f_{sx} \quad (2.13)$$

$$f_y = f_{cy} + \rho_{sy} \cdot f_{sy} \quad (2.14)$$

$$v_{xy} = v_{cx} + \rho_{sx} \cdot v_{sx} \quad (2.15)$$

Assuming  $v_{cx} = v_{cy} = v_{cxy}$  then the concrete stress conditions are fully defined if  $f_{cx}$ ,  $f_{cy}$  and  $v_{cxy}$  are known. The concrete element will resist concrete shear stresses  $v_{cxy}$ , horizontal concrete stresses  $f_{cx}$  and vertical concrete stresses  $f_{cy}$ ;  $f_x$  and  $f_y$  are stress in X and Y-directions;  $f_{sx}$  and  $f_{sy}$  are horizontal and vertical stresses of steel;  $\rho_{sx}$  and  $\rho_{sy}$  are reinforcement ratio in X and Y-directions;  $v_{xy}$  is shear stress; The average concrete stress is illustrated in Figure 2.14 and described by the following relationships:

$$f_{cx} = f_{c1} - \frac{v_{cxy}}{\tan \theta_c} \quad (2.16)$$

$$f_{cy} = f_{c1} - \frac{v_{cxy}}{\tan \theta_c} \quad (2.17)$$

$$f_{c2} = f_{c1} - v_{cxy} \cdot \left( \tan \theta_c + \frac{1}{\tan \theta_c} \right) \quad (2.18)$$

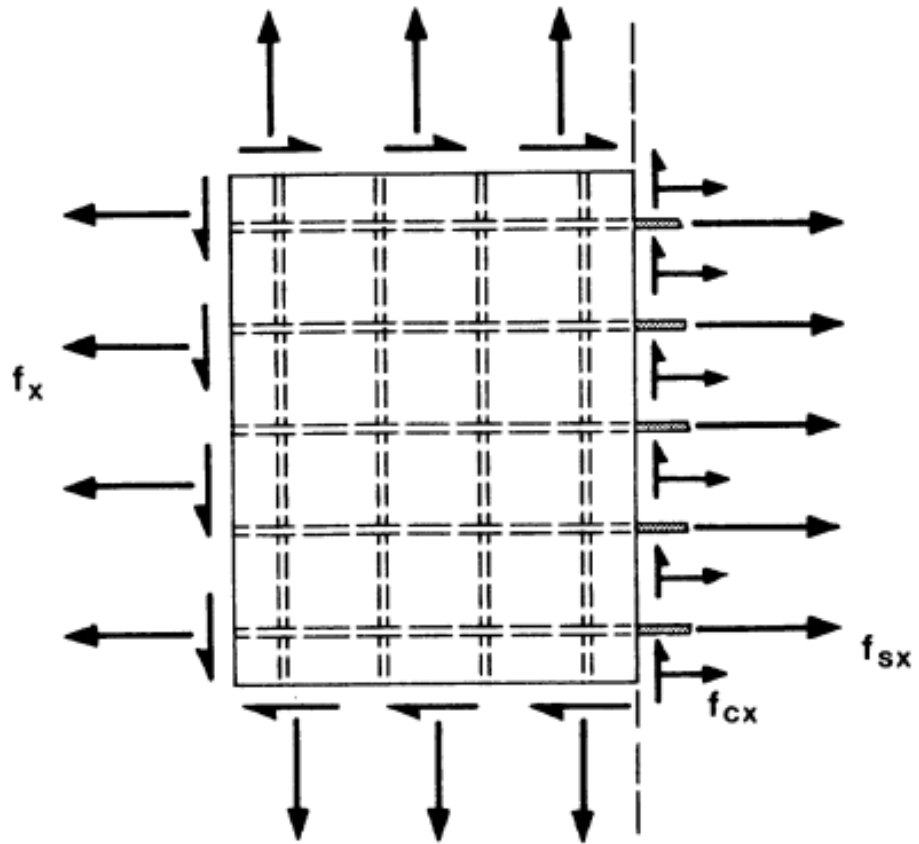


Figure 2.13 The Free body diagram of a part of element (Vecchio and Collins, 1986)

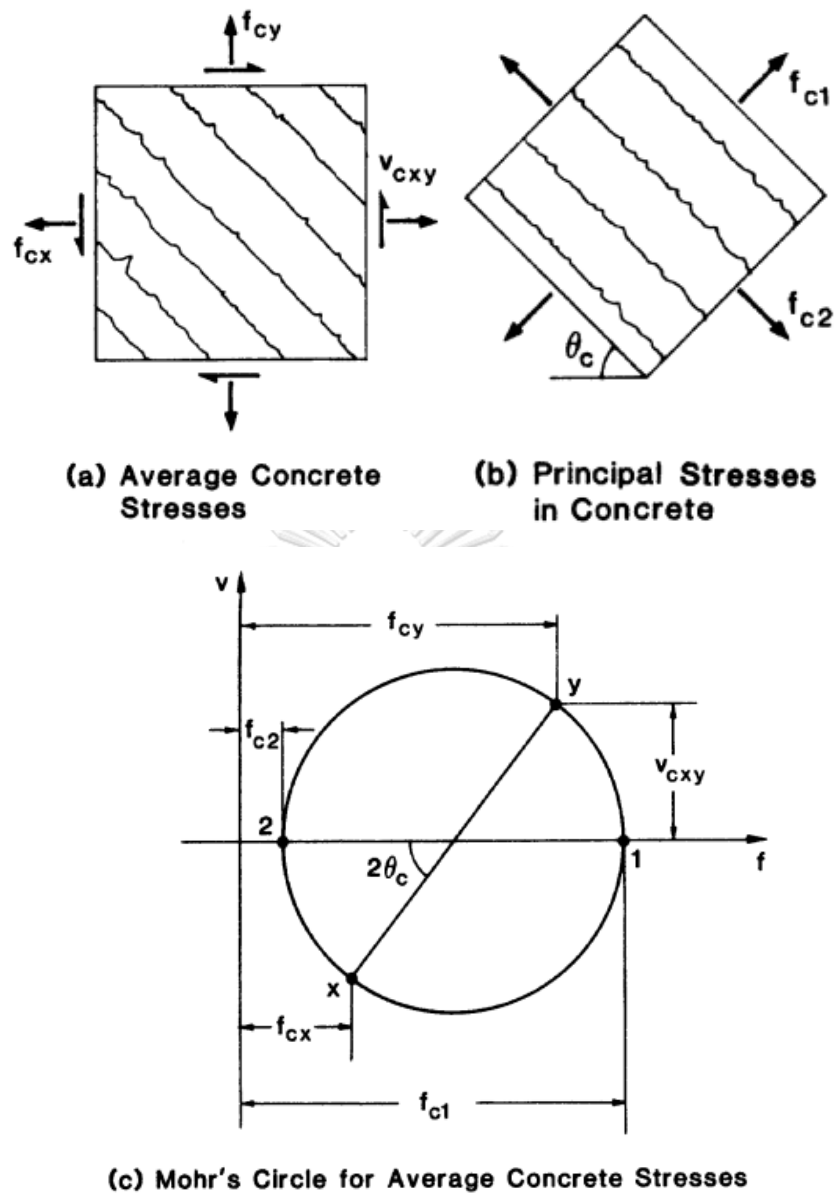


Figure 2.14 Stress in cracked concrete (Vecchio and Collins, 1986)

### 2.2.3.3 Material constitutive relationships

The Figure 2.15 shows the stress-strain relationship for concrete in compression in the principal direction. Cracked concrete is weaker when it subjected to biaxial strains compared to a concrete uniaxial stress-strain relationship. Therefore, the principal compressive strength might be significantly lower than the uniaxial strength when concrete is subjected to significant tensile strain transverse to the principal



compression. The reduction in concrete strength (peak stress) in such case can be predicted by the following equations:

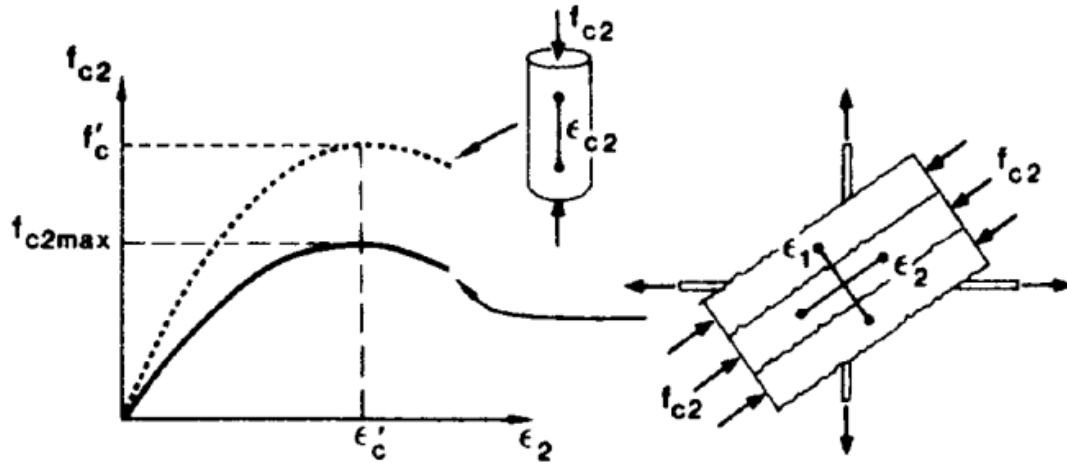


Figure 2.15 Concrete average stress-strain relationship in compression  
(Vecchio and Collins, 1986)

$$f_{c2max} = \frac{f'_c}{0.8 - 0.34 \frac{\epsilon_1}{\epsilon_c}} \leq f'_c \quad (2.19)$$

$$f_{c2} = f_{c2max} \left[ 2 \frac{\epsilon_2}{\epsilon_c} - \left( \frac{\epsilon_2}{\epsilon_c} \right)^2 \right] \quad (2.20)$$

where  $f_{c2max}$  is peak stress of concrete under biaxial strains;  $\epsilon_1$  is a concrete principle tensile strain;  $f'_c$  is concrete peak stress under uniaxial compression;  $\epsilon'_c$  is concrete-strain corresponding to concrete peak compressive stress and is usually equal -0.002;  $f_{c2}$  is concrete compressive stress in the principal direction;  $\epsilon_2$  is a concrete compressive strain in the principal direction;  $f_{c1}$  is concrete tensile stress in principal direction. The relationship for the average principal tensile strain is linear up until cracking and then shows decreasing values of  $f_{c1}$  with increasing of  $\epsilon_1$  as expressed in Figure 2.16 and formulas:

$$f_{c1} = E_c \epsilon_1 \quad \text{where} \quad \epsilon_1 \leq \epsilon_{cr} \quad (2.21)$$

$$f_{c1} = \frac{f_{cr}}{1 + \sqrt{200\epsilon_1}} \quad \text{where } \epsilon_1 > \epsilon_{cr} \quad (2.22)$$

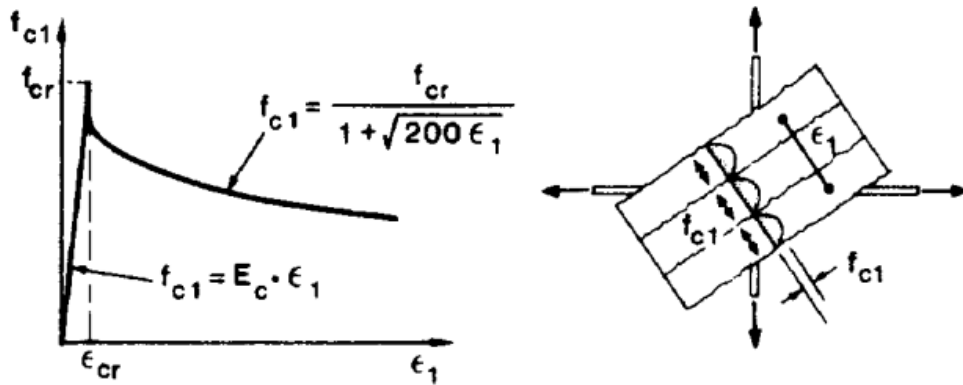


Figure 2.16 Average concrete stress-strain relationship in tension  
(Vecchio and Collins, 1986)

Eq. (2.22) was later changed to a more conservative equation (Bentz et al., 2006; Collins et al., 1996; Rahal and Collins, 1999) as follows:

$$f_{c1} = \frac{f_{cr}}{1 + \sqrt{500\epsilon_1}} \quad (2.23)$$

After cracking occurs in a concrete panel, shear is carried by the aggregate interlock mechanism along a crack. The maximum shear stress that can be resisted and the diagonal cracked width is shown in Figure 2.17 and given by the equations:

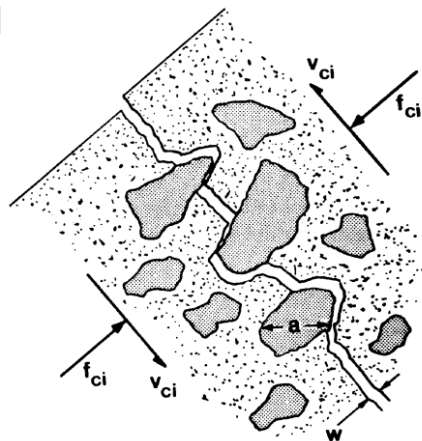


Figure 2.17 Transmitted shear stress across crack by aggregate interlocking  
(Vecchio and Collins, 1986)

$$v_{ci\max} = \frac{0.18\sqrt{f'_c}}{0.31 + 24w(a+16)} \text{ SI units (MPa)} \quad (2.24)$$

where  $a$  is the maximum aggregate size (mm), and  $w$  is crack width (mm) determined from:

$$w = s_\theta \varepsilon_1 \quad (2.25)$$

where  $s_\theta$  is crack spacing as shown in Figure 2.17 is determined from:

$$s_\theta = \frac{1}{\frac{\sin \theta}{s_{mx}} + \frac{\cos \theta}{s_{my}}} \quad (2.26)$$

$s_{mx}$  and  $s_{my}$  are the crack controlled parameters of x-direction reinforcement and y-direction reinforcement, respectively. For members with a minimum amount of reinforcement, crack spacing might be conservatively assumed as  $s_\theta = 300$  mm (Bentz et al., 2006; Collins et al., 1996; Rahal and Collins, 1999).

A bilinear stress-strain relationship as shown in Figure 2.18 is used for reinforcement. The axial stress in the reinforcement will be assumed to depend on only one strain parameter that is the axial strain in the reinforcement. The average shear stress resisted by the reinforcement is assumed to be zero. Therefore

$$f_{sx} = E_s \varepsilon_x \leq y_{yx} \quad (2.27)$$

$$f_{sy} = E_s \varepsilon_y \leq y_{yy} \quad (2.28)$$

$$v_{sx} = v_{sy} = 0 \quad (2.29)$$

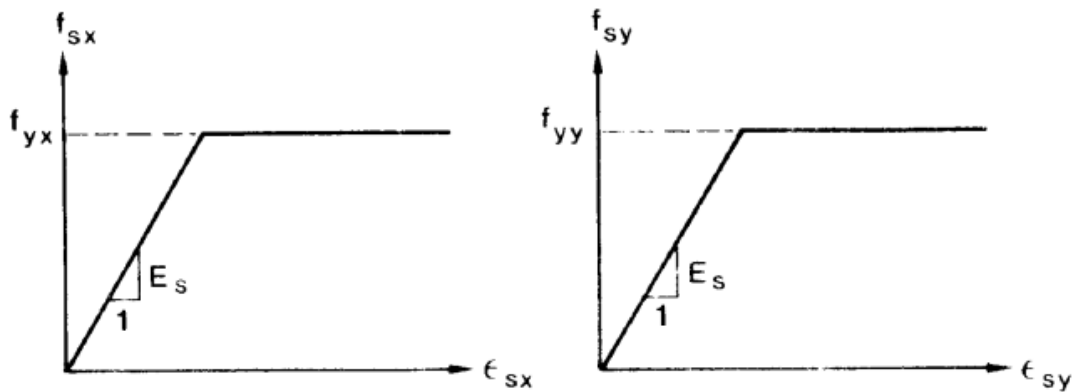


Figure 2.18 Stress-strain relationship for steel reinforcement  
(Vecchio and Collins, 1986)

Various solution techniques for the MCFT presented by Vecchio and Collins (1986). It was tedious to calculate all the methods by hand. The difficult procedure requires individual concrete layers and reinforcing bar elements to be analyzed separately for the entire cross section (Vecchio and Collins, 1988). A simple procedure was established by Collins et al. (1996) for design of shear strength which uses an assumption that shear stress remains constant over the whole depth of the web. This is the basis of AASHTO LRFD bridge design specification. The first edition was published in 1994.

## 2.3 Recent code provisions

In this section, some of the current code provisions for design of shear capacity of reinforced concrete beams are reviewed. The most used shear design procedures for RC member with and without shear reinforcement (ACI 318-14; AASHTO LRFD 2012) are evaluated in this thesis as follows:

### 2.3.1 American Concrete Institute 318 (2014)

ACI 318-14 code provides simple equations to calculate the shear strength at first diagonal crack of RC beams based on the concept of average shear stress acting on effective cross-section. In a member without shear reinforcement, shear is assumed to be carried by concrete. In a member with shear reinforcement, a portion of shear strength is assumed to be resisted by concrete and the remainder by shear

reinforcement. The 45-degree truss model was used to represent the steel contribution to shear strength.

The basic design equation for the shear strength of the reinforced concrete beam is:

$$\phi V_n \geq V_u \quad (2.30)$$

where

$\phi$  = strength reduction factor, which is equal to 0.75 for shear

$V_u$  = factored shear force at the considered section

$V_n$  = nominal shear strength of a section computed by Eq. (2.31)

$$V_n = V_c + V_s \quad (2.31)$$

where

$V_c$  = concrete contribution to the shear strength (N)

$V_s$  = shear contribution provided by shear reinforcement (N)

Joint ACI-ASCE Committee 326 (1962) proposed the following equation to calculate the concrete contribution to shear strength,  $V_c$  the smallest value from equation below: (ACI 318-14 Section 22.5.5.1)

$$V_c = \left( 0.16\lambda\sqrt{f'_c} + 17\rho_w \frac{V_u d}{M_u} \right) b_w d$$

$$V_c = \left( 0.16\lambda\sqrt{f'_c} + 17\rho_w \right) b_w d \quad (2.32)$$

$$V_c = 0.29\lambda\sqrt{f'_c} b_w d$$

For ordinary RC beams without axial force, ACI 318-14 allows the following equation to be used instead of the second term in Eq. (2.32). The concrete contribution to shear strength shall be calculated by (ACI 318-14 Section 22.5.5.1):

$$V_c = 0.17\lambda\sqrt{f'_c} b_w d \quad (2.33)$$

The shear resisted by the stirrups can be calculated by the equation as follows:  
For vertical transverse reinforcement shown in Figure 2.19 and Eq. (2.34):

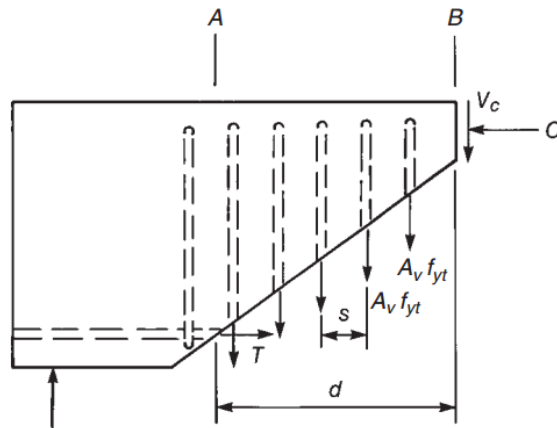


Figure 2.19 Shear resisted by vertical stirrups (MacGregor et al., 1997)

$$V_s = \frac{A_v f_{yt} d}{s} \quad (2.34)$$

(ACI 318-14 Section 22.5.5.3)

For inclined transverse reinforcement shown in Figure 2.20, shear resisted by stirrups are determined by Eq. (2.35) (ACI 318-14 Section 22.10.5.4).

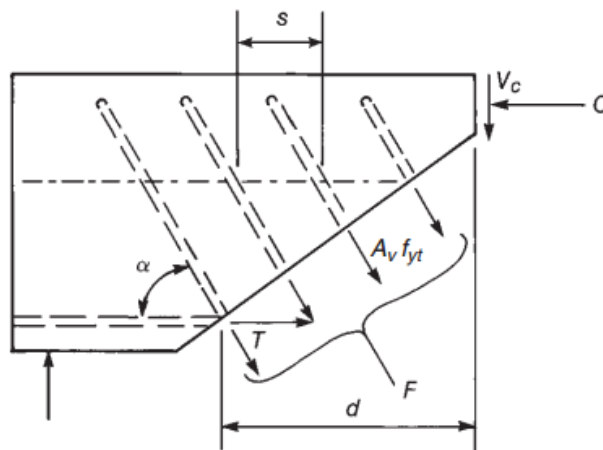


Figure 2.20 Shear resisted by inclined stirrups (MacGregor et al., 1997)

$$V_s = \frac{A_v f_{yt} (\sin \alpha + \cos \alpha) d}{s} \quad (2.35)$$

$$A_{v,\min} = 0.062 \sqrt{f_c'} \frac{b_w s}{f_{yt}} \geq \frac{0.35 b_w s}{f_{yt}} \quad (2.36)$$

where

$f'_c$  = concrete cylinder compressive strength (MPa)

$\lambda$  = modification factor for lightweight concrete

(ACI 318-14 Section 19.2.4.2)

$b_w$  = web width (mm)

$d$  = effective depth of the beam (mm)

$A_s$  = area of non-prestressed longitudinal tension reinforcement (mm<sup>2</sup>)

$\rho_w$  = main flexural reinforcement ratio

$A_v$  = area of shear reinforcement within spacing  $s$  (mm<sup>2</sup>)

$V_u$  = factored shear force at the section of the beam (N)

$M_u$  = factored moment at the section (N.m)

$f_{yt}$  = specified yield strength of transverse reinforcement (MPa)

$s$  = center-to-center spacing of transverse reinforcement (mm)

$\alpha$  = angle between inclined stirrups and a longitudinal axis

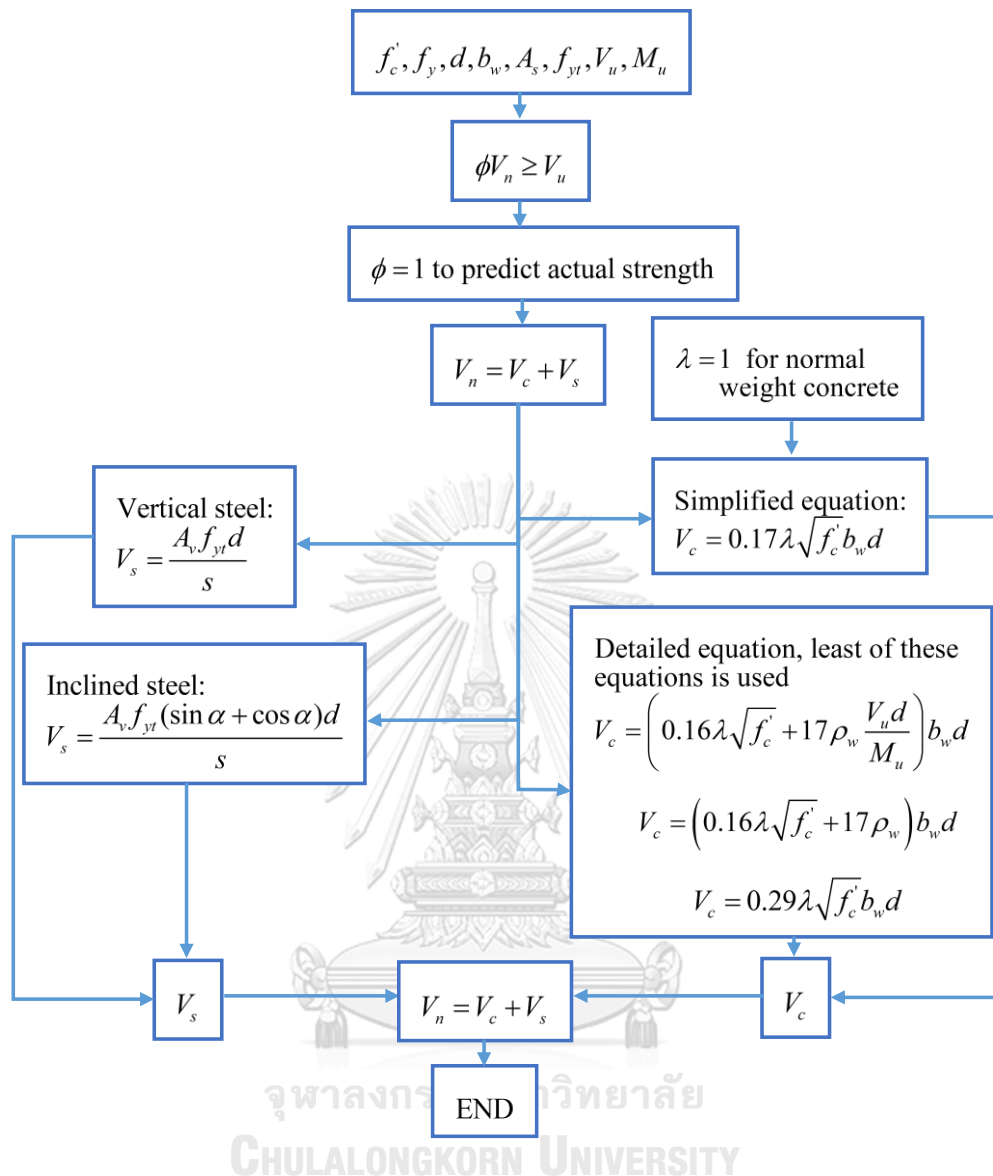


Figure 2.21 Calculation flowchart of shear capacity by ACI 318 (2014)

### 2.3.2 AASHTO LRFD (2012)

The shear provisions in the AASHTO (American Association of State Highway and Transportation Officials) LRFD Bridge Design Specification (2012) is the procedure design or determine the shear strength of a section, which the basis of this was derived from the Modified Compression Field Theory (MCFT) rather than empirical equations. The nominal shear strength of a section shall be calculated as the lesser of the Eq. (2.37) and (2.38) as follows:



$$V_n = V_c + V_s + V_p \quad (2.37)$$

$$V_{n,\max} = 0.25 f'_c b_v d_v + V_p \quad (2.38)$$

$$V_c = 0.083 \beta \sqrt{f'_c} b_v d_v \quad (2.39)$$

$$V_s = \frac{A_v f_y d_v (\cot \alpha + \cot \theta) \sin \alpha}{s} \quad (2.40)$$

$$V_s = \frac{A_v f_y d_v \cot \theta}{s} \quad (2.41)$$

when the angle of inclined stirrups to the longitudinal axis  $\alpha$  is 90 degree, the Eq. (2.40) becomes Eq. (2.41) where

$V_n$  = nominal shear strength (N)

$V_c$  = shear resistance provided by concrete (N)

$V_s$  = shear resistance by the shear reinforcement (N)

$V_p$  = component in the direction of the applied shear of the effective prestressing force (N)

$V_c$  is a function of a factor  $\beta$  which shows the ability of diagonally cracked concrete to transmit tension and shear; the factor  $\beta$  is inversely proportional to the strain in longitudinal tension reinforcement  $\varepsilon_s$  of the section; the value of  $\beta$  is determined as follow for the section that containing at least the minimum amount of shear reinforcement.

$$\beta = \frac{4.8}{(1 + 750\varepsilon_s)} \quad (2.42)$$

If sections do not contain at least the minimum amount of shear reinforcement, the value of  $\beta$  is determined as follow:

$$\beta = \frac{4.8}{(1 + 750\varepsilon_s)} \frac{1300}{(1000 + s_{xe})} \quad (2.43)$$

The crack spacing parameter  $s_{xe}$  can determined as

$$s_{se} = s_x \frac{35}{a_g + 16} \quad \text{where } 300 \text{ mm} \leq s_{se} \leq 2000 \text{ mm} \quad (2.44)$$

The inclination angle of the diagonal compressive stresses can be determined as follow:

$$\theta = 29 + 3500\varepsilon_s \quad (2.45)$$

The strain in longitudinal tension reinforcement ( $\varepsilon_s$ ) is calculated using the equation as follow:

$$\varepsilon_s = \frac{\left| \frac{M_u}{d_v} \right| + 0.5N_u + |V_u - V_p| - A_{ps}f_{po}}{E_s A_s + E_p A_{ps}} \quad (2.46)$$

The minimum area of transverse reinforcement is given by:

$$A_{v,\min} = 0.083\sqrt{f'_c} \frac{b_v s}{f_y} \quad (2.47)$$

The maximum spacing of transverse reinforcement is given by:

$$S_{\max} = 0.8d_v \leq 600 \text{ mm} \quad \text{if } v_u < 0.125f'_c \quad (2.48)$$

$$S_{\max} = 0.4d_v \leq 300 \text{ mm} \quad \text{if } v_u \geq 0.125f'_c \quad (2.49)$$

$$v_u = \frac{|V_u - \phi V_p|}{\phi b_v d_v} \quad (2.50)$$

where

$A_v$  = area of shear reinforcement within a distance  $s$  ( $\text{mm}^2$ )

$f_v$  = specified yield strength of shear reinforcement (MPa)

$d_v$  = effective shear depth measured from distance perpendicular to the neutral axis, between the resultants of the tensile and compressive forces due to flexure (mm). it need not be taken to be less than the greater of  $0.9d_e$  or  $0.72h$  (mm)

$$d_e = \frac{A_{ps} f_{ps} d_p + A_s f_y d_s}{A_{ps} f_{ps} + A_s f_y} \quad (2.51)$$

$$d_v = \frac{M_n}{A_{ps} f_{ps} + A_s f_y} \quad (2.52)$$

- $b_v$  = effective web width (mm)
- $s$  = spacing of transverse reinforcement (mm)
- $M_u$  = absolute value of the factored moment, not to be taken less than  $|V_u - V_p| d_v$  (N.m)
- $V_u$  = factored shear force (N)
- $N_u$  = factored axial force, taken as positive of tensile and negative if compressive (N)
- $A_{ps}$  = area of pre-stressing steel on the flexural tension side of the member (mm<sup>2</sup>)
- $f_{po}$  =  $E_p$  times locked-in difference in strain at ultimate load between the pre-stressing tendons and surrounding concrete (MPa)
- $E_s$  = modulus of elasticity of reinforcing bars (MPa)
- $E_p$  = modulus of elasticity of pre-stressing steel (MPa)
- $A_s$  = area of non-prestressed tension reinforcement on the flexural-tension side of the member at ultimate load (MPa)
- $s_x$  = crack-spacing parameter, the lesser of either  $d_v$  or the maximum distance between layers of longitudinal-crack-control reinforcement (mm)
- $v_u$  = factored shear stresses (MPa)
- $\phi$  = resistance factored for shear
- $a_g$  = maximum aggregate size (mm)

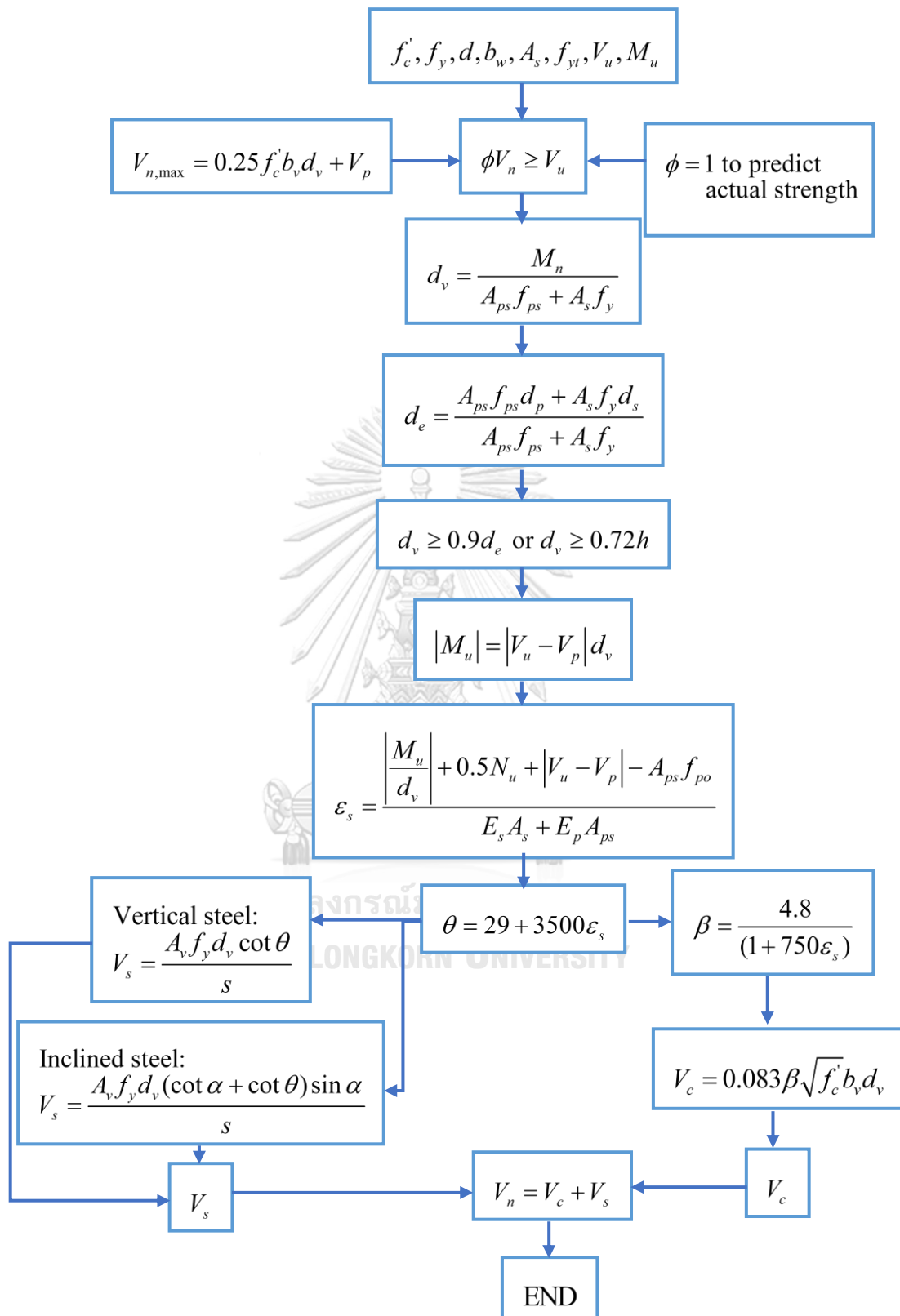


Figure 2.22 Calculation flowchart of shear capacity by AASHTO LRFD (2012)

## 2.4 Strut-and-tie model (STM)

### 2.4.1 Overview

Typically, RC members are designed to resist shear and flexural forces based on the assumption that strains vary linearly at a section. Referring to Bernoulli hypothesis or beam theory, the mechanical behavior of a beam is commonly defined by assuming that plane sections remain plane. The B-regions of a structure, the internal state of stress can be derived from section forces before and after the concrete cracks. Therefore, the design of these regions is referred to a section design.

A deep beam is a structural member whose behavior is controlled by shear deformations. In practice, engineers usually meet deep beams when designing transfer girders, pile support foundation or bridge bents. The structural design standards, AASHTO LRFD and ACI 318, adopted the use of strut-and-tie modeling (STM) for strength design of deep beams or other regions of discontinuity in 1994 and 2002, respectively. Based on the theory of plasticity, STM is a design method that idealizes stress fields as axial members of a truss. The primary advance of STM is its versatility. It is valid for any given loading and geometry. However, the primary weakness of STM is also its versatility.

A deep beam design must be treated differently than a sectional design because assumption utilized to derive sectional theory are no longer valid. A deep beam is a member whose shear span-to-depth ( $a/d$ ) ratio is relatively small such that nonlinear shearing strains dominate the behavior. Generally, a region of a beam with  $a/d$  ratio less than 2.0 to 2.5 is considered to behave as a deep-beam. The beam shown in Figure 2.23 has  $a/d$  ratio approximately two to the right of the concentrated load and five to the left of the load. The left side of the beam (section A-A) contains a B-region and stresses can be determined according to sectional method. The right side of the beam (section B-B) is considered a deep beam region. Shear strains govern the behavior and beam theory can not be used to determine the internal state of stress.

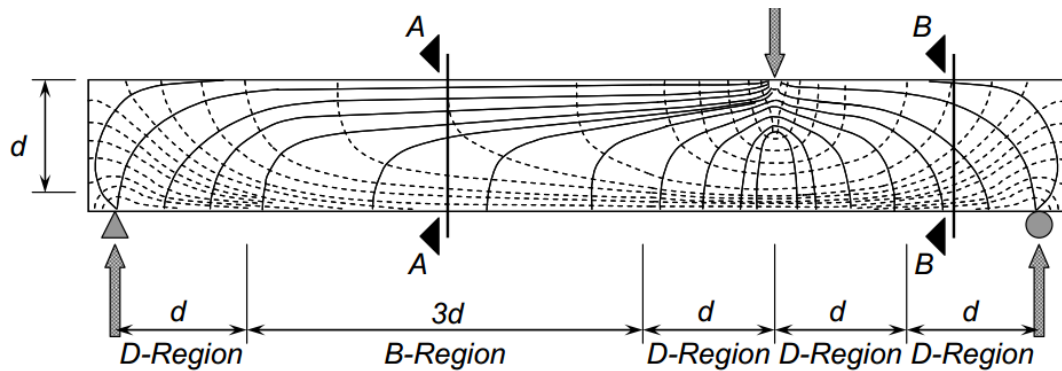


Figure 2.23 Stress trajectories in B-regions and near discontinuities (D-regions)  
(Birrcher et al., 2009)

#### 2.4.2 Theoretical background

A STM idealizes the complex flow of stresses in a structural member as elements in a truss member. The compressive stress fields are resisted by concrete struts, and tensile stress fields are resisted by reinforcing steel ties. Strut and ties intersect at a region called nodes. Strut, tie, and node are the three elements that comprise a STM and they must be proportional to resist the applied loads. According to the lower bound theory of plasticity, the capacity of a STM is always less than actual capacity of structure to redistribute forces into the assumed truss elements. The stresses applied to elements must not exceed their yield or plastic flow capacity. Failure of a STM can be attributed to the crushing of the struts, crushing of concrete at the face of a node, yield of the ties, or anchorage failure of the ties.

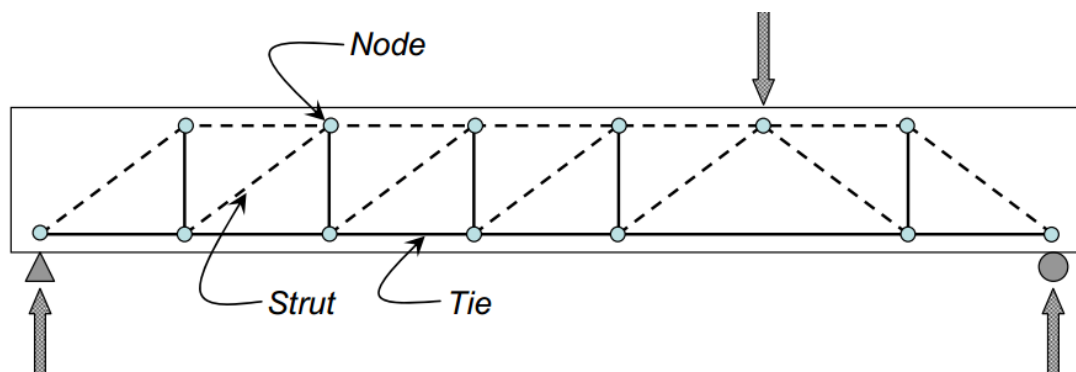


Figure 2.24 Strut-and-tie model of a simply supported beam under a concentrated load  
(Birrcher et al., 2009)

As an example, the loads supported by beam show in Figure 2.23 can be supported by determinate truss show in Figure 2.24. The same truss model is shown in Figure 2.25 with concrete struts, nodes, and reinforcement drawn to scale.

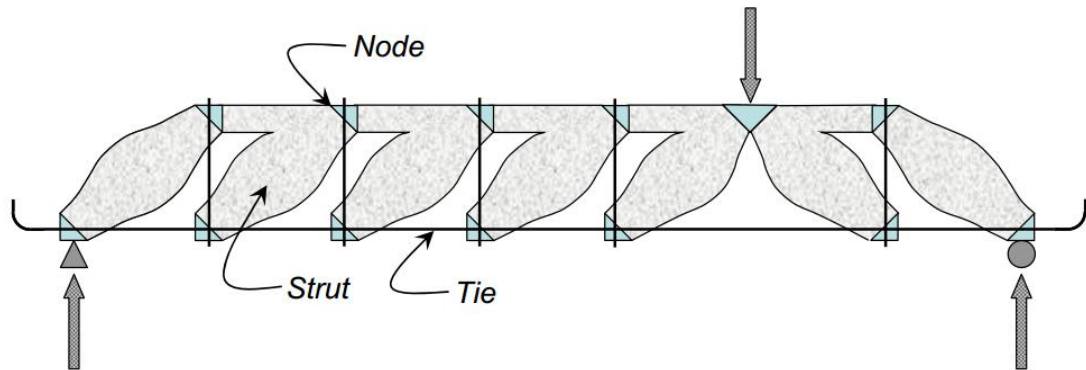


Figure 2.25 RC beam approximated as a truss by STM (Birrcher et al., 2009)

### 2.4.3 Code provisions in ACI 318 (2014)

Guidance for determining the size of struts, nodes, and ties has been given in ACI 318RM-14 are summarized as follows.

For each applicable forced load combination, design strength of each strut, tie, and nodal in a strut-and-tie model satisfy  $\phi S_u \geq U$ , including the following (a) through (c):

(a) Struts:  $\phi F_{ns} \geq F_{us}$

(b) Ties:  $\phi F_{nt} \geq F_{ut}$

(c) Nodal zones:  $\phi F_{nm} \geq F_{us}$

Strength reduction factors  $\phi = 0.75$  for shear.

#### 2.4.3.1 Strength of struts

The effective strength of strut is computed from

$$f_{ce} = 0.85\beta_s f'_c \quad (2.53)$$

The value of  $\beta_s$  is dependent on shape of idealized strut as well as sufficiency of transverse reinforcement. It accounts for the effects of cracking confinement within the strut. The value of  $\beta_s$  are summarized in Table 2-1

Table 2-1 Strut coefficient  $\beta_s$ 

Strut geometry and location	Reinforcement crossing a strut	$\beta_s$	
Struts with uniform cross-sectional area along length	N/A	1.0	(a)
Struts located in a region of a member where the width of the compressed concrete at mid-length of the strut can spread laterally (bottle-shaped struts)	Satisfying section 23.5	0.75	(b)
	Not Satisfying section 23.5	$0.6\lambda$	(c)
Strut located in tension members or the tension zones of members	N/A	0.4	(d)
All other cases	N/A	$0.6\lambda$	(e)

The nominal compressive strength of a strut ( $F_{ns}$ ) shall be calculated by (a) or (b):

(a) Strut without longitudinal reinforcement

$$F_{ns} = f_{ce} A_{cs} \quad (2.54)$$

(b) Strut with longitudinal reinforcement

$$F_{ns} = f_{ce} A_{cs} + A'_s f'_s \quad (2.55)$$

where

$F_{ns}$  shall be evaluated at each end of the strut and taken as the lesser value (N)

$A_{cs}$  = cross-sectional area at the end of the strut under consideration ( $\text{mm}^2$ )

$A'_s$  = area of compression reinforcement along the length of the strut ( $\text{mm}^2$ )

$f'_s$  = stress in the compression reinforcement at the nominal strength of the strut,

it shall be permitted to take  $f'_s$  equal to  $f_y$  for grade 40 (280 MPa) and 60 (420 MPa) reinforcement.



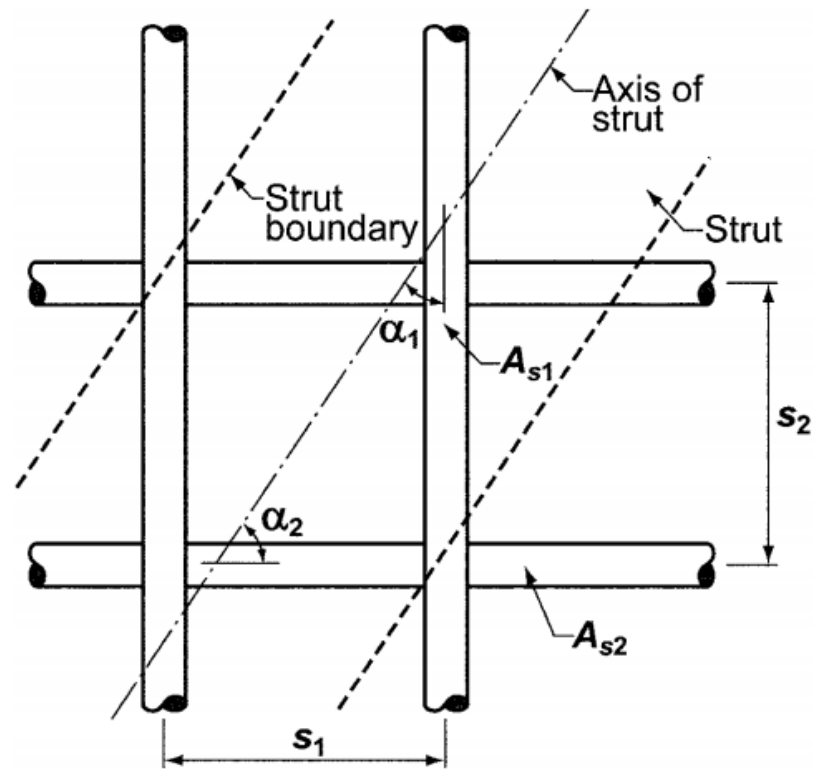


Figure 2.26 Reinforcement crossing a strut

For bottle-shaped struts designed using  $\beta_s = 0.75$  reinforcement to resist transverse tension resulting from spreading of the compressive force in the strut shall cross the strut axis. Transverse reinforcement shall be provided to control longitudinal splitting, For  $f'_c \leq 42 \text{ MPa}$  ACI code considers the transverse reinforcement to be satisfied if the strut is crossed by layers as Figure 2.26 of reinforcement that satisfy.

$$\sum \frac{A_{s_i}}{b_s s_i} \sin \alpha_i \geq 0.003 \quad (2.56)$$

where

$A_{s_i}$  = the total area of distributed reinforcement at spacing  $s_i$  in the  $i$ -th direction of reinforcement crossing a strut at an angle  $\alpha_i$  to the axis of a strut ( $\text{mm}^2$ )

$b_s$  = the width of strut (mm).

### 2.4.3.2 Strength of nodal zones

Once nodal dimensions are defined, the nominal strength of nodal zone can be computed from the following equation:

$$F_{nz} = f_{ce} A_{nz} \quad (2.57)$$

$$f_{ce} = 0.85 \beta_n f'_c \quad (2.58)$$

where

$A_{nz}$  = area of the face of nodal zone taken perpendicular to the line of action of the force from strut or tie (mm<sup>2</sup>)

$f_{ce}$  = effective compressive strength of the concrete in the nodal zone (MPa)

The value of  $\beta_n$  is dependent on type of nodal zone as shown in Table 2-2.

Table 2-2 Nodal zone coefficient  $\beta_n$

Configuration of nodal zone	$\beta_n$	
Nodal zone bounded by struts, bearing areas, or both	1.0	(a)
Nodal zone anchoring one tie	0.80	(b)
Nodal zone anchoring two or more ties	0.60	(c)

### 2.4.3.3 Strength of ties

Nominal strength of ties  $F_{nt}$  is contributed by the strength of the reinforcing steel and pre-stressing steel within the tie. Concrete in tension does not contribute any strength to ties in STM.

$$F_{nt} = A_{ts} f_y + A_{tp} (f_{se} + \Delta f_p) \quad (2.59)$$

where

$A_{ts}$  = area of reinforcing steel (mm<sup>2</sup>)

$f_y$  = yield strength of reinforcing steel (MPa)

$A_{tp}$  = area of pre-stressing steel, if any (mm<sup>2</sup>)

$f_{py}$  = specified yield strength of prepressing reinforcement (MPa)

$f_{se}$  = effective stress in pre-stressing steel (initial stress) (MPa)

$\Delta f_p$  = increase in pre-stressing steel stress due to factored load increment (MPa)

where  $(f_{se} + \Delta f_p)$  shall not exceed  $f_{py}$

In Eq. (2.59), it shall be permitted to take  $\Delta f_p$  equal to 420 MPa for bonded pre-stressing steel and 70 MPa for unbounded pre-stressing steel. Higher values of  $\Delta f_p$  shall be permitted if justified by analysis

Effective width of tie ( $w_t$ ) depends on the distribution of tie reinforcement. It can be taken as the diameter of the bars in the tie plus twice the cover to the surface of the bar as shown in Figure 2.27.

A practical upper limit of the tie width can be taken as the width corresponding to the width in a hydrostatic nodal zone, calculated as

$$w_{t,\max} = \frac{F_{nt}}{f_{ce} b_s} \quad (2.60)$$

where

$f_{ce}$  = the effective nodal zone compressive stress (MPa)

$b_s$  = thickness of strut (mm)

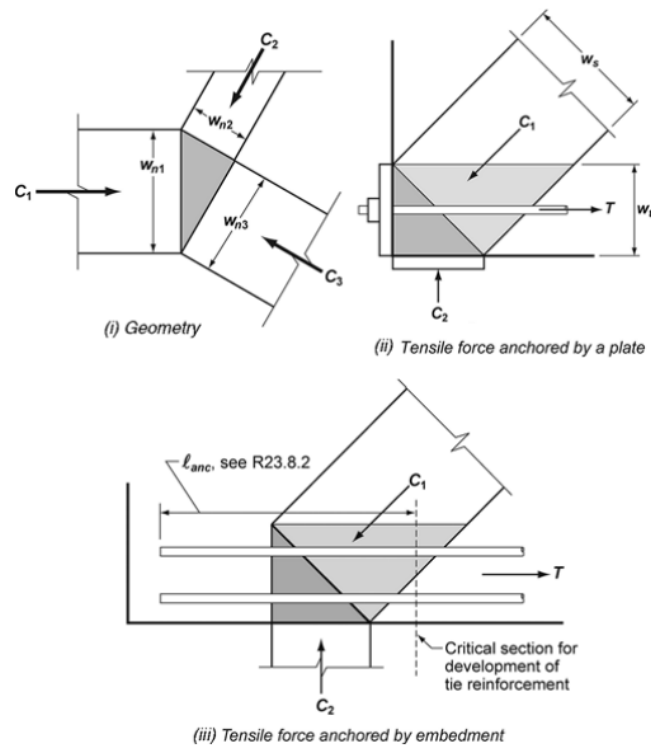


Figure 2.27 Hydrostatic nodes (ACI 318, 2014)

Ties must be anchored adequately before they leave the nodal zone. If the combined lengths of the nodal zone and extended nodal zone (Figure 2.27) are inadequate to provide for the development length of the reinforcement, additional anchorage may be obtained by extending the reinforcement beyond the nodal zone, using 90 degree hooks, or by using a mechanical anchor.

#### 2.4.3.4 Shear strength requirement for deep beam

Deep beams are defined as the beam having clear spans to total member depth ( $L/h$ ) less than or equal to 4, also for beam with concentrated load placed within twice of total beam depth from support  $\frac{a}{d} \geq 2$  is considered as deep beam.

The nominal shear in deep beam may not exceed

$$V_{n,max} = 0.83\sqrt{f'_c}b_w d \quad (2.61)$$

The minimum steel requirement for horizontal and vertical reinforcement within deep beam.

Minimum vertical web reinforcement

$$A_v \geq 0.0025b_w s$$

Minimum longitudinal web reinforcement

$$A_{vh} \geq 0.0025b_w s_2$$

$A_{vh}$  = area of distributed longitudinal web reinforcement (mm<sup>2</sup>)

$A_v$  = area of distributed longitudinal web reinforcement (mm<sup>2</sup>)

$s, s_2$  = spacing of distributed vertical and longitudinal reinforcement (mm)

$s$  and  $s_2$  may not exceed  $d/5$  or 300 mm

#### 2.4.4 Code provisions in AASHTO LRFD (2012)

The factored resistance  $P_r$  of strut and ties shall be taken as that of axially loaded components:

$$P_r = \phi P_n \quad (2.62)$$

where

$P_n$  = nominal resistance of strut or tie (N)

$\phi$  = resistance factor for tension or compression

##### 2.4.4.1 Strength of struts

The nominal compressive strength of a strut ( $F_{ns}$ ) shall be calculated by (a) or (b):

(a) Strut without longitudinal reinforcement

$$P_n = f_{cu} A_{cs} \quad (2.63)$$

(b) Strut with longitudinal reinforcement

$$P_n = f_{cu} A_{cs} + f_y A_{ss} \quad (2.64)$$

where

$P_n$  = nominal resistance of a compressive strut (N)

$A_{cs}$  = effective cross-sectional area of strut (mm<sup>2</sup>); the value of  $A_{cs}$  shall be taken from the smaller end of the strut

$A_{ss}$  = area of reinforcement in the compressive strut ( $\text{mm}^2$ )

$f_{cu}$  = limiting compressive stress (MPa)

$f_y$  = yield strength of steel longitudinal reinforcement (MPa)

The limiting compressive stress ( $f_{cu}$ ) shall be taken as:

$$f_{cu} = \frac{f'_c}{0.8 + 170\varepsilon_1} \leq 0.85f'_c \quad (2.65)$$

in which

$$\varepsilon_1 = \varepsilon_s + (\varepsilon_s + 0.002) \cot^2 \alpha_s \quad (2.66)$$

where

$\alpha_s$  = smallest angle between the compressive strut and adjoining tension ties  
(degree)

$\varepsilon_s$  = tensile strain in the concrete in the direction of the tension tie (mm/mm)

$f'_c$  = specified compressive strength (MPa)

#### 2.4.4.2 Strength of ties

Tension tie reinforcement shall be anchored to the nodal zones by specified embedment length, hooks, or mechanical anchorage.

The nominal resistance of a tension tie shall be taken as:

$$P_n = f_y A_{st} + A_{ps} (f_{pe} + f_y) \quad (2.67)$$

where

$A_{st}$  = total area of longitudinal steel reinforcement in the tie ( $\text{mm}^2$ )

$A_{ps}$  = area of pre-stressing steel ( $\text{mm}^2$ )

$f_{pe}$  = stress in pre-stressing steel due to pre-stress after losses (MPa)

#### 2.4.4.3 Strength of nodal zone

The concrete compressive stress in the node region of the strut shall not exceed:

1. For node regions bonded by compressive struts and bearing areas:  $0.85\phi f'_c$

2. For node regions anchoring a one-direction tension tie:  $0.75\phi f'_c$
3. For node regions anchoring tension ties in more than one direction:  $0.65\phi f'_c$

$\phi$  = resistance factor for bearing on concrete

The tension tie reinforcement shall be uniformly distributed over an effective area of concrete at least equal to the tension tie force divided by the stress limits specified herein

#### 2.4.4.4 Crack control reinforcement

The spacing of the bars in these grids shall not exceed the smallest of  $d/4$  or 300 mm Figure 2.28.

The reinforcement in the vertical and horizontal direction shall satisfy following:

$$\frac{A_v}{b_s s_v} \geq 0.003 \quad (2.68)$$

$$\frac{A_h}{b_w s_h} \geq 0.003 \quad (2.69)$$

where

$A_h$  = total area of horizontal crack control reinforcement within spacing  $s_h$  ( $\text{mm}^2$ )

$A_v$  = total area of vertical crack control reinforcement within spacing  $s_v$  ( $\text{mm}^2$ )

$b_w$  = width of member's web (mm)

$s_v, s_h$  = spacing of vertical and horizontal crack control reinforcement (mm)

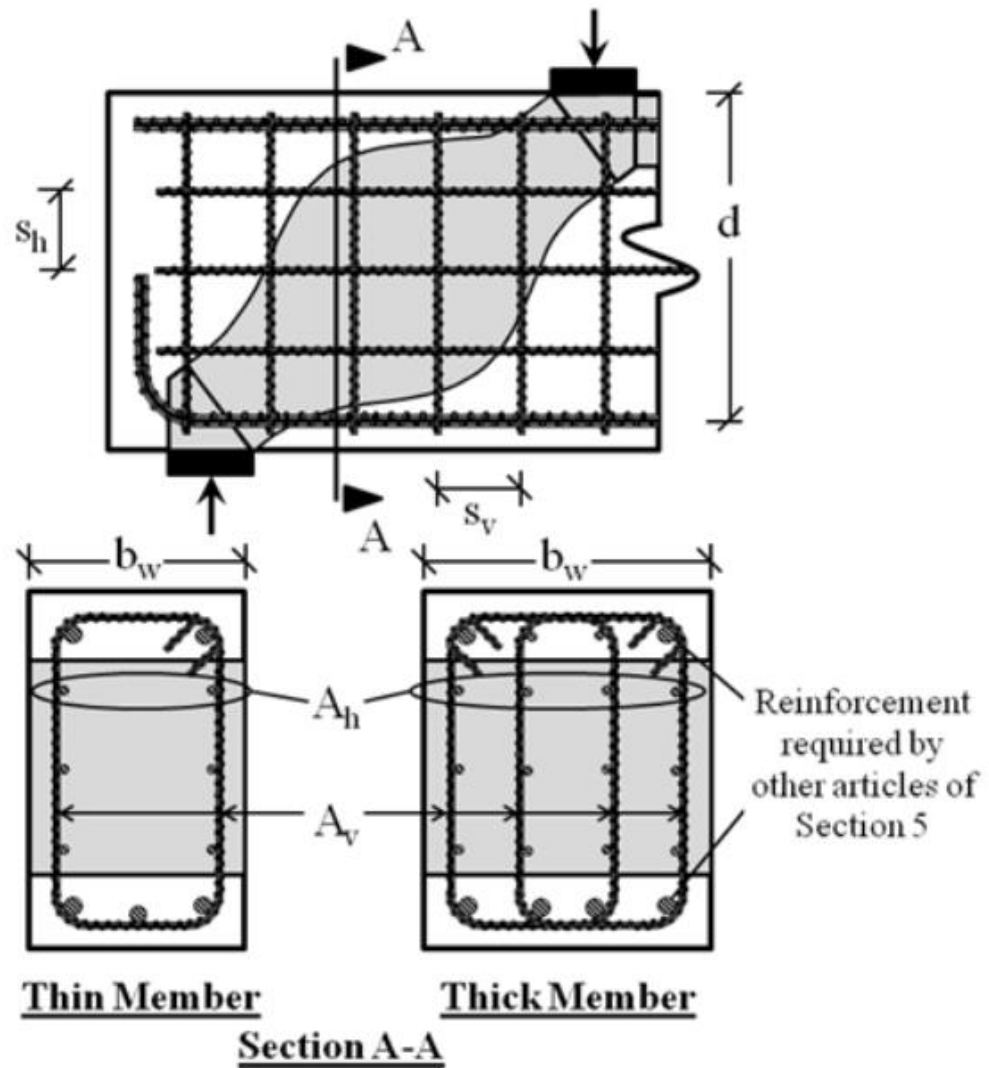


Figure 2.28 Crack control reinforcement (AASHTO LRFD, 2012)



### 2.4.5 Procedure of STM

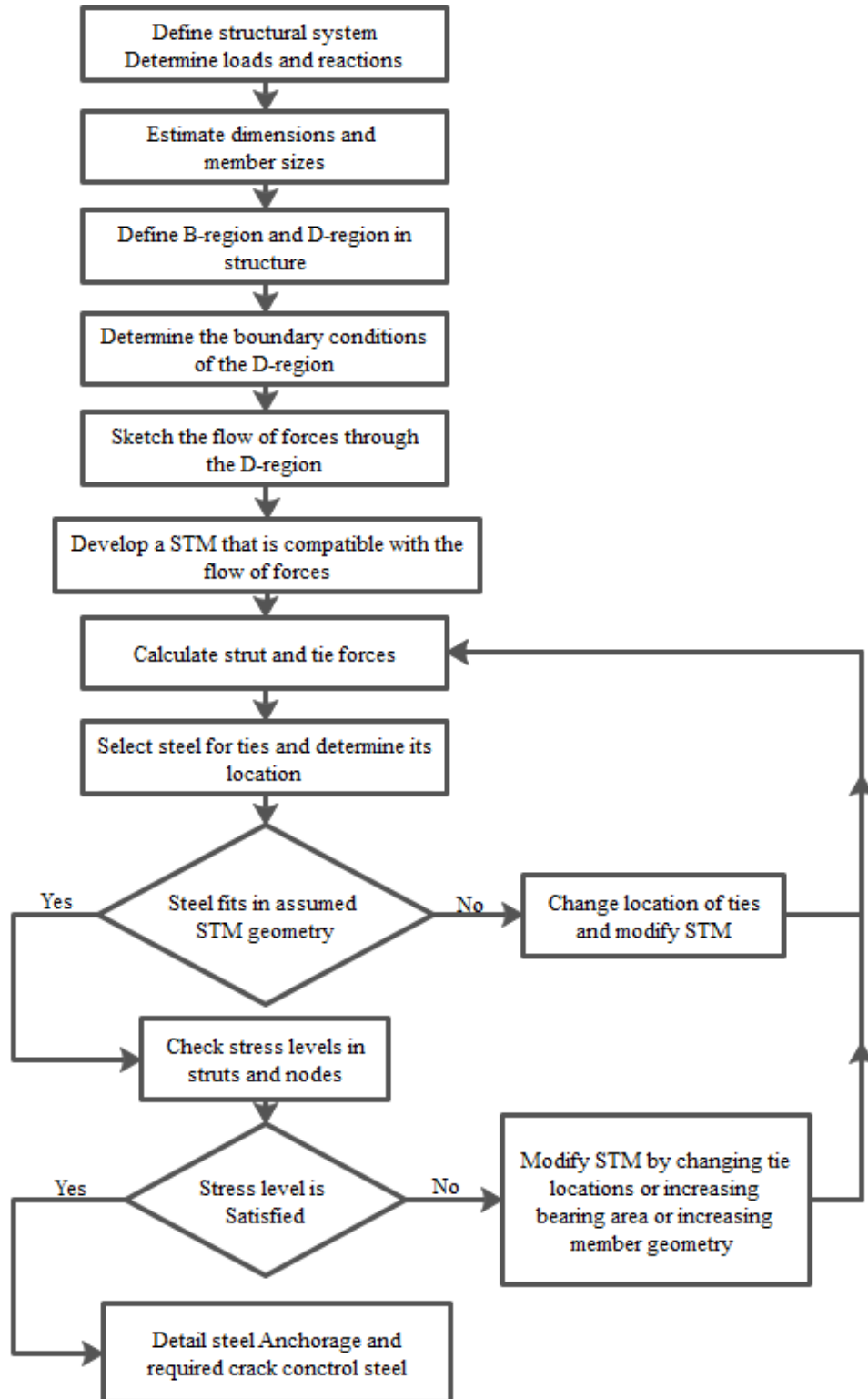


Figure 2.29 Calculation flowchart of STM

## 2.5 Past experimental studies of RC beams with embedded steel trusses

### 2.5.1 RC beams with embedded steel trusses

Zhang et al. (2016) conducted five beam specimens with the small shear span-depth ratio. The structural performance and ultimate shear strength were investigated in this study, and the comparative study was considered regarding shear strength, elastic deflection, and elastoplastic. The beam specimens have material properties and configuration are shown in Table 2-3 and Table 2-4, and Figure 2.30 to Figure 2.33 as follow:

Table 2-3 Material properties of steel (Zhang et al., 2016)

Type of steel	Size (mm)	Yield strength $f_y$ (MPa)	Ultimate strength $f_u$ (MPa)	Modulus of elasticity $E_s$ (GPa)
Reinforcing round bar	$\phi 8$	363	465	210
Reinforcing deformed bar	$\phi 12$	405	522	200
Reinforcing deformed bar	$\phi 16$	378	472	200
Reinforcing deformed bar	$\phi 22$	393	557	200
Flat bar	30 x 4	266	363	200
Angle	40 x 40 x 4	345	519	200
Angle	30 x 30 x 3	348	522	200

Table 2-4 Material properties of concrete (Zhang et al., 2016)

Test specimen	SRCB1	SRCB2	SRCB3	SRCB4	SRCB5
Compressive strength, $f_c'$ (MPa)	41.54	41.73	44.11	40.41	42.36
Modulus of elasticity, $E_c$ (GPa)	34.11	34.10	34.56	33.72	34.13

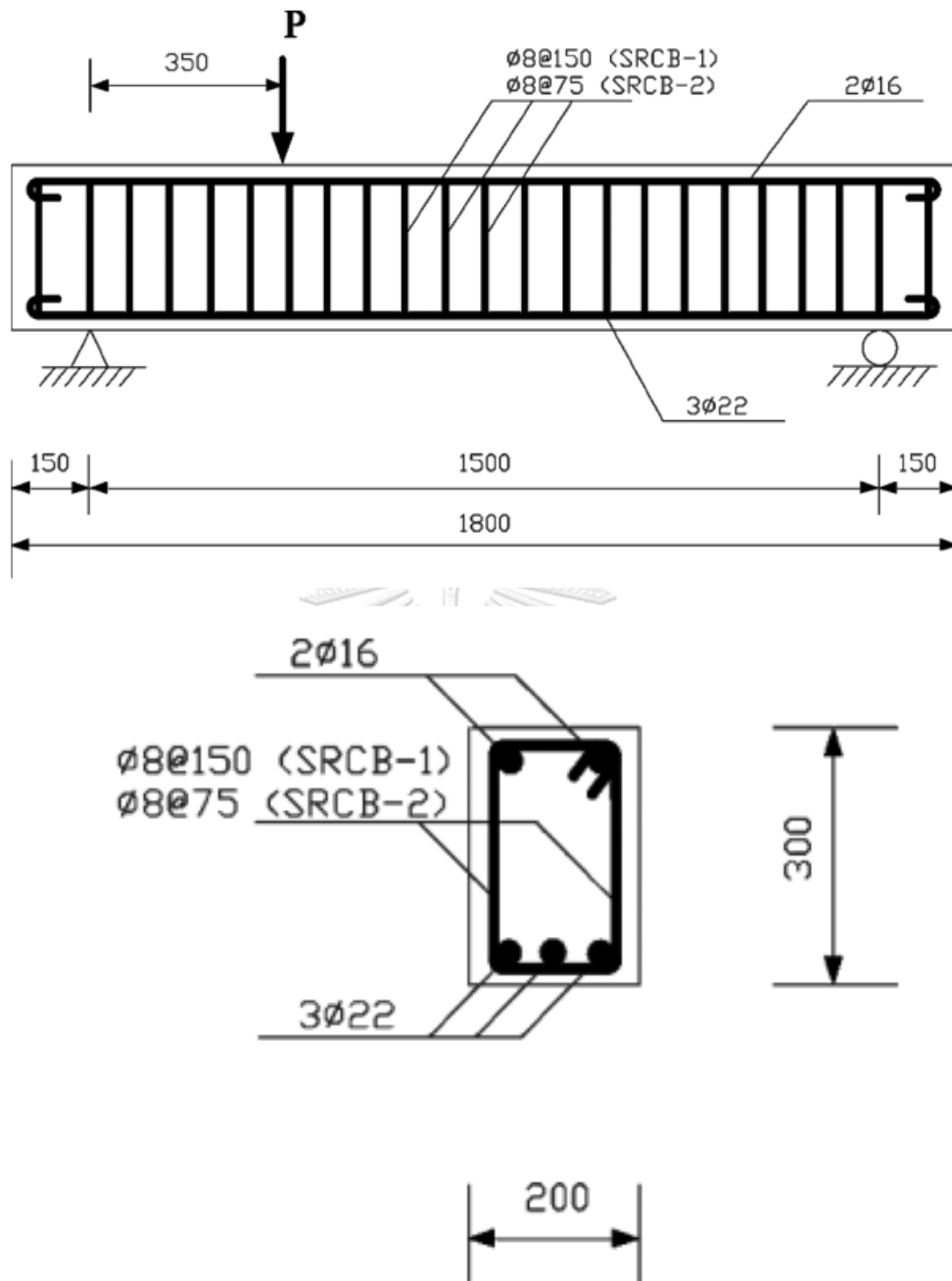


Figure 2.30 Profile and cross-section detail of SRCB1 and SRCB2  
(Zhang et al., 2016)

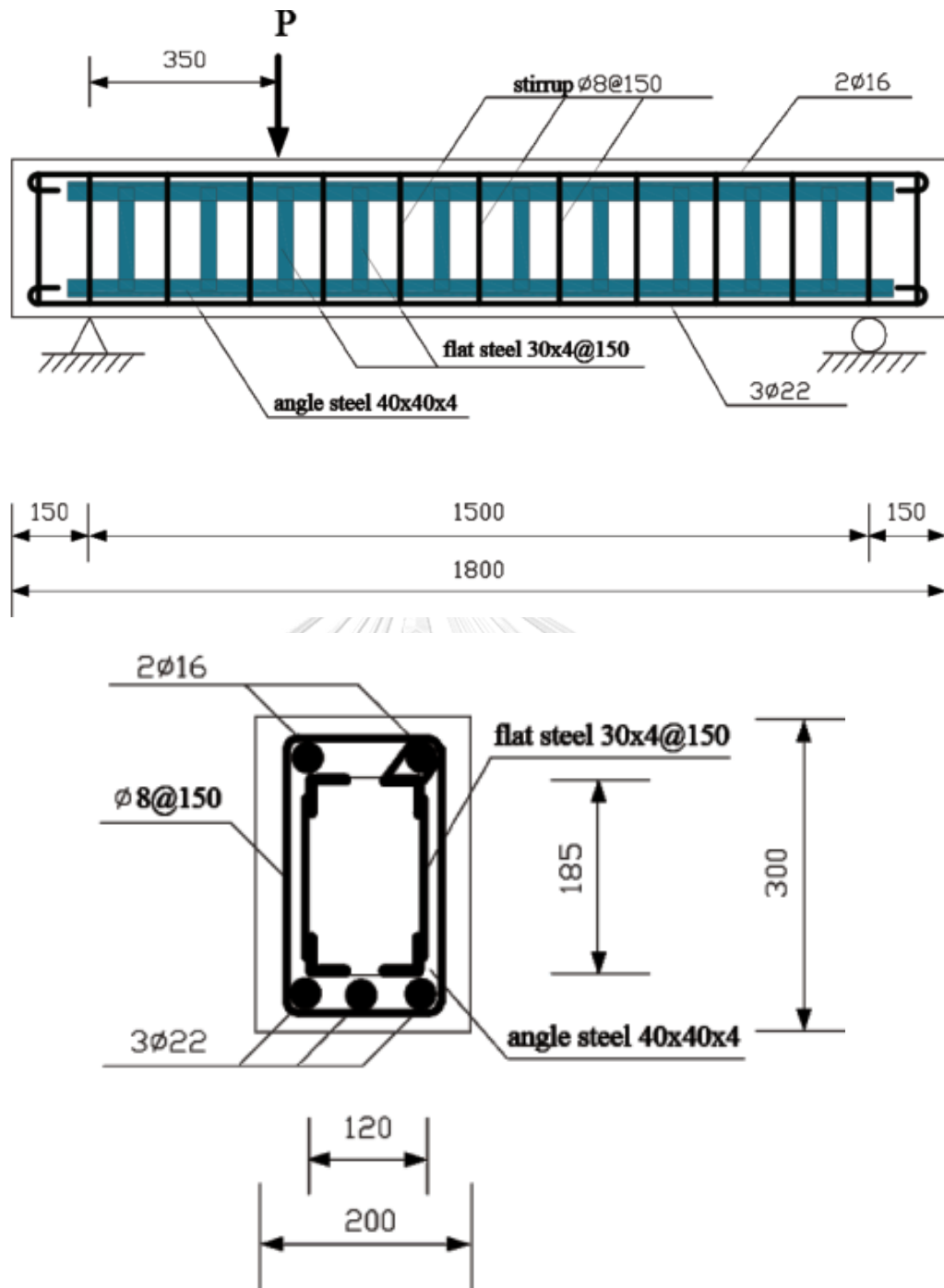


Figure 2.31 Profile and cross-section detail of SCRB3 (Zhang et al., 2016)

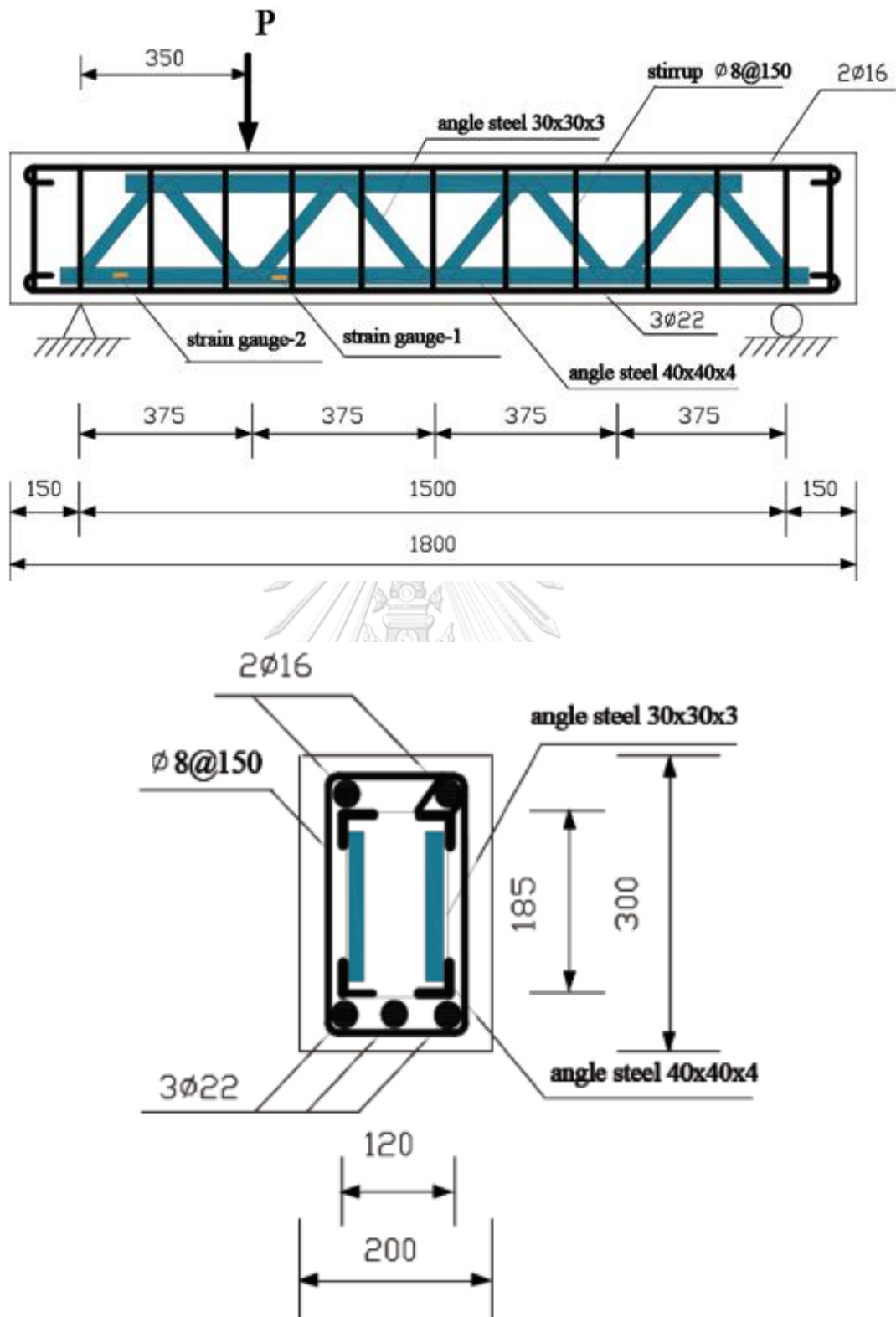


Figure 2.32 Profile and cross-section detail of SRCB4 (Zhang et al., 2016)

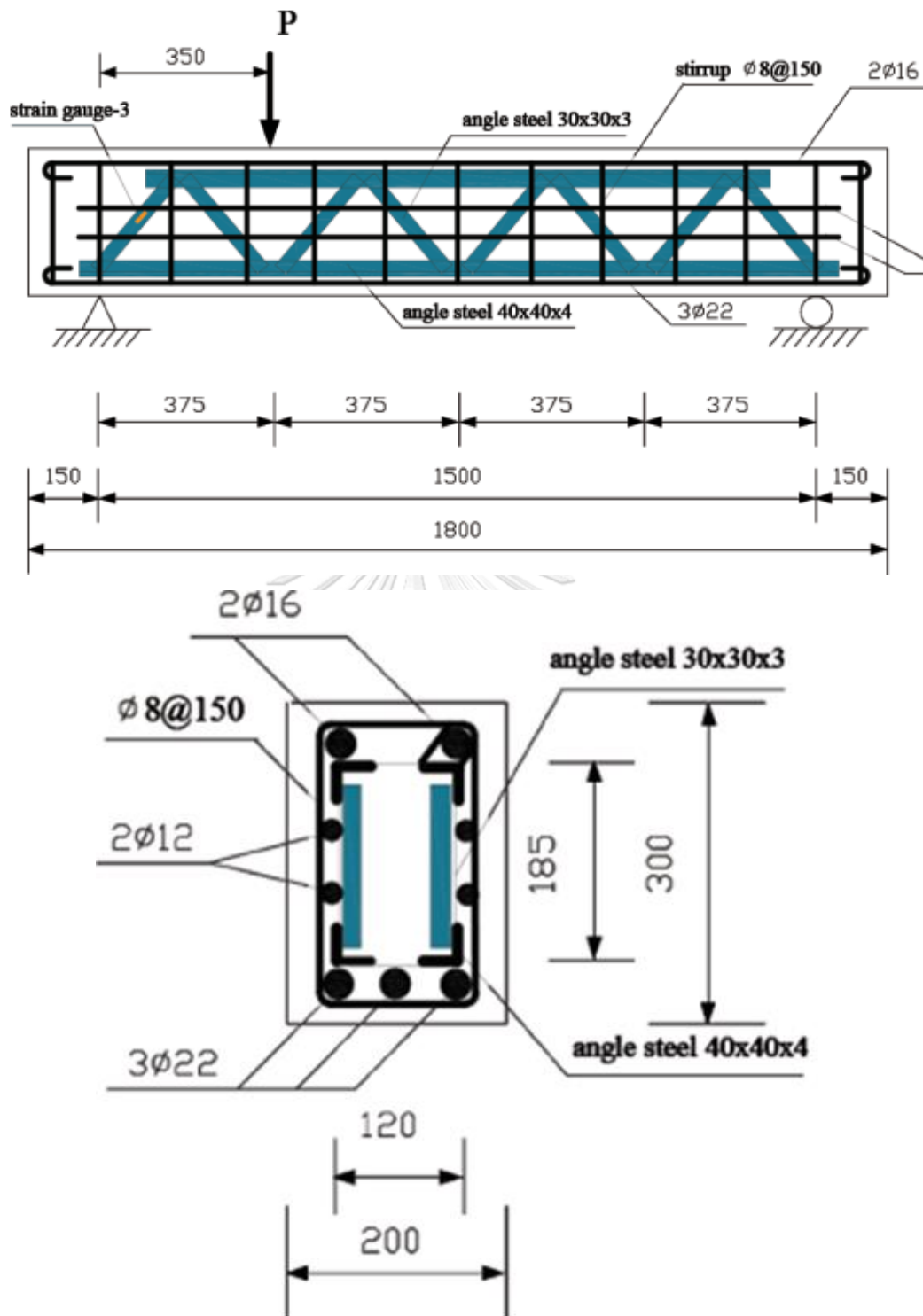


Figure 2.33 Profile and cross-section detail of SRCB5 (Zhang et al., 2016)

Table 2-5 Structural performance of test specimens (Zhang et al., 2016)

Test specimen	SRCB1	SRCB2	SRCB3	SRCB4	SRCB5
Yield load, $P_y$ (kN)	343.4	399.7	480.0	503.4	589.7
Yield load increase compared to SRCB1 (%)	—	16.4	39.8	46.6	71.7
Yield load increase compared to SRCB2 (%)	—	—	20.1	26.0	47.5
Ultimate load, $P_u$ (kN)	364.1	459.0	514.8	553.1	656.9
Ultimate load increase compared to SRCB1 (%)	—	26.0	41.3	51.9	80.4
Ultimate load increase compared to SRCB2 (%)	—	—	12.2	20.5	43.1
Elastic stiffness, $k_e$ (kN/mm)	57.73	92.65	111.76	84.85	111.57
Elastic stiffness increase compared to SRCB1 (%)	—	60.5	93.6	47.0	93.3
Elastoplastic stiffness, $k_{ep}$ (kN/mm)	4.464	6.984	29.12	13.35	26.59
Elastoplastic stiffness increase compared to SRCB1 (%)	—	56.5	552.3	199.0	495.7

The test results showed in Table 2-5, and observed that the reinforced concrete beams with embedded steel truss frame (SRCB4 and SRCB5) have shear-flexural failure, which provided ductile failure mode and better deflection stiffness. The compressive strength of concrete (SRCB4 and SRCB5) was almost entirely used in the shear compression region due to the distribution of concrete crack of reinforced concrete beams with embedded steel truss frame are relatively adequate. Therefore, the ultimate shear strength of SRCB4 and SRCB5 were improved.

The deflection development of five beam specimens under a loading process was shown in Figure 2.34. The load-deflection relationship illustrates that the deflection stiffness of these specimens at the elastic deformation stage and elastoplastic deformation stage after yielding of the steel specimens.

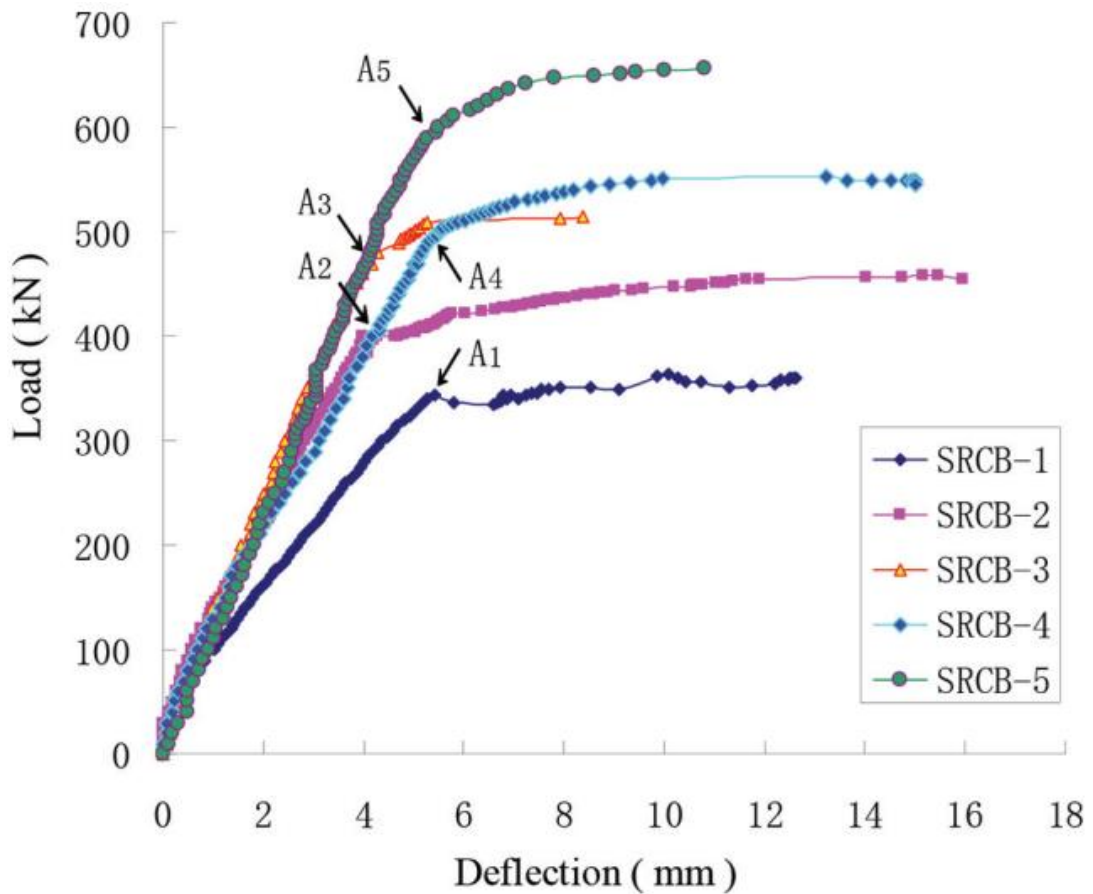


Figure 2.34 Load-deflection curve under loading point (Zhang et al., 2016)

Finally, Comparison the specimens shown in Table 2-3 and Figure 2.34 can be concluded that SRCB5 has not only the most excellent ultimate shear strength but also the best deformation stiffness of these five specimens. Compared with the conventional RC beam SRCB1, the SRCB5 improved the ultimate shear-strength, elastic deformation stiffness, and elastoplastic deformation stiffness by 80.4%, 93.3%, 495.72% respectively.

Zhang et al. (2016) was also proposed ultimate shear strength model for a reinforced concrete beam with embedded steel trusses in accordant with the test results of (SRCB-3, SRCB-4, SRCB-5). Three equations can be built based the equilibrium condition of internal-forces in the failure section at the ultimate stage as shown in Figure 2.35.



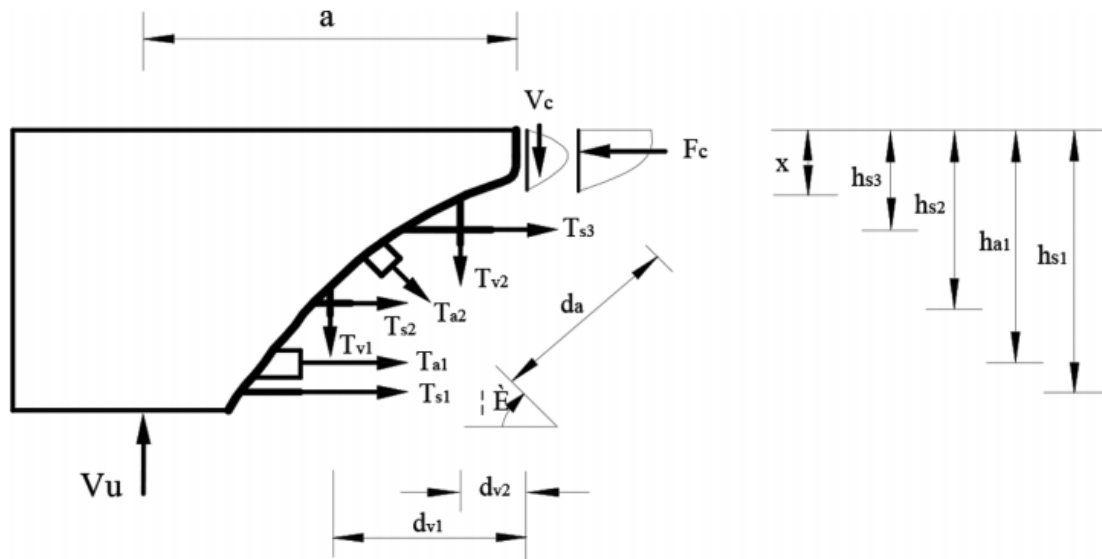


Figure 2.35 Analytical model of interior-force on the failure section  
(Zhang et al., 2016)

$$F_c = \sum_{i=1}^m T_{si} \quad (2.70)$$

$$V_y = V_c + \sum_{i=1}^n T_{vi} \quad (2.71)$$

$$V_u a = \sum_{i=1}^m T_{si} h_{si} + \sum_{i=1}^n t_{vi} d_{vi} - F_c \frac{x}{2} \quad (2.72)$$

$F_c$  = compression force of concrete in the shear-compression zone

$\sum_{i=1}^m T_{si}$  = total ultimate tensile forces of longitudinal reinforcement and steel angle

$\sum_{i=1}^n T_{vi}$  = total ultimate tensile forces of vertical stirrups and the vertical

component of steel angle

$V_c$  = shear-force carried by entire concrete along the equivalent compressive depth of the beam

$h_{si}$  = distances measure from top surface of the beam angle steel to the centroidal position of longitudinal reinforcements and angle steel

- $d_{vi}$  = distances from the centroidal position of vertical of the vertical stirrup and the vertical component the of angle steel to the loading point
- $a$  = shear-span of the beam in the shear-compression zone
- $V_u$  = ultimate shear-flexural strength of the reinforced concrete with embedded steel trusses

Figure 2.36 is shown the distribution of normal compressive stress and shear stress of the concrete in the shear-compression zone. It can be presented as follows:

$$\sigma_o = \frac{F_c}{bx} \quad (2.73)$$

$$\tau_{\max} = 1.5 \frac{V_c}{bx} \quad (2.74)$$

$\sigma_o$  = average normal compression stress;  $\tau_{\max}$  is the maximum shear stress which equals  $1.5\tau_o$ ;  $x$  is equivalent compression depth

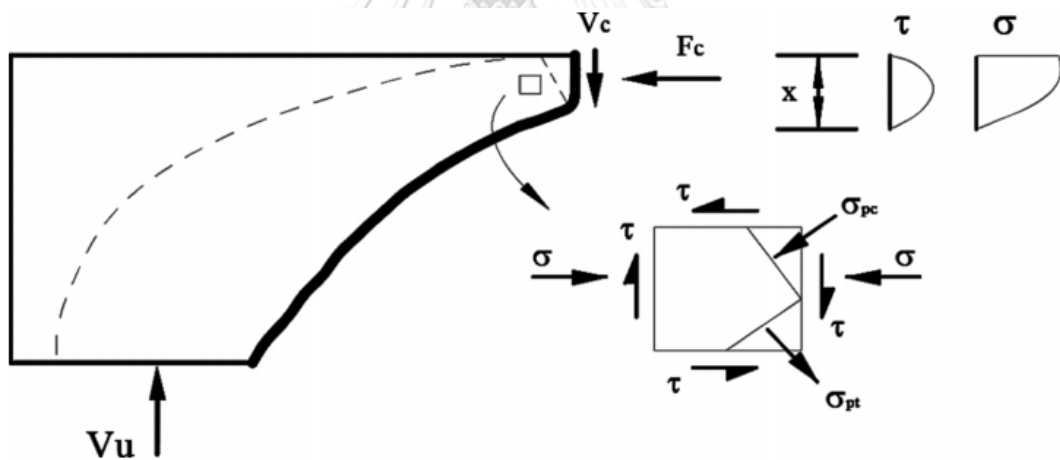


Figure 2.36 Analytical-model of stress in shear compression zone (Zhang et al., 2016).

$\sigma_{pc}$  and  $\sigma_{pt}$  are the principal compressive-stress and the principal tensile-stress obtained as follows:

$$\sigma_{pc} = \frac{\sigma_o}{2} + \sqrt{\left(\frac{\sigma_o}{2}\right)^2 + \tau_{\max}^2} \quad (2.75)$$

$$\sigma_{pc} = \nu f_c' \quad (2.76)$$

$$\nu f_c' = \frac{\sigma_0}{2} + \sqrt{\left(\frac{\sigma_0}{2}\right)^2 + \tau_{\max}^2} \quad (2.77)$$

$\nu$  = softened coefficient of compression strength of concrete; the average value may be taken as 0.6 or 0.7;  $f_c'$  is the concrete cylinder compressive-strength; The value of  $x$  compute as follows:

$$Ax^2 + Bx + C = 0 \quad (2.78)$$

$$A = \frac{\left(\sum_{i=1}^m T_{si}\right)^2}{4a^2b^2} - (\nu f_c')^2 \quad (2.79)$$

$$B = \frac{\nu f_c' \sum_{i=1}^m T_{si}}{b} - \frac{\left(\sum_{i=1}^m T_{si} h_{si} + \sum_{i=1}^n T_{vi} d_{vi} - a \sum_{i=1}^n T_{vi}\right) \sum_{i=1}^m T_{si}}{a^2b^2} \quad (2.80)$$

$$C = \frac{\left(\sum_{i=1}^m T_{si} h_{si} + \sum_{i=1}^n T_{vi} d_{vi} - a \sum_{i=1}^n T_{vi}\right)^2}{a^2b^2} \quad (2.81)$$

$$x = \frac{-B \pm \sqrt{B^2 - 4AC}}{2A} \quad (2.82)$$

The ultimate shear-flexural strength can be computed as follow, and the ultimate-load comparisons of test results and calculation are shown in the Eq. (2.83).

$$V_u = \frac{\sum_{i=1}^m T_{si} h_{si} + \sum_{i=1}^n T_{vi} d_{vi}}{a} - \frac{\sum_{i=1}^m T_{si}}{2a} x \quad (2.83)$$

Table 2-6 Comparison of the test results and calculation (Zhang et al., 2016)

Test specimen	SRCB3	SRCB4	SRCB5
Test results $P_u^T, kN$	514.83	553.10	656.89
Calculation results $P_u^c, kN$	489.50	522.21	601.51
Relative deviation $\frac{P_u^c - P_u^T}{P_u^T}, \%$	-4.9	-5.6	-8.43

### 2.5.2 Steel-truss RC transfer beam in tall buildings

Wu et al. (2011) carried out the experiment on steel truss reinforced concrete transfer beam (STRC) to apply to tall building in China. The specimens were designed as Table 2-6 and material properties of the concrete and steel showed in Table 2-7.

Table 2-7 Details of specimens (Wu et al., 2011)

Specimens	L1 (RC)	L2 (chevron)	L3 (chevron)	L4 (triangle)
Cross section (mm x mm)	200x1300	200x1300	200x1300	200x1300
Bottom rebar (ratio)	9 $\phi$ 25 (1.7%)	9 $\phi$ 25 (1.7%)	9 $\phi$ 25 (1.7%)	3 $\phi$ 20+4 $\phi$ 18+2 $\phi$ 14 (0.9%)
Top rebar (ratio)	9 $\phi$ 18 (0.9%)	9 $\phi$ 18 (0.9%)	5 $\phi$ 18+4 $\phi$ 1 4 (0.7%)	5 $\phi$ 18+4 $\phi$ 14(0.7%)
Stirrups	$\phi$ 14@100	$\phi$ 14@100	$\phi$ 10@100	$\phi$ 10@150
Web reinforcement	$\phi$ 14@100	$\phi$ 14@100	$\phi$ 10@100	$\phi$ 10@150
Steel truss	None	Chevron	Chevron	Triangle
Steel-plate Thickness (mm)	None	10	10	10

Table 2-8 Concrete and steel material (Wu et al., 2011)

Diameter of bar (mm)	Yield strength of steel $f_y$	Ultimate strength of steel $f_u$
	(MPa)	(MPa)
10	400	565
12	425	600
14	405	605
18	375	585
20	375	590
25	380	595
Steel plate (Q235)	300	450

Four STRC transfer beams were designed as L1-L4 with scale 1:4 and tested. The concrete compressive-strength of specimens L1, L2, L3, and L4 are 30.9, 39.0, 35.0 and 42.6 MPa, respectively. The five-meter-long specimens described in Figure 2.37.

The results of the experiment are illustrated as the load-deflection relationship in Figure 2.38. From the experimental investigations, Wu et al. (2011) summarized that the bearing capacity of the STRC transfer beam increased by 30-40%, and 30-50% of rigidity was improved compared with RC transfer beam. The loads were mainly transferred by compressive diagonal SRC struts and, SRC struts and horizontal ties formed a self-balanced system.

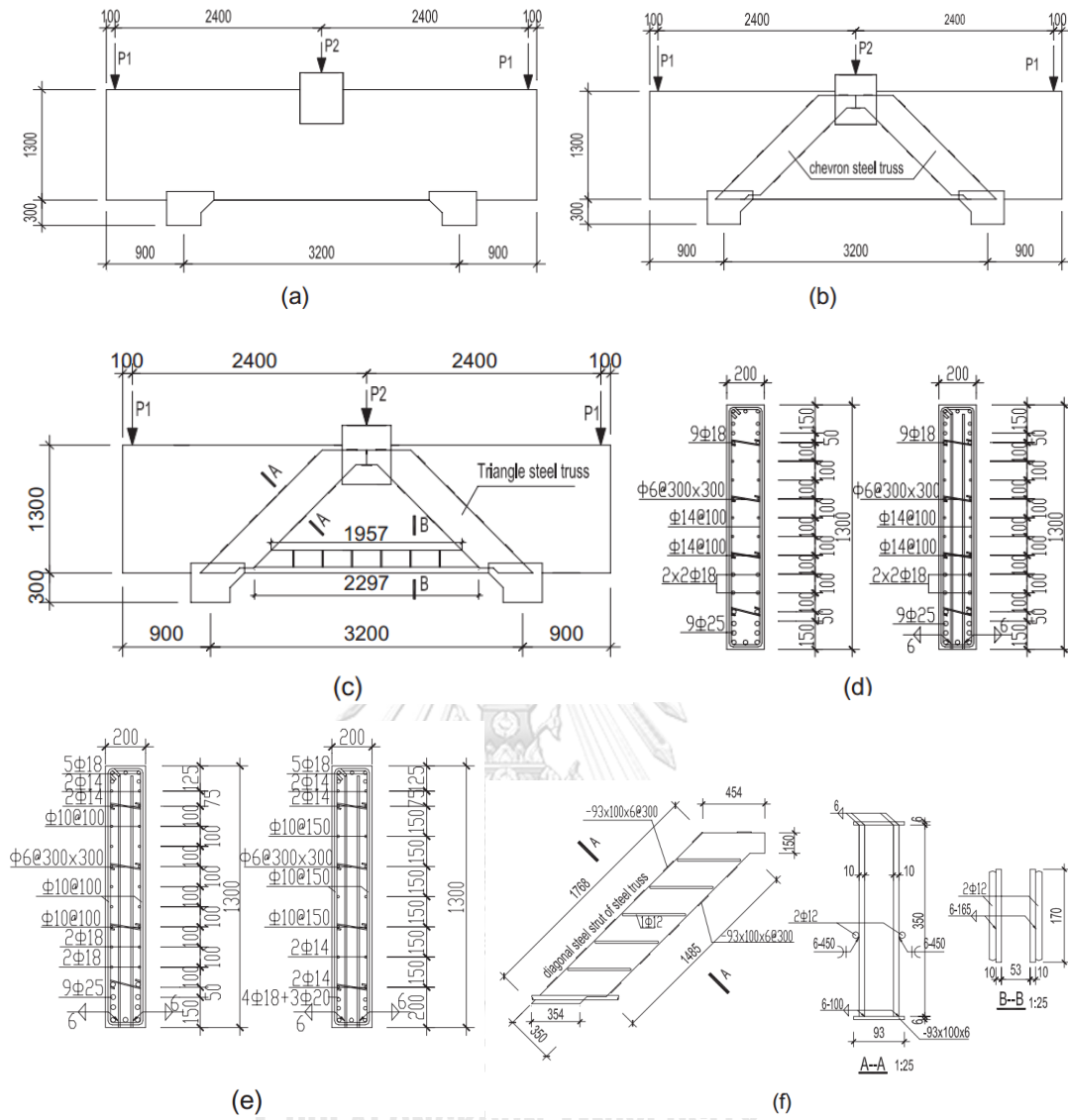


Figure 2.37 Design configuration of the specimens (mm) (Wu et al., 2011)

Note: the drawing scale is 1:100 except specially indicated: (a) Specimen L1 (RC transfer beam), (b) Specimens L2 and L3 (chevron STRC), (c) Specimen L4 (triangular STRC transfer beam), (d) Reinforcements of specimens L1 and L2, (e) Reinforcements of specimens L3 and L4, and (f) Details of one steel struts as a member of steel truss and sections A and B.

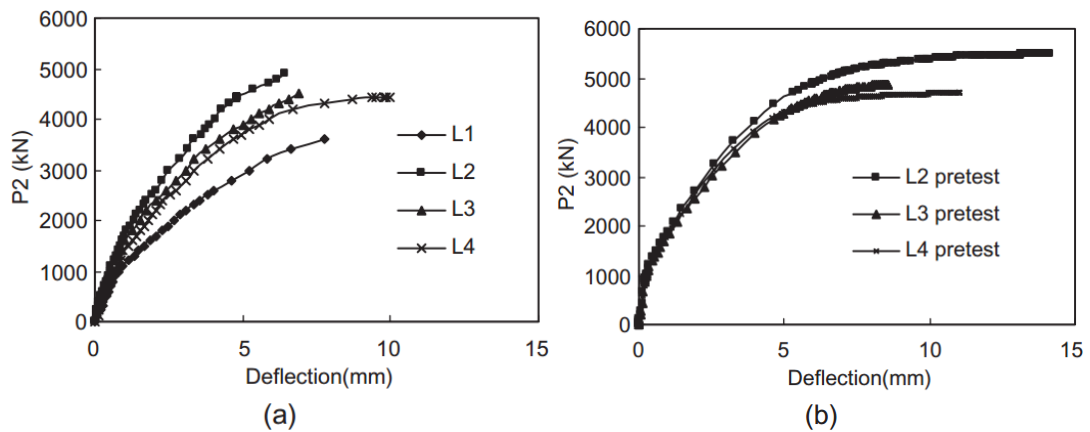


Figure 2.38 Load-deflection curves (Wu et al., 2011)

## 2.6 Previous works on finite element analysis of RC and composite beams

Mahmoud (2016), developed a three-dimensional nonlinear FEM to discover the fracture behaviors of continuous double steel-concrete composite beams (Figure 2.39) with underlining on the beam slab interface. FEM was presented by using ANSYS 11 finite element package. Concrete was modeled using Solid65 element, Link 8 element was used to model steel reinforcement, the head studs shear connectors was done the BEAM 188 elements, and SOLID185 was used to model the steel beam. TARGE170 and CONTA173 elements were used to present the slab-steel beam interface.

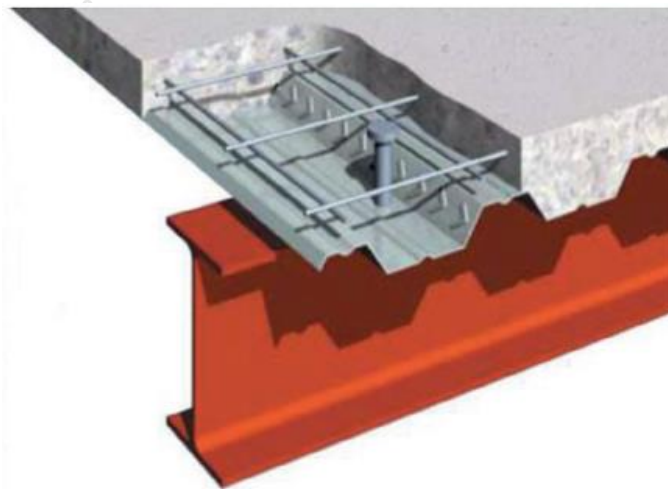


Figure 2.39 Steel-concrete composite section with studs shear connects  
(Mahmoud, 2016)

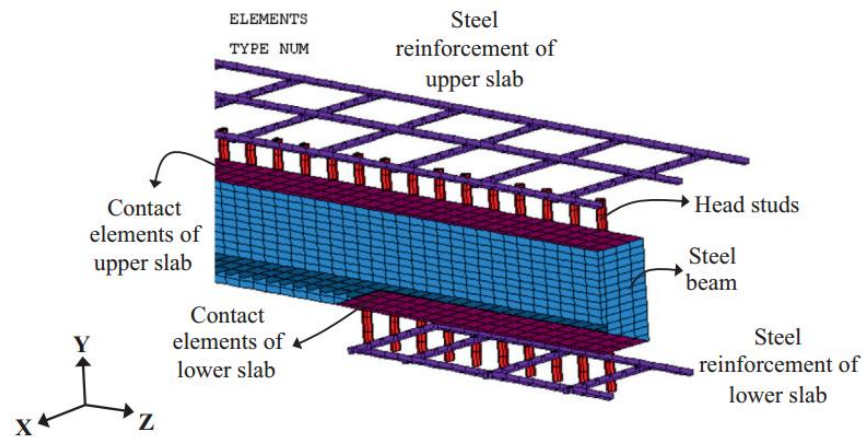


Figure 2.40 The finite element modeling of steel and contact elements  
(Mahmoud, 2016)

FE model is displayed in Figure 2.40. By comparing results with previous available experimental data, it was found that the FE analysis of steel-concrete composite beams in this study provides acceptable accuracy (Mahmoud, 2016).

Özcan et al. (2009) studied on the experimental and FE analysis on the steel fiber-reinforced concrete (SFRC) beams ultimate behavior. Three SFRC beams with 250x350x2000 (mm) were used in the study; their FE models are illustrated in Figure 2.41; the material properties of the model are shown in

Table 2-8.



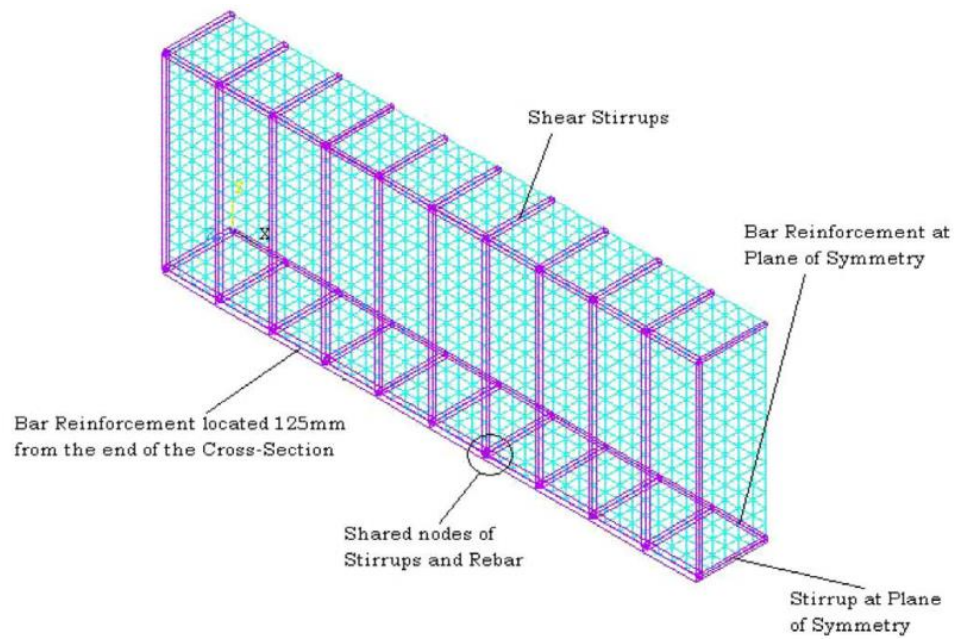


Figure 2.41 The specimen configuration (Özcan et al., 2009)

Table 2-9 Summary of material properties for SFRC beam (Özcan et al., 2009)

Beam	Concrete					Steel		
	$E_c$	$f_c$	$f_t$	$\nu$	$\beta_t$	$E_c$	$f_t$	$\nu$
	(GPa)	(MPa)	(MPa)			(GPa)	(MPa)	
	27.5	20.6	1.59	0.2	0.3	200	420	0.3

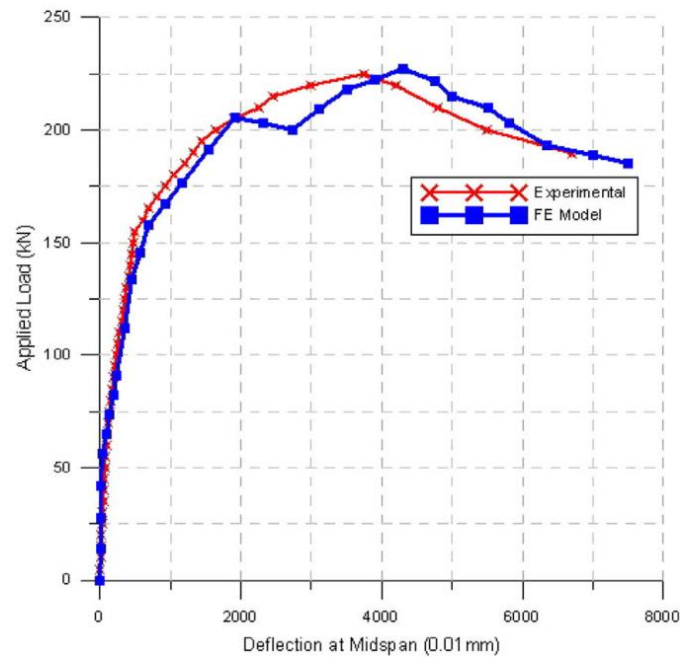


Figure 2.42 Experimental and FEM load-deflection responses (Özcan et al., 2009)

The results obtained from experiment and FE analysis were compared as shown in Figure 2.42. It demonstrated that FE failure behavior indicated a good agreement with experimental failure behavior (Özcan et al., 2009).

Vasudevan and Kothandaraman (2014) carried out the nonlinear FE analysis of RC beams with additional external bars. Models were created using ANSYS 12.0 software. Six control beams and fourteen retrofitted beams with external bars at the soffit level were studied. Dimension of specimens were 2000x250x200 mm; Solid65, Link8, and Solid45 elements were utilized to model concrete, steel rebar, and steel plate at support and loading point, respectively. The contact between external bars and the beam soffit was modeled using COMBIND39. Figure 2.43 displayed the detailed specimens; material properties of concrete and steel for FEM were described in Table 2-10. The FE model configuration was shown in Figure 2.44.

Table 2-10 Concrete and steel materials (Vasudevan and Kothandaraman, 2014)

Property	Value	Property	Value
Yield strength of hanger bars (MPa)	556	Shear transfer coefficient for open crack	0.3

Yield strength of stirrups (MPa)	550	Shear transfer coefficient for closed crack	1
Tangent modulus for steel (MPa)	20	Uniaxial crushing stress value	-1
Poisson ratio of concrete	0.2	Stiffness multiplier constant $T_c$	0.6
Poisson ratio of steel	0.3		

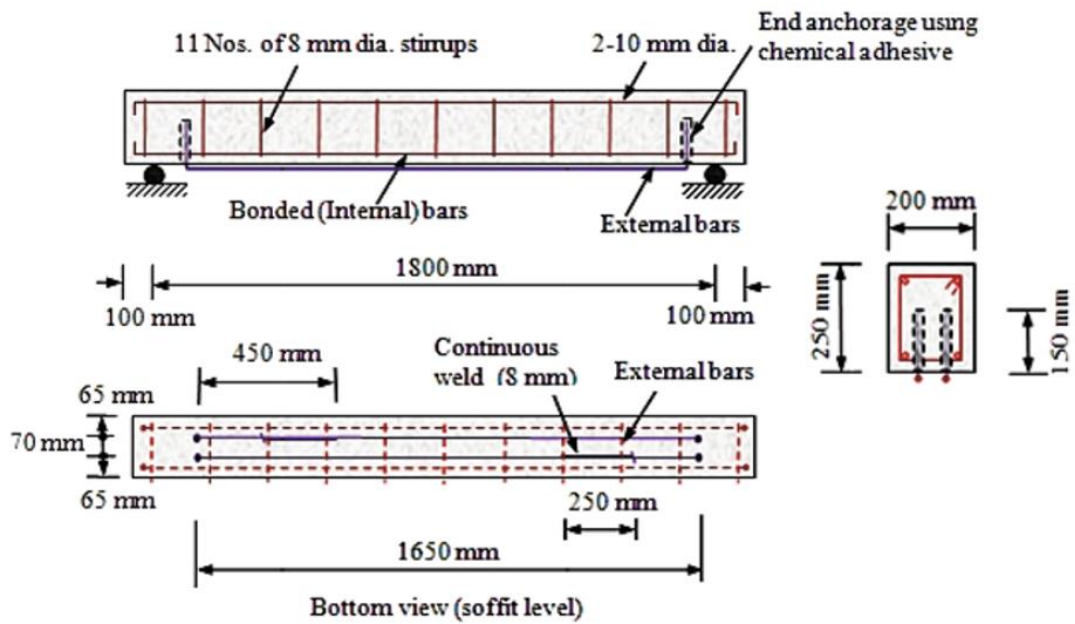


Figure 2.43 Details of the specimen (Vasudevan and Kothandaraman, 2014)

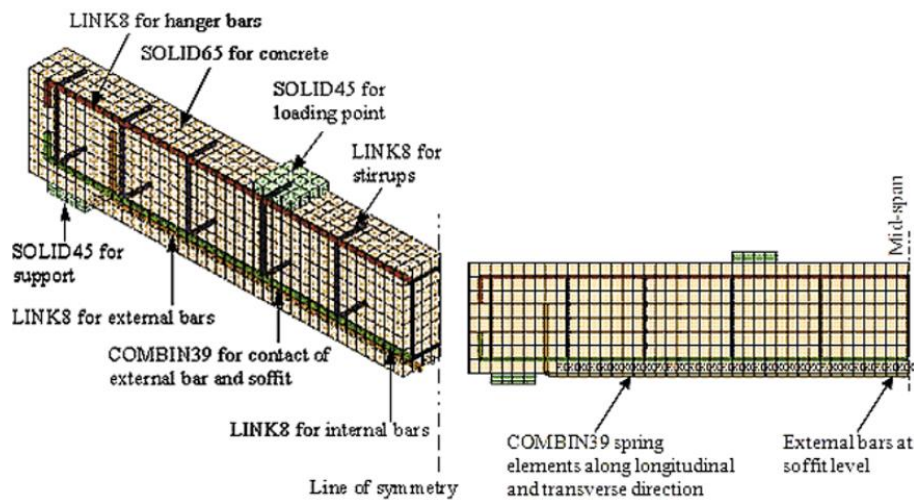


Figure 2.44 Finite element model with reinforcement

(Vasudevan and Kothandaraman, 2014)

Vasudevan and Kothandaraman (2014) presented results such as the deflected shape of the beam, strain variation along the length and depth of the beam, crack propagation at various loading stages. Figure 2.45 compares results of FEA and test, which indicates that FEA provides good agreement with the test results.

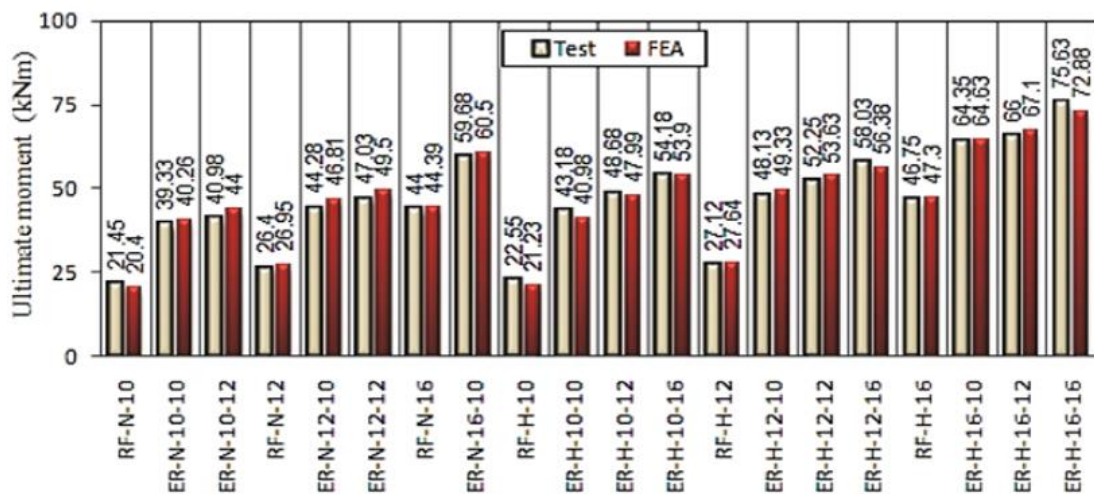


Figure 2.45 Comparison of the ultimate bending moment capacity

(Vasudevan and Kothandaraman, 2014)

Machacek and Cudejko (2009) investigated behavior of two steel and concrete composite truss girders. The experimental and numerical investigations were conducted. Details of a specimen is shown in Figure 2.46.

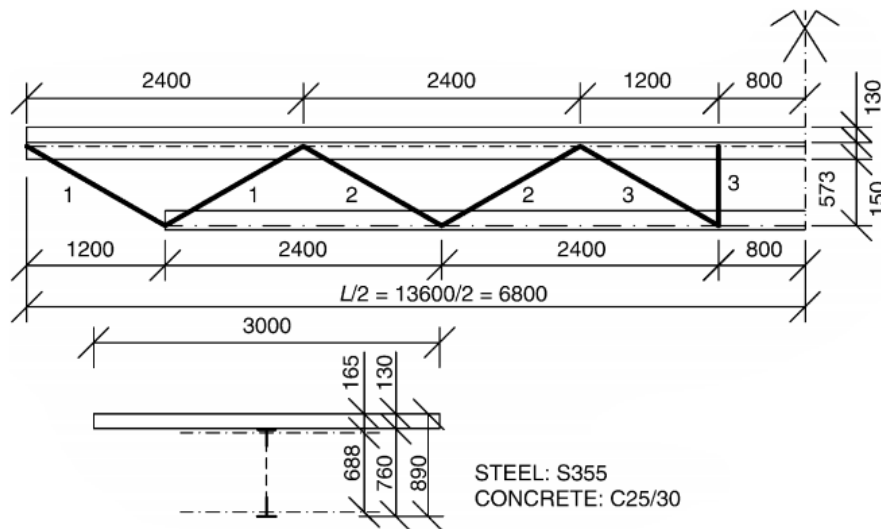


Figure 2.46 Composite truss configuration used for a basic investigation of shear flow at the steel-concrete interface (Machacek and Cudejko, 2009)

FE modeling by ANSYS software was used for simulation. Solid65 was used for the concrete slab; BEAM24 was used for bottom-chord and web bars; SHELL43 was used for upper-chord of the truss girders. Nonlinear two nodes spring element (COMBIN39) was applied to simulate nonlinear behavior. Figure 2.47 shows the FE model of truss girder and concrete slab sub-assembly.

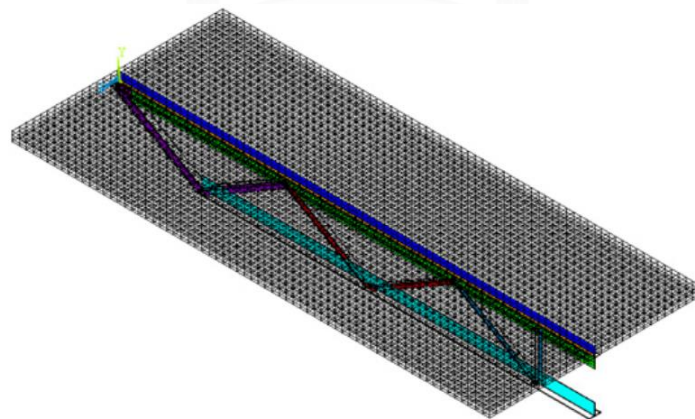


Figure 2.47 Axonometric view of FE modeling (Machacek and Cudejko, 2009)

The results of composite truss girders developed in FE model has successfully been verified by experimental results as shown in Figure 2.48.

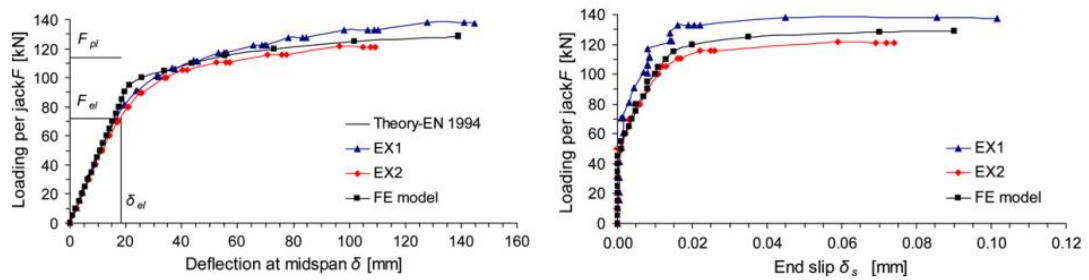


Figure 2.48 Load-deflection curves (Machacek and Cudejko, 2009)

## 2.7 Summary of literature reviews

1. RC beam reinforced with embedded steel trusses can improve strength and stiffness.
2. Steel truss embedded in the RC beam is a good alternative for improving the capacity of the beam and is practically possible for construction.
3. Finite element analysis has been utilized to study on mechanical behavior of various materials in a member such as RC, steel, composite members.
4. Many of researchers used ANSYS to develop their models.
5. Those models provide a reasonable prediction of beam strength.
6. Finite element analysis of the RC beam with embedded steel trusses has not yet been investigated.

## CHAPTER 3

### CALCULATION BY CODE METHODS

The code provisions by ACI 318-14 and AASHTO 2012 were employed to predict the shear capacity of the beams which including the conventional shear design formula and strut-and-tie model (STM).

The studied beams were shown in Table 3-1. Detail configurations of each beam referred to Figure 2.30 to Figure 2.32. Material properties referred to Table 2-3 and Table 2-4 were used in this study and restated here Table 3-2 and Table 3-3.

Table 3-1 The studied beams

Test specimens	Dimension (mm)					Remark
	Width	Height	Support Length	Total Length	a/d ratio	
SRCB1	200	300	1500	1800	1.39	No truss
SRCB2	200	300	1500	1800	1.39	No truss
SRCB3	200	300	1500	1800	1.39	With trusses
SRCB4	200	300	1500	1800	1.39	With trusses

Table 3-2 Steel properties of current studied beams

Type of steel	Size	Yield strength $f_y$	Ultimate strength $f_u$	Modulus of elasticity $E_s$
	mm	MPa	MPa	GPa
Stirrup round bar	$\phi 8$	363	465	210
Longitudinal deformed bar	$\phi 12$	405	522	200
Longitudinal deformed bar	$\phi 16$	378	472	200
Longitudinal deformed bar	$\phi 22$	393	557	200
Flat bar	30 x 4	266	363	200
Angle	40 x 40 x 4	345	519	200
Angle	30 x 30 x 3	348	522	200

Table 3-3 Concrete properties of current studied beams

Test specimen	SRCB1	SRCB2	SRCB3	SRCB4
Compressive strength, $f'_c$ MPa	41.54	41.73	44.11	40.41
Modulus of elasticity, $E_c$ GPa	34.11	34.1	34.56	33.72

The assumption and parameter for calculation were summarized as follows:

- The material properties of each beam are referred to Table 2-3 and Table 2-4
- The demand  $V_u$  and  $M_u$  were computed from the forces from the experimental study shown in Table 2-5.
- The actual ultimate tensile stress of steel and compressive strength of concrete of each beam were used the calculation.
- For the studied beams SRCB3, SRCB4 shown in Table 3-1 and details configuration shown in Figure 2.21 and Figure 2.32, the longitudinal steel truss members were assumed and treated as another longitudinal reinforcing bar. The bond slip between concrete and steel trusses were assumed to be neglected.
- The diagonal and vertical truss members were assumed as inclined and vertical reinforcing stirrups.

### 3.1 Calculation of shear strength by conventional shear strength formulas

The calculation procedure to predict shear strength by conventional shear formula illustrated in the flowchart Figure 2.21 and Figure 2.22 for ACI 318 (2014) and AASHTO LRFD (2012) respectively.

#### 3.1.1 Result of shear strength per ACI 318 and AASHTO LRFD

Shear capacity were summarized in the

Table 3-4 which displayed the maximum values of each method.



Table 3-4 Shear capacity of studied beams by conventional shear formula

STUDY BEAMS	SRCB1	SRCB2	SRCB3	SRCB4
ULTIMATE LOAD, $P_u$ (kN)	364	459	515	553
EXPERIMENTAL, $V_u$ (kN)	<b>279</b>	<b>352</b>	<b>395</b>	<b>424</b>
ACI 318-14, $V_c$ (kN)	66	66	75	72
ACI 318-14, $V_s$ (kN)	78	222	224	249
ACI 318-14, $V_n=V_c+V_s$ (kN)	<b>144</b>	<b>288</b>	<b>299</b>	<b>321</b>
ACI 318-14, $V_{max}$ (kN)	<b>267</b>	<b>269</b>	<b>277</b>	<b>265</b>
AASHTO LRFD, $V_c$ (kN)	35	30	38	35
AASHTO LRFD, $V_s$ (kN)	84	152	249	255
AASHTO LRFD, $V_n=V_c+V_s$ (kN)	<b>119</b>	<b>182</b>	<b>287</b>	<b>290</b>
AASHTO LRFD, $V_{max}$ (kN)	<b>469</b>	<b>471</b>	<b>498</b>	<b>456</b>

### 3.2 Calculation of shear strength by strut-and-tie model (STM)

The calculation procedure of STM to predict shear strength of study beams showed in flowchart Figure 2.29. The truss layout of beams for STM Figure 3.1

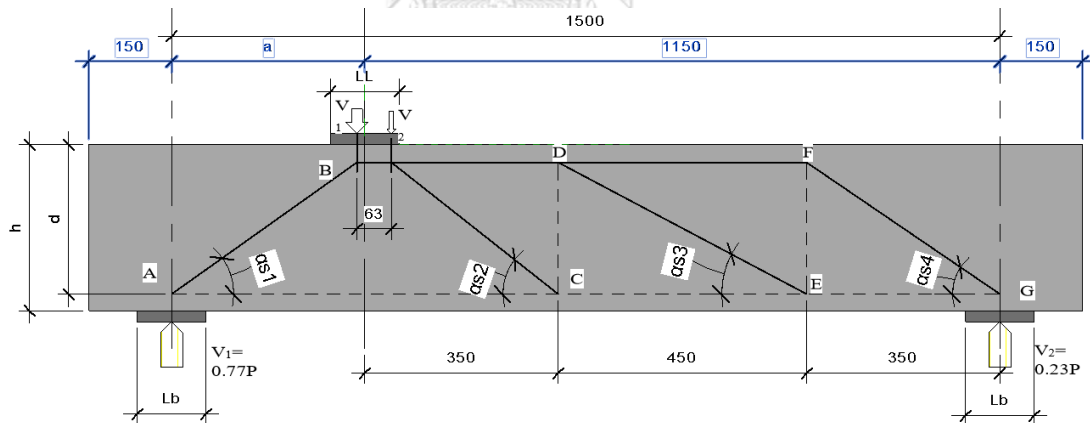


Figure 3.1 Truss layout of STM calculation

The internal forces of each element of truss in Figure 3.1 were computed as follow from Eqs. (3.1) to Eq. (3.11), which the ultimate referred to Table 3-4. Internal forces of studied beam SRCB1 were computed from Eqs. (3.1) to Eq. (3.11). Internal forces of other beams were computed in the same manner, which summarized in Table 3-5.

#### **From equilibrium at node A:**

$$\sum F_y = V_{u1} + F_{AB} \sin \alpha_{s1} = 0 \text{ implies } F_{AB} = -510 \quad (3.1)$$

$$\sum F_x = F_{AB} \cos \alpha_{s1} + F_{AC} = 0 \text{ implies } F_{AC} = -427 \quad (3.2)$$

**From equilibrium at node B:**

$$\sum F_y = -V_{u1} - F_{BC} \sin \alpha_{s2} = 0 \text{ implies } F_{BC} = -145 \quad (3.3)$$

$$\sum F_x = F_{BD} + F_{CB} \cos \alpha_{s1} + F_{AB} \cos \alpha_{s1} = 0 \text{ implies } F_{BD} = -310 \quad (3.4)$$

**From equilibrium at node C:**

$$\sum F_y = F_{CD} + F_{BC} \sin \alpha_{s2} = 0 \text{ implies } F_{CD} = 85 \quad (3.5)$$

$$\sum F_x = -F_{AC} - F_{BC} \cos \alpha_{s2} + F_{CE} = 0 \text{ implies } F_{CE} = 310 \quad (3.6)$$

**From equilibrium at node D:**

$$\sum F_y = -F_{CD} - F_{DE} \sin \alpha_{s3} = 0 \text{ implies } F_{DE} = -194 \quad (3.7)$$

$$\sum F_x = -F_{BD} + F_{DE} \cos \alpha_{s3} = 0 \text{ implies } F_{DF} = -136 \quad (3.8)$$

**From equilibrium at node E:**

$$\sum F_y = F_{EF} + F_{DE} \sin \alpha_{s3} = 0 \text{ implies } F_{EF} = 85 \quad (3.9)$$

$$\sum F_x = -F_{CE} - F_{DE} \cos \alpha_{s3} + F_{EG} = 0 \text{ implies } F_{EG} = 136 \quad (3.10)$$

**From equilibrium at node F:**

$$\sum F_y = -F_{EF} - F_{FG} \sin \alpha_{s4} = 0 \text{ implies } F_{FG} = -160 \quad (3.11)$$

Table 3-5 Summary of internal forces in truss members for STM

Member	Internal force flow (kN)			
	SRCB1	SRCB2	SRCB3	SRCB4
Ultimate load $P_u$	364	459	515	553
AB	-510	-642	-717	-777
AC	427	537	598	651
BC	-145	-182	-203	-220
BD	-310	-390	-434	-472
CD	85	107	120	129
CE	310	390	434	472
DE	-194	-244	-272	-295
DF	-136	-171	-190	-207
EF	85	107	120	129
EG	136	171	190	207
FG	-160	-201	-225	-244

### 3.2.1 ACI 318 (2014)

To compute the shear capacity by STM, first the capacity of strut, tie, and nodal capacity Figure 3.2 were determined following the procedure Figure 2.29.

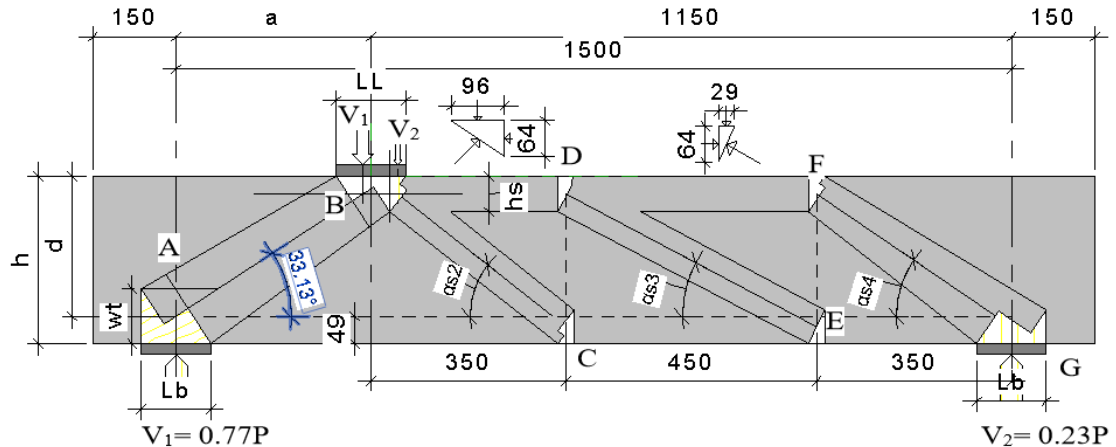


Figure 3.2 The strut, tie, and nodal zone configuration of STM

#### 3.2.1.1 SRCB1 beam

The beam detail configuration refers to Figure 2.30 and the idealized Strut, tie and nodal forces of Figure 3.2 were computed as follow:

##### ➤ Assumption and given data

Modification factor of lightweight concrete	$\lambda = 1$	
Compressive strength of concrete	$f'_c = 41.54$	MPa
Ultimate strength of stirrups	$f_u = 465$	MPa
Ultimate strength of bottom rebar	$f_u = 557$	MPa
Ultimate strength of top rebar	$f_u = 472$	MPa
Height of beam	$h = 300$	mm
Concrete cover	$c = 30$	mm
Width of beam	$b_w = 200$	mm
Effective depth of beam	$d = 251$	mm
Distance from extreme compression fiber	$d'_s = 46$	mm
Total length of beam	$L = 1800$	mm
Support to support length	$L_n = 1500$	mm
Shear reduction factor	$\phi = 1$	(to predict test results)
Distance of loading point	$a = 350$	mm
Factored point load	$P_u = 364,138$	N
Factored shear	$V_{u1} = 279,172$	N

Factored shear	$V_{u2} =$	84,966	N
Factored moment	$M_u =$	97,710,363	N.mm
Number of top rebar	2DB16	$A'_s = 402$	mm <sup>2</sup>
Number of bottom rebar	3DB22	$A_s = 1,140$	mm <sup>2</sup>
Stirrups spacing	DB8@	150	mm
Criterion of shear-span-to-depth ratio,	$a/d =$	1.394	
Length of the loading face	$ll =$	125	mm
Length of the bearing face correspond to load $l_{l1} =$		96	mm
Length of the bearing face correspond to load	$l_{l2} =$	29	mm
Length of the bearing face	$l_b =$	125	mm
Height of the back face of tension tie	$w_t =$	98	mm
Height of the back face of top compression	$h_s = \beta_1 c = \frac{(A_s f_s - A'_s f'_s)}{0.85 b_w f'_c} =$		63 mm
Distance from loading from left part Figure 3.2 $a_{left} =$		335	mm
Angle of diagonal strut,	$\alpha_{s1} = \arctan \left( \frac{d-h/2}{a_{left}} \right) =$		33.197 degree
Angle of diagonal strut,	$\alpha_{s2} =$	36	degree
Angle of diagonal strut,	$\alpha_{s3} =$	26	degree
Angle of diagonal strut,	$\alpha_{s4} =$	32	degree

### **Node A:**

#### **➤ Capacity of nodal zone**

Width of compression strut,  $w_s = l_b \sin \alpha_s + w_t \cos \alpha_s =$  150 mm

At node A is C-C-T  $\beta_n =$  0.8

The effective compressive strength of concrete

$$f_{ce(A)} = 0.85 \beta_n f'_c = 28 \text{ MPa}$$

Check stress at the base face of node A

$$f_{base(A)} = V_{u1} / b_w l_b = 11.17 \text{ MPa}$$

The nominal compressive strength of nodal zone

$$F_{nn(A)} = f_{ce(A)} A_{nz(A)} = 706,180 \text{ N}$$

$$\phi F_{nn(A)} = 706,180 \text{ N}$$

#### **➤ Capacity of compressive strut A-B from node A**

At node A is C-C-T	$\beta_s =$	0.75	
The effective compressive strength of concrete			
$f_{ce(A-B)} = 0.85\beta_s f'_c =$		26	MPa
The nominal compressive strength of strut A-B at A			
$F_{ns(A-B)} = f_{ce(A-B)} A_{cs} =$		796,812	N
$\phi F_{ns(A-B)} =$		796,812	N
Shear strength $V_{capacity} = F_{ns(A-B)} \sin \alpha_{s1} =$		<b>436,268</b>	N

### **Node B:**

#### ➤ Capacity of nodal zone

Width of compression strut,  $w_s = l_{11} \sin \alpha_s + h_s \cos \alpha_s =$  105 mm

At node B is C-C-C  $\beta_n =$  1

The effective compressive strength of concrete

$f_{ce(B)} = 0.85\beta_n f'_c =$  35 MPa

Check stress at the top face of node B

$f_{top(B)} = V_{u1} / b_w l_{11} =$  14.57 MPa

Check stress on vertical face of left part of node

$f_{top(B)} = F_{BD} / b_w h_s =$  24.55 MPa

Stress at the top face of node B was satisfied

#### ➤ Capacity of compressive strut A-B from node B

At node B is C-C-C  $\beta_s =$  1

The effective compressive strength of concrete

$f_{ce(A-B)} = 0.85\beta_s f'_c =$  35 MPa

The nominal compressive strength of strut A-B at B

$F_{ns(A-B)} = f_{ce(A-B)} A_{cs} =$  743,243 N

$\phi F_{ns(A-B)} =$  743,243 N

Shear strength  $V_{capacity} = F_{ns(A-B)} \sin \alpha_{s1} =$  **406,938** N

#### ➤ Strength of tie

$F_{nt} = A_{st} f_y =$  635,202 N

$$\phi F_{nt} = A_{st} f_y = 635,202 \quad \text{N}$$

➤ **Check provided minimum reinforcement**

$$\rho_v = \frac{A_v}{b_s w} \geq 0.0025 \quad 0.0034 \quad \text{Satisfied}$$

$$\rho_h = \frac{A_{vh}}{b_s w} \geq 0.0015 \quad - \quad \text{Not Satisfied}$$

$$\alpha_1 = 90 - \alpha_{s1} = 59 \quad \text{degree}$$

$$\alpha_2 = \alpha_{s1} = 31 \quad \text{degree}$$

$$\rho_v \sin \alpha_1 = 0.0029$$

$$\rho_{vh} \sin \alpha_2 = 0.0029$$

$$\sum \frac{A_{si}}{b_{s1}} \sin \alpha_i \geq 0.003 \quad 0.0029 \quad \text{Not Satisfied}$$

### 3.2.1.2 SRCB2 beam

The beam detail configuration refers to Figure 2.30 and the idealized Strut, tie and nodal forces of Figure 3.2 were computed as follow:

➤ **Assumption and given data**

Modification factor of lightweight concrete	$\lambda = 1$	
Compressive strength of concrete	$f'_c = 41.73$	MPa
Ultimate strength of stirrups	$f_u = 465$	MPa
Ultimate strength of bottom rebar	$f_u = 557$	MPa
Ultimate strength of top rebar	$f_u = 472$	MPa
Height of beam	$h = 300$	mm
Concrete cover	$c = 30$	mm
Width of beam	$b_w = 200$	mm
Effective depth of beam	$d = 251$	mm
Distance from extreme compression fiber	$d'_s = 46$	mm
Total length of beam	$L = 1800$	mm
Support to support length	$L_n = 1500$	mm
Shear reduction factor	$\phi = 1$	(to predict test results)
Distance of loading point	$a = 350$	mm
Factored point load	$P_u = 458,966$	N
Factored shear	$V_{u1} = 351,874$	N
Factored shear	$V_{u2} = 107,092$	N

Factored moment	$M_u = 123,155,877$	N.mm
Number of top rebar	2DB16	$A'_s = 402$ mm <sup>2</sup>
Number of bottom rebar	3DB22	$A_s = 1,140$ mm <sup>2</sup>
Stirrups spacing	DB8@	75 mm
Criterion of shear-span-to-depth ratio,	$a/d = 1.394$	
Length of the loading face	$l = 125$	mm
Length of the bearing face correspond to load	$l_{l1} = 96$	mm
Length of the bearing face correspond to load	$l_{l2} = 29$	mm
Length of the bearing face	$l_b = 125$	mm
Height of the back face of tension tie	$w_t = 98$	mm
Height of the back face of top compression	$h_s = \beta_1 c = \frac{(A_s f_s - A'_s f'_s)}{0.85 b_w f'_c}$	63 mm
Distance from loading from left part Figure 3.2	$a_{left} = 335$	mm
Angle of diagonal strut,	$\alpha_{s1} = \arctan\left(\frac{d-h/2}{a_{left}}\right) =$	33.214 degree
Angle of diagonal strut,	$\alpha_{s2} = 36$	degree
Angle of diagonal strut,	$\alpha_{s3} = 26$	degree
Angle of diagonal strut,	$\alpha_{s4} = 32$	degree

### Node A:

#### ➤ Capacity of nodal zone

$$\text{Width of compression strut, } w_s = l_b \sin \alpha_s + w_t \cos \alpha_s = 150 \text{ mm}$$

$$\text{At node A is C-C-T } \beta_n = 0.8$$

The effective compressive strength of concrete

$$f_{ce(A)} = 0.85 \beta_n f'_c = 28 \text{ MPa}$$

Check stress at the base face of node A

$$f_{base(A)} = V_{u1} / b_w l_b = 14.07 \text{ MPa}$$

The nominal compressive strength of nodal zone

$$F_{nn(A)} = f_{ce(A)} A_{nz(A)} = 709,410 \text{ N}$$

$$\phi F_{nn(A)} = 709,410 \text{ N}$$

#### ➤ Capacity of compressive strut A-B from node A

$$\text{At node A is C-C-T } \beta_s = 0.75$$

The effective compressive strength of concrete

$$f_{ce(A-B)} = 0.85\beta_s f'_c = 27 \quad \text{MPa}$$

The nominal compressive strength of strut A-B at A

$$F_{ns(A-B)} = f_{ce(A-B)} A_{cs} = 800,538 \quad \text{N}$$

$$\phi F_{ns(A-B)} = 800,538 \quad \text{N}$$

$$\text{Shear strength } V_{capacity} = F_{ns(A-B)} \sin \alpha_{s1} = 438,509 \quad \text{N}$$

### Node B:

#### ➤ Capacity of nodal zone

$$\text{Width of compression strut, } w_s = l_{l1} \sin \alpha_s + h_s \cos \alpha_s = 105 \quad \text{mm}$$

$$\text{At node B is C-C-C} \quad \beta_n = 1$$

The effective compressive strength of concrete

$$f_{ce(B)} = 0.85\beta_n f'_c = 35 \quad \text{MPa}$$

Check stress at the top face of node B

$$f_{top(B)} = V_{u1} / b_w l_{l1} = 18.36 \quad \text{MPa}$$

Check stress on vertical face of left part of node

$$f_{top(B)} = F_{BD} / b_w h_s = 31.07 \quad \text{MPa}$$

Stress at the top face of node B was satisfied

#### ➤ Capacity of compressive strut A-B from node B

$$\text{At node B is C-C-C} \quad \beta_s = 1$$

The effective compressive strength of concrete

$$f_{ce(A-B)} = 0.85\beta_s f'_c = 35 \quad \text{MPa}$$

The nominal compressive strength of strut A-B at B

$$F_{ns(A-B)} = f_{ce(A-B)} A_{cs} = 745,035 \quad \text{N}$$

$$\phi F_{ns(A-B)} = 745,035 \quad \text{N}$$

$$\text{Shear strength } V_{capacity} = F_{ns(A-B)} \sin \alpha_{s1} = 408,106 \quad \text{N}$$

#### ➤ Strength of tie

$$F_{nt} = A_{st} f_y = 635,202 \quad \text{N}$$

$$\phi F_{nt} = A_{st} f_y = 635,202 \quad \text{N}$$



➤ **Check provided minimum reinforcement**

$\rho_v = \frac{A_v}{b_s w} \geq 0.0025 =$	0.0067	Satisfied
$\rho_h = \frac{A_{vh}}{b_s w} \geq 0.0015 =$	–	Not Satisfied
$\alpha_1 = 90 - \alpha_{s1} =$	57	degree
$\alpha_2 = \alpha_{s1} =$	33	degree
$\rho_v \sin \alpha_1 =$	0.0056	
$\rho_{vh} \sin \alpha_2 =$		
$\sum \frac{A_{si}}{b_{s1}} \sin \alpha_i \geq 0.003$	0.0056	Satisfied

3.2.1.3 SRCB3 beam

The beam detail configuration refers to Figure 2.30 and the idealized Strut, tie and nodal forces of Figure 3.2 were computed as follow:

➤ **Assumption and given data**

Modification factor of lightweight concrete	$\lambda = 1$	
Compressive strength of concrete	$f'_c = 44.11$	MPa
Ultimate strength of stirrups	$f_u = 465$	MPa
Ultimate strength of bottom rebar	$f_u = 557$	MPa
Ultimate strength of top rebar	$f_u = 472$	MPa
Ultimate strength of bot-chord-truss	$f_u = 519$	MPa
Height of beam	$h = 300$	mm
Concrete cover	$c = 30$	mm
Width of beam	$b_w = 200$	mm
Effective depth of beam	$d = 251$	mm
Distance from extreme compression fiber	$d'_s = 46$	mm
Total length of beam	$L = 1800$	mm
Support to support length	$L_n = 1500$	mm
Shear reduction factor	$\phi = 1$	(to predict test results)
Distance of loading point	$a = 350$	mm
Factored point load	$P_u = 514,828$	N
Factored shear	$V_{u1} = 394,701$	N
Factored shear	$V_{u2} = 120,127$	N

Factored moment	$M_u =$	138,145,513	N.mm
Number of top rebar	2DB16	$A'_s = 402$	mm <sup>2</sup>
Number of bottom rebar	3DB22	$A_s = 1,140$	mm <sup>2</sup>
Stirrups spacing	DB8@	150	mm
Bottom chord of steel,	No: 2	$A_s = 616$	mm <sup>2</sup>
Criterion of shear-span-to-depth ratio,	$a/d =$	1.394	
Length of the loading face	$ll =$	125	mm
Length of the bearing face correspond to load	$l_{11} =$	96	mm
Length of the bearing face correspond to load	$l_{12} =$	29	mm
Length of the bearing face	$l_b =$	125	mm
Height of the back face of tension tie	$w_t =$	98	mm
Height of the back face of top compression	$h_s = \beta_1 c = \frac{(A_s f_s - A'_s f'_s)}{0.85 b_w f'_c}$		59 mm
Distance from loading from left part Figure 3.2	$a_{left} =$	335	mm
Angle of diagonal strut,	$\alpha_{s1} = \arctan\left(\frac{d-h/2}{a_{left}}\right) =$	33.42	degree
Angle of diagonal strut,	$\alpha_{s2} =$	36	degree
Angle of diagonal strut,	$\alpha_{s3} =$	26	degree
Angle of diagonal strut,	$\alpha_{s4} =$	32	degree

### **Node A:**

#### **➤ Capacity of nodal zone**

Width of compression strut,  $w_s = l_b \sin \alpha_s + w_t \cos \alpha_s =$  151 mm

At node A is C-C-T  $\beta_n =$  0.8

The effective compressive strength of concrete

$$f_{ce(A)} = 0.85 \beta_n f'_c = 30 \text{ MPa}$$

Check stress at the base face of node A

$$f_{base(A)} = V_{u1} / b_w l_b = 15.79 \text{ MPa}$$

The nominal compressive strength of nodal zone

$$F_{nn(A)} = f_{ce(A)} A_{nz(A)} = 749,870 \text{ N}$$

$$\phi F_{nn(A)} = 749,870 \text{ N}$$

#### **➤ Capacity of compressive strut A-B from node A**

At node A is C-C-T  $\beta_s =$  0.75

The effective compressive strength of concrete

$$f_{ce(A-B)} = 0.85\beta_s f'_c = 28 \quad \text{MPa}$$

The nominal compressive strength of strut A-B at A

$$F_{ns(A-B)} = f_{ce(A-B)} A_{cs} = 847,199 \quad \text{N}$$

$$\phi F_{ns(A-B)} = 847,199 \quad \text{N}$$

$$\text{Shear strength } V_{capacity} = F_{ns(A-B)} \sin \alpha_{s1} = 466,565 \quad \text{N}$$

### **Node B:**

#### **➤ Capacity of nodal zone**

$$\text{Width of compression strut, } w_s = l_{l1} \sin \alpha_s + h_s \cos \alpha_s = 102 \quad \text{mm}$$

$$\text{At node B is C-C-C} \quad \beta_n = 1$$

The effective compressive strength of concrete

$$f_{ce(B)} = 0.85\beta_n f'_c = 37 \quad \text{MPa}$$

Check stress at the top face of node B

$$f_{top(B)} = V_{u1} / b_w l_{l1} = 20.59 \quad \text{MPa}$$

Check stress on vertical face of left part of node

$$f_{top(B)} = F_{BD} / b_w h_s = 36.56 \quad \text{MPa}$$

Stress at the top face of node B was satisfied

#### **➤ Capacity of compressive strut A-B from node B**

$$\text{At node B is C-C-C} \quad \beta_s = 1$$

The effective compressive strength of concrete

$$f_{ce(A-B)} = 0.85\beta_s f'_c = 37 \quad \text{MPa}$$

The nominal compressive strength of strut A-B at B

$$F_{ns(A-B)} = f_{ce(A-B)} A_{cs} = 767,529 \quad \text{N}$$

$$\phi F_{ns(A-B)} = 767,529 \quad \text{N}$$

$$\text{Shear strength } V_{capacity} = F_{ns(A-B)} \sin \alpha_{s1} = 422,690 \quad \text{N}$$

#### **➤ Strength of tie**

$$F_{nt} = A_{st} f_y = 906,950 \quad \text{N}$$

$$\phi F_{nt} = A_{st} f_y = 906,950 \quad \text{N}$$

➤ **Check provided minimum reinforcement**

$\rho_v = \frac{A_v}{b_s w} \geq 0.0025 =$	0.0034	Satisfied
$\rho_h = \frac{A_{vh}}{b_s w} \geq 0.0015 =$	–	Not Satisfied
$\alpha_1 = 90 - \alpha_{s1} =$	57	degree
$\alpha_2 = \alpha_{s1} =$	33	degree
$\rho_v \sin \alpha_1 =$	0.0028	
$\rho_{vh} \sin \alpha_2 =$		
$\sum \frac{A_{si}}{b_{s1}} \sin \alpha_i \geq 0.003 =$	0.0028	Not Satisfied

### 3.2.1.4 SRCB4 beam

The beam detail configuration refers to Figure 2.32 and the idealized Strut, tie and nodal forces of Figure 3.2 were computed as follow:

➤ **Assumption and given data**

Modification factor of lightweight concrete	$\lambda = 1$	
Compressive strength of concrete	$f'_c = 40.41$	MPa
Ultimate strength of stirrups	$f_u = 465$	MPa
Ultimate strength of bottom rebar	$f_u = 557$	MPa
Ultimate strength of top rebar	$f_u = 472$	MPa
Ultimate strength of bot-chord-truss	$f_u = 519$	MPa
Height of beam	$h = 300$	mm
Concrete cover	$c = 30$	mm
Width of beam	$b_w = 200$	mm
Effective depth of beam	$d = 251$	mm
Distance from extreme compression fiber	$d'_s = 46$	mm
Total length of beam	$L = 1800$	mm
Support to support length	$L_n = 1500$	mm
Shear reduction factor	$\phi = 1$	(to predict test results)
Distance of loading point	$a = 350$	mm
Factored point load	$P_u = 553,103$	N
Factored shear	$V_{u1} = 424,046$	N

Factored shear	$V_{u2} = 129,057$	N
Factored moment	$M_u = 148,415,972$	N.mm
Number of top rebar	2DB16	$A_s' = 402$ mm <sup>2</sup>
Number of bottom rebar	3DB22	$A_s = 1,140$ mm <sup>2</sup>
Stirrups spacing	DB8@	150 mm
Bottom chord of steel,	No: 2	$A_s = 616$ mm <sup>2</sup>
Criterion of shear-span-to-depth ratio,	$a/d = 1.394$	
Length of the loading face	$l_l = 125$	mm
Length of the bearing face correspond to load	$l_{l1} = 96$	mm
Length of the bearing face correspond to load	$l_{l2} = 29$	mm
Length of the bearing face	$l_b = 125$	mm
Height of the back face of tension tie	$w_t = 98$	mm
Height of the back face of top compression	$h_s = \beta_1 c = \frac{(A_s f_s - A_s' f_s')}{0.85 b_w f_c}$	65 mm
Distance from loading from left part Figure 3.2	$a_{left} = 335$	mm
Angle of diagonal strut,	$\alpha_{s1} = \arctan\left(\frac{d-h/2}{a_{left}}\right)$	33.09 degree
Angle of diagonal strut,	$\alpha_{s2} = 36$	degree
Angle of diagonal strut,	$\alpha_{s3} = 26$	degree
Angle of diagonal strut,	$\alpha_{s4} = 32$	degree

### Node A:

#### ➤ Capacity of nodal zone

Width of compression strut,  $w_s = l_b \sin \alpha_s + w_t \cos \alpha_s = 150$  mm

At node A is C-C-T  $\beta_n = 0.8$

The effective compressive strength of concrete

$$f_{ce(A)} = 0.85 \beta_n f_c' = 27 \text{ MPa}$$

Check stress at the base face of node A

$$f_{base(A)} = V_{u1} / b_w l_b = 16.96 \text{ MPa}$$

The nominal compressive strength of nodal zone

$$F_{nn(A)} = f_{ce(A)} A_{nz(A)} = 686,970 \text{ N}$$

$$\phi F_{nn(A)} = 686,970 \text{ N}$$

#### ➤ Capacity of compressive strut A-B from node A

At node A is C-C-T  $\beta_s = 0.75$

The effective compressive strength of concrete

$$f_{ce(A-B)} = 0.85\beta_s f'_c = 25.76 \quad \text{MPa}$$

The nominal compressive strength of strut A-B at A

$$F_{ns(A-B)} = f_{ce(A-B)} A_{cs} = 774,651 \quad \text{N}$$

$$\phi F_{ns(A-B)} = 774,651 \quad \text{N}$$

$$\text{Shear strength } V_{capacity} = F_{ns(A-B)} \sin \alpha_{s1} = 422,934 \quad \text{N}$$

### **Node B:**

#### **➤ Capacity of nodal zone**

$$\text{Width of compression strut, } w_s = l_{l1} \sin \alpha_s + h_s \cos \alpha_s = 107 \quad \text{mm}$$

$$\text{At node B is C-C-C} \quad \beta_n = 1$$

The effective compressive strength of concrete

$$f_{ce(B)} = 0.85\beta_n f'_c = 34.35 \quad \text{MPa}$$

Check stress at the top face of node B

$$f_{top(B)} = V_{u1} / b_w l_{l1} = 22.12 \quad \text{MPa}$$

Check stress on vertical face of left part of node

$$f_{top(B)} = F_{BD} / b_w h_s = 36.43 \quad \text{MPa}$$

Stress at the top face of node B was satisfied

#### **➤ Capacity of compressive strut A-B from node B**

$$\text{At node B is C-C-C} \quad \beta_s = 1$$

The effective compressive strength of concrete

$$f_{ce(A-B)} = 0.85\beta_s f'_c = 34.35 \quad \text{MPa}$$

The nominal compressive strength of strut A-B at B

$$F_{ns(A-B)} = f_{ce(A-B)} A_{cs} = 774,651 \quad \text{N}$$

$$\phi F_{ns(A-B)} = 774,651 \quad \text{N}$$

$$\text{Shear strength } V_{capacity} = F_{ns(A-B)} \sin \alpha_{s1} = 400,000 \quad \text{N}$$

#### **➤ Strength of tie**

$$F_{nt} = A_{st} f_y = 906,950 \quad \text{N}$$

$$\phi F_{nt} = A_{st} f_y = 906,950 \quad \text{N}$$

➤ **Check provided minimum reinforcement**

$\rho_v = \frac{A_v}{b_s w} \geq 0.0025 =$	0.0034	Satisfied
$\rho_h = \frac{A_{vh}}{b_s w} \geq 0.0015 =$	–	Not Satisfied
$\alpha_1 = 90 - \alpha_{s1} =$	57	degree
$\alpha_2 = \alpha_{s1} =$	33	degree
$\rho_v \sin \alpha_1 =$	0.0028	
$\rho_{vh} \sin \alpha_2 =$		
$\sum \frac{A_{si}}{b_{s1}} \sin \alpha_i \geq 0.003 =$	0.0028	Not Satisfied

### 3.2.2 AASHTO LRFD (2012)

#### 3.2.2.1 SRCB1 beam

The beam detail configuration refers to Figure 2.30 and the idealized Strut, tie and nodal forces of Figure 3.2 were computed as follow:

#### Assumption and given data

Modification factor of lightweight concrete	$\lambda = 1$	
Compressive strength of concrete	$f'_c = 41.54$	MPa
Young's modulus of bottom rebar	$E_s = 200,000$	MPa
Ultimate strength of stirrups	$f_u = 465$	MPa
Ultimate strength of bottom rebar	$f_u = 557$	MPa
Ultimate strength of top rebar	$f_u = 472$	MPa
Height of beam	$h = 300$	mm
Concrete cover	$c = 30$	mm
Width of beam	$b_w = 200$	mm
Effective depth of beam	$d = 251$	mm
Distance from extreme compression fiber	$d'_s = 46$	mm
Total length of beam	$L = 1800$	mm
Support to support length	$L_n = 1500$	mm
Shear reduction factor	$\phi = 1$	(to predict test results)
Distance of loading point	$a = 350$	mm

Factored point load	$P_u =$	364,138	N
Factored shear	$V_{u1} =$	279,172	N
Factored shear	$V_{u2} =$	84,966	N
Factored moment	$M_u =$	97,710,363	N.mm
Number of top rebar	2DB16	$A'_s = 402$	mm <sup>2</sup>
Number of bottom rebar	3DB22	$A_s = 1,140$	mm <sup>2</sup>
Stirrups spacing	DB8@	150	mm
Criterion of shear-span-to-depth ratio,	$a/d =$	1.394	
Length of the loading face	$ll =$	125	mm
Length of the bearing face correspond to load	$l_{11} =$	96	mm
Length of the bearing face correspond to load	$l_{12} =$	29	mm
Length of the bearing face	$l_b =$	125	mm
Height of the back face of tension tie	$w_t =$	98	mm
Height of the back face of top compression	$h_s = \beta_1 c = \frac{(A_s f_s - A'_s f'_s)}{0.85 b_w f'_c} =$	63	mm
Distance from loading from left part Figure 3.2	$a_{left} =$	335	mm
Angle of diagonal strut,	$\alpha_{s1} = \arctan\left(\frac{d-h/2}{a_{left}}\right) =$	33.197	degree
Angle of diagonal strut,	$\alpha_{s2} =$	36	degree
Angle of diagonal strut,	$\alpha_{s3} =$	26	degree
Angle of diagonal strut,	$\alpha_{s4} =$	32	degree

➤ **Strength of tie**

Nominal strength of tie

$$P_n = A_{st} f_y = 635,202 \quad \text{N}$$

$$\phi P_n = A_{st} f_y = 635,202 \quad \text{N}$$

$$F_{AC} = 426,671 \quad \text{N}$$

➤ **Capacity of nodal zone**

$$f_s = \frac{F_{AC}}{A_s} = 187 \quad \text{MPa}$$

Note: only half of tension force  $F_{AC}$ , assumed the strain varies over the width of the strut.

$$\varepsilon_s = \frac{f_s}{E_s} = 0.0009$$



$$\varepsilon_1 = \varepsilon_s + (\varepsilon_s + 0.002) \cot^2 \alpha_{s1} = 0.0078$$

$$f_{cu} = \frac{f'_c}{0.8 + 170\varepsilon_1} \leq 0.85 f'_c = 19.6 \quad \text{MPa}$$

$$f_{cu} = 0.85 f'_c = 35.3 \quad \text{MPa}$$

### The nominal compressive strength from node A

Width of compression strut,  $w_s = l_b \sin \alpha_s + w_t \cos \alpha_s = 150 \quad \text{mm}$

$$P_{n(A)} = f_{cu(A)} A_{cs(A)} = 588,295 \quad \text{N}$$

$$\phi P_{n(A)} = 588,295 \quad \text{N}$$

Shear strength  $V_{capacity} = P_{n(A)} \sin \alpha_{s1} = 322,101 \quad \text{N}$

### The nominal compressive strength from node B

Width of compression strut,  $w_s = l_{11} \sin \alpha_s + h_t \cos \alpha_s = 105 \quad \text{mm}$

$$P_{n(B)} = f_{cu(B)} A_{cs(B)} = 743.243 \quad \text{N}$$

$$\phi P_{n(B)} = 743.243 \quad \text{N}$$

Shear strength  $V_{capacity} = P_{n(B)} \sin \alpha_{s1} = 406,938 \quad \text{N}$

### ➤ Capacity of nodal zone

Check stress at the base face of the node A

$$f_{base(A)} = V_{u1} / b_w l_b = 11.17 \quad \text{MPa}$$

Check stress at the base face of the node B

$$f_{top(B)} = V_{u1} / b_w l_{11} = 14.57 \quad \text{MPa}$$

Check stress at vertical face of left part of node B

$$f_{vertical(B)} = F_{BD} / b_w h_s = 22.55 \quad \text{MPa}$$

Limiting concrete compressive stress at the node

$$f_{cu(C-C-C)} = 0.85 \phi f'_c = 35.31 \quad \text{MPa}$$

$$f_{cu(C-C-T)} = 0.75 \phi f'_c = 31.16 \quad \text{MPa}$$

$$f_{cu(C-T-T)} = 0.65 \phi f'_c = 27.00 \quad \text{MPa}$$

### ➤ Check provided minimum reinforcement

$\rho_v = \frac{A_v}{b_s w} \geq 0.003 =$	0.0034	Satisfied
$\rho_h = \frac{A_{vh}}{b_s w} \geq 0.003 =$	-	Not Satisfied
$\alpha_2 = 90 - \alpha_{s1} =$	57	degree
$\alpha_2 = \alpha_{s1} =$	33	degree
$\rho_v \sin \alpha_1 =$	0.0028	
$\rho_{vh} \sin \alpha_2 =$		
$\sum \frac{A_{si}}{b_{s1}} \sin \alpha_i \geq 0.003$	0.0028	Not Satisfied

### 3.2.2.2 SRCB2 beam

The beam detail configuration refers to Figure 2.30 and the idealized Strut, tie and nodal forces of Figure 3.2 were computed as follow:

#### Assumption and given data

Modification factor of lightweight concrete	$\lambda = 1$	
Compressive strength of concrete	$f'_c = 41.73$	MPa
Young's modulus of bottom rebar	$E_s = 200,000$	MPa
Ultimate strength of stirrups	$f_u = 465$	MPa
Ultimate strength of bottom rebar	$f_u = 557$	MPa
Ultimate strength of top rebar	$f_u = 472$	MPa
Height of beam	$h = 300$	mm
Concrete cover	$c = 30$	mm
Width of beam	$b_w = 200$	mm
Effective depth of beam	$d = 251$	mm
Distance from extreme compression fiber	$d'_s = 46$	mm
Total length of beam	$L = 1800$	mm
Support to support length	$L_n = 1500$	mm
Shear reduction factor	$\phi = 1$	(to predict test results)
Distance of loading point	$a = 350$	mm
Factored point load	$P_u = 458,966$	N
Factored shear	$V_{u1} = 351,874$	N
Factored shear	$V_{u2} = 107,092$	N
Factored moment	$M_u = 123,155,877$	N.mm

Number of top rebar	2DB16	$A'_s = 402$	$\text{mm}^2$
Number of bottom rebar	3DB22	$A_s = 1,140$	$\text{mm}^2$
Stirrups spacing	DB8@	75	mm
Criterion of shear-span-to-depth ratio,	$a/d =$	1.394	
Length of the loading face	$l =$	125	Mm
Length of the bearing face correspond to load	$l_{11} =$	96	mm
Length of the bearing face correspond to load	$l_{12} =$	29	mm
Length of the bearing face	$l_b =$	125	mm
Height of the back face of tension tie	$w_t =$	98	mm
Height of the back face of top compression	$h_s = \beta_1 c = \frac{(A_s f_s - A'_s f'_s)}{0.85 b_w f'_c} =$		63 mm
Distance from loading from left part Figure 3.2	$a_{left} =$	335	mm
Angle of diagonal strut,	$\alpha_{s1} = \arctan\left(\frac{d-h/2}{a_{left}}\right) =$		33.21 degree
Angle of diagonal strut,	$\alpha_{s2} =$	36	degree
Angle of diagonal strut,	$\alpha_{s3} =$	26	degree
Angle of diagonal strut,	$\alpha_{s4} =$	32	degree

➤ **Strength of tie**

Nominal strength of tie

$$P_n = A_{st} f_y = 635,202 \quad \text{N}$$

$$\phi P_n = A_{st} f_y = 635,202 \quad \text{N}$$

$$F_{AC} = 537,433 \quad \text{N}$$

➤ **Capacity of nodal zone**

$$f_s = \frac{F_{AC}}{A_s} = 236 \quad \text{MPa}$$

Note: only half of tension force  $F_{AC}$ , assumed the strain varies over the width of the strut.

$$\varepsilon_s = \frac{f_s}{E_s} = 0.0012$$

$$\varepsilon_1 = \varepsilon_s + (\varepsilon_s + 0.002) \cot^2 \alpha_{s1} = 0.0086$$

$$f_{cu} = \frac{f'_c}{0.8 + 170\varepsilon_1} \leq 0.85 f'_c = 18.46 \quad \text{MPa}$$

$$f_{cu} = 0.85 f'_c = 35.5 \quad \text{MPa}$$

**The nominal compressive strength from node A**

$$\text{Width of compression strut, } w_s = l_b \sin \alpha_s + w_t \cos \alpha_s = 150 \quad \text{mm}$$

$$P_{n(A)} = f_{cu(A)} A_{cs(A)} = 555,476 \quad \text{N}$$

$$\phi P_{n(A)} = 555,476 \quad \text{N}$$

$$\text{Shear strength } V_{capacity} = P_{n(A)} \sin \alpha_{s1} = 304,272 \quad \text{N}$$

**The nominal compressive strength from node B**

$$\text{Width of compression strut, } w_s = l_{l1} \sin \alpha_s + h_t \cos \alpha_s = 105 \quad \text{mm}$$

$$P_{n(B)} = f_{cu(B)} A_{cs(B)} = 745,035 \quad \text{N}$$

$$\phi P_{n(B)} = 745,035 \quad \text{N}$$

$$\text{Shear strength } V_{capacity} = P_{n(B)} \sin \alpha_{s1} = 408,106 \quad \text{N}$$

**➤ Capacity of nodal zone**

Check stress at the base face of the node A

$$f_{base(A)} = V_{u1} / b_w l_b = 14.07 \quad \text{MPa}$$

Check stress at the base face of the node B

$$f_{top(B)} = V_{u1} / b_w l_{l1} = 18.36 \quad \text{MPa}$$

Check stress at vertical face of left part of node B

$$f_{vertical(B)} = F_{BD} / b_w h_s = 31.07 \quad \text{MPa}$$

Limiting concrete compressive stress at the node

$$f_{cu(C-C-C)} = 0.85 \phi f'_c = 35.47 \quad \text{MPa}$$

$$f_{cu(C-C-T)} = 0.75 \phi f'_c = 31.30 \quad \text{MPa}$$

$$f_{cu(C-T-T)} = 0.65 \phi f'_c = 27.12 \quad \text{MPa}$$

**➤ Check provided minimum reinforcement**

$$\rho_v = \frac{A_v}{b_s w} \geq 0.003 = 0.0067 \quad \text{Satisfied}$$

$$\rho_h = \frac{A_{vh}}{b_s w} \geq 0.003 = - \quad \text{Not Satisfied}$$

$$\alpha_2 = 90 - \alpha_{s1} = 57 \quad \text{degree}$$

$$\alpha_2 = \alpha_{s1} = 33 \quad \text{degree}$$

$$\rho_v \sin \alpha_1 = 0.0056$$

$$\rho_{vh} \sin \alpha_2 =$$

$$\sum \frac{A_{si}}{bs_1} \sin \alpha_i \geq 0.003 = 0.0056 \quad \text{Satisfied}$$

### 3.2.2.3 SRCB3 beam

The beam detail configuration refers to Figure 2.31 and the idealized Strut, tie and nodal forces of Figure 3.2 were computed as follow:

#### ➤ Assumption and given data

Modification factor of lightweight concrete	$\lambda = 1$	
Compressive strength of concrete	$f'_c = 44.11$	MPa
Young's modulus of bottom rebar	$E_s = 200,000$	MPa
Ultimate strength of stirrups	$f_u = 465$	MPa
Ultimate strength of bottom rebar	$f_u = 557$	MPa
Ultimate strength of top rebar	$f_u = 472$	MPa
Ultimate strength of bot-chord-truss	$f_u = 519$	MPa
Height of beam	$h = 300$	mm
Concrete cover	$c = 30$	mm
Width of beam	$b_w = 200$	mm
Effective depth of beam	$d = 251$	mm
Distance from extreme compression fiber	$d'_s = 46$	mm
Total length of beam	$L = 1800$	mm
Support to support length	$L_n = 1500$	mm
Shear reduction factor	$\phi = 1$ (to predict test results)	
Distance of loading point	$a = 350$	mm
Factored point load	$P_u = 514,828$	N
Factored shear	$V_{u1} = 394,701$	N
Factored shear	$V_{u2} = 120,127$	N
Factored moment	$M_u = 138,145,513$	N.mm
Number of top rebar	2DB16 $A'_s = 402$	mm <sup>2</sup>
Number of bottom rebar	3DB22 $A_s = 1,140$	mm <sup>2</sup>
Stirrups spacing	DB8 150	mm
Bottom chord of steel,	No: 2 $A_s = 616$	mm <sup>2</sup>
Criterion of shear-span-to-depth ratio,	$a/d = 1.394$	
Length of the loading face	$l_l = 125$	mm
Length of the bearing face correspond to load	$l_{l1} = 96$	mm

Length of the bearing face correspond to load	$l_{t2} = 29$	mm
Length of the bearing face	$l_b = 125$	mm
Height of the back face of tension tie	$w_t = 98$	mm
Height of the back face of top compression	$h_s = \beta_1 c = \frac{(A_s f_s - A'_s f'_s)}{0.85 b_w f'_c} =$	65 mm
Distance from loading from left part Figure 3.2	$a_{left} = 335$	mm
Angle of diagonal strut,	$\alpha_{s1} = \arctan\left(\frac{d - h/2}{a_{left}}\right) =$	33.42 degree
Angle of diagonal strut,	$\alpha_{s2} = 36$	degree
Angle of diagonal strut,	$\alpha_{s3} = 26$	degree
Angle of diagonal strut,	$\alpha_{s4} = 32$	degree

➤ **Strength of tie**

Nominal strength of tie

$$P_n = A_{st} f_y = 954,906 \quad \text{N}$$

$$\phi P_n = A_{st} f_y = 954,906 \quad \text{N}$$

$$F_{AC} = 598,231 \quad \text{N}$$

➤ **Capacity of nodal zone**

$$f_s = \frac{F_{AC}}{A_s} = 170.30 \quad \text{MPa}$$

Note: only half of tension force  $F_{AC}$ , assumed the strain varies over the width of the strut.

$$\varepsilon_s = \frac{f_s}{E_s} = 0.00085$$

$$\varepsilon_1 = \varepsilon_s + (\varepsilon_s + 0.002) \cot^2 \alpha_{s1} = 0.0074$$

$$f_{cu} = \frac{f'_c}{0.8 + 170 \varepsilon_1} \leq 0.85 f'_c = 21 \quad \text{MPa}$$

$$f_{cu} = 0.85 f'_c = 37.5 \quad \text{MPa}$$

**The nominal compressive strength from node A**

$$\text{Width of compression strut, } w_s = l_b \sin \alpha_s + w_t \cos \alpha_s = 151 \quad \text{mm}$$

$$P_{n(A)} = f_{cu(A)} A_{cs(A)} = 645,637 \quad \text{N}$$

$$\phi P_{n(A)} = 645,637 \quad \text{N}$$

Shear strength $V_{capacity} = P_{n(A)} \sin \alpha_{s1} =$	<b>355,562</b>	N
---	----------------	---

**The nominal compressive strength from node B**

Width of compression strut, $w_s = l_{l1} \sin \alpha_s + h_t \cos \alpha_s =$	102	mm
--	-----	----

$P_{n(B)} = f_{cu(B)} A_{cs(B)} =$	767,526	N
------------------------------------	---------	---

$\phi P_{n(B)} =$	767,526	N
-------------------	---------	---

Shear strength $V_{capacity} = P_{n(B)} \sin \alpha_{s1} =$	<b>422,690</b>	N
---	----------------	---

➤ **Capacity of nodal zone**

Check stress at the base face of the node A

$f_{base(A)} = V_{u1} / b_w l_b =$	11.17	MPa
------------------------------------	-------	-----

Check stress at the base face of the node B

$f_{top(B)} = V_{u1} / b_w l_{l1} =$	14.57	MPa
--------------------------------------	-------	-----

Check stress at vertical face of left part of node B

$f_{vertical(B)} = F_{BD} / b_w h_s =$	22.55	MPa
--	-------	-----

Limiting concrete compressive stress at the node

$f_{cu(C-C-C)} = 0.85 \phi f'_c =$	37.49	MPa
------------------------------------	-------	-----

$f_{cu(C-C-T)} = 0.75 \phi f'_c =$	33.08	MPa
------------------------------------	-------	-----

$f_{cu(C-T-T)} = 0.65 \phi f'_c =$	28.67	MPa
------------------------------------	-------	-----

➤ **Check provided minimum reinforcement**

$\rho_v = \frac{A_v}{b_s w} \geq 0.003 =$	0.0034	Satisfied
---	--------	-----------

$\rho_h = \frac{A_{vh}}{b_s w} \geq 0.003 =$	-	Not Satisfied
--	---	---------------

$\alpha_2 = 90 - \alpha_{s1} =$	57	degree
---------------------------------	----	--------

$\alpha_2 = \alpha_{s1} =$	33	degree
----------------------------	----	--------

$\rho_v \sin \alpha_1 =$	0.0028	
--------------------------	--------	--

$\rho_{vh} \sin \alpha_2 =$	-	
-----------------------------	---	--

$\sum \frac{A_{si}}{b s_1} \sin \alpha_i \geq 0.003 =$	0.0028	Not Satisfied
--	--------	---------------

### 3.2.2.4 SRCB4 beam

The beam detail configuration refers to Figure 2.32 and the idealized Strut, tie and nodal forces of Figure 3.2 were computed as follow:

#### ➤ Assumption and given data

Modification factor of lightweight concrete	$\lambda = 1$	
Compressive strength of concrete	$f'_c = 40.41$	MPa
Young's modulus of bottom rebar	$E_s = 200,000$	MPa
Ultimate strength of stirrups	$f_u = 465$	MPa
Ultimate strength of bottom rebar	$f_u = 557$	MPa
Ultimate strength of top rebar	$f_u = 472$	MPa
Ultimate strength of bot-chord-truss	$f_u = 519$	MPa
Height of beam	$h = 300$	mm
Concrete cover	$c = 30$	mm
Width of beam	$b_w = 200$	mm
Effective depth of beam	$d = 251$	mm
Distance from extreme compression fiber	$d'_s = 46$	mm
Total length of beam	$L = 1800$	mm
Support to support length	$L_n = 1500$	mm
Shear reduction factor	$\phi = 1$ (to predict test results)	
Distance of loading point	$a = 350$	mm
Factored point load	$P_u = 553,103$	N
Factored shear	$V_{u1} = 424,046$	N
Factored shear	$V_{u2} = 129,057$	N
Factored moment	$M_u = 148,415,972$	N.mm
Number of top rebar	2DB16 $A'_s = 402$	mm <sup>2</sup>
Number of bottom rebar	3DB22 $A_s = 1,140$	mm <sup>2</sup>
Stirrups spacing	DB8@ 150	mm
Bottom chord of steel,	No: 2 $A_s = 616$	mm <sup>2</sup>
Criterion of shear-span-to-depth ratio,	$a/d = 1.394$	
Length of the loading face	$ll = 125$	mm
Length of the bearing face correspond to load	$l_{11} = 96$	mm
Length of the bearing face correspond to load	$l_{12} = 29$	mm
Length of the bearing face	$l_b = 125$	mm
Height of the back face of tension tie	$w_t = 98$	mm
Height of the back face of top compression	$h_s = \beta_1 c = \frac{(A_s f_s - A'_s f'_s)}{0.85 b_w f'_c} =$	65 mm
Distance from loading from left part Figure 3.2	$a_{left} = 335$	mm



Angle of diagonal strut,	$\alpha_{s1} = \arctan\left(\frac{d-h/2}{a_{left}}\right) =$	33.09	degree
Angle of diagonal strut,	$\alpha_{s2} =$	36	degree
Angle of diagonal strut,	$\alpha_{s3} =$	26	degree
Angle of diagonal strut,	$\alpha_{s4} =$	32	degree

➤ **Strength of tie**

Nominal strength of tie

$$P_n = A_{st} f_y = 954,906 \quad \text{N}$$

$$\phi P_n = A_{st} f_y = 954,906 \quad \text{N}$$

$$F_{AC} = 650,702 \quad \text{N}$$

➤ **Capacity of nodal zone**

$$f_s = \frac{F_{AC}}{A_s} = 185.24 \quad \text{MPa}$$

Note: only half of tension force  $F_{AC}$ , assumed the strain varies over the width of the strut.

$$\varepsilon_s = \frac{f_s}{E_s} = 0.00093$$

$$\varepsilon_1 = \varepsilon_s + (\varepsilon_s + 0.002) \cot^2 \alpha_{s1} = 0.00781$$

$$f_{cu} = \frac{f'_c}{0.8 + 170\varepsilon_1} \leq 0.85 f'_c = 19 \quad \text{MPa}$$

$$f_{cu} = 0.85 f'_c = 34.3 \quad \text{MPa}$$

**The nominal compressive strength from node A**

$$\text{Width of compression strut, } w_s = l_b \sin \alpha_s + w_t \cos \alpha_s = 150 \quad \text{mm}$$

$$P_{n(A)} = f_{cu(A)} A_{cs(A)} = 760,609 \quad \text{N}$$

$$\phi P_{n(A)} = 760,609 \quad \text{N}$$

$$\text{Shear strength } V_{capacity} = P_{n(A)} \sin \alpha_{s1} = 415,276 \quad \text{N}$$

**The nominal compressive strength from node B**

$$\text{Width of compression strut, } w_s = l_{11} \sin \alpha_s + h_t \cos \alpha_s = 107 \quad \text{mm}$$

$$P_{n(B)} = f_{cu(B)} A_{cs(B)} = 922,399 \quad \text{N}$$

$\phi P_{n(B)} =$	922,399	N
Shear strength $V_{capacity} = P_{n(B)} \sin \alpha_{s1} =$	<b>503,606</b>	N
<b>➤ Capacity of nodal zone</b>		
Check stress at the base face of the node A		
$f_{base(A)} = V_{u1} / b_w l_b =$	16.96	MPa
Check stress at the base face of the node B		
$f_{top(B)} = V_{u1} / b_w l_{l1} =$	22.12	MPa
Check stress at vertical face of left part of node B		
$f_{vertical(B)} = F_{BD} / b_w h_s =$	36.43	MPa
Limiting concrete compressive stress at the node		
$f_{cu(C-C-C)} = 0.85\phi f'_c =$	35.35	MPa
$f_{cu(C-C-T)} = 0.75\phi f'_c =$	30.31	MPa
$f_{cu(C-T-T)} = 0.65\phi f'_c =$	26.37	MPa
<b>➤ Check provided minimum reinforcement</b>		
$\rho_v = \frac{A_v}{b_s w} \geq 0.003 =$	0.0034	Satisfied
$\rho_h = \frac{A_{vh}}{b_s w} \geq 0.003 =$	–	Not Satisfied
$\alpha_2 = 90 - \alpha_{s1} =$	57	degree
$\alpha_2 = \alpha_{s1} =$	33	degree
$\rho_v \sin \alpha_1 =$	0.0028	
$\rho_{vh} \sin \alpha_2 =$		
$\sum \frac{A_{si}}{b_{s1}} \sin \alpha_i \geq 0.003 =$	0.0028	Not Satisfied

### 3.2.3 Summary of shear strength by STM

The shear strength predicted by STM in both ACI 318 (2014) and AASHTO LRFD (2012) were summed up in Table 3-6.

Table 3-6 Shear strength by STM following ACI 318 and AASHTO LRFD

STUDY BEAMS	SRCB1	SRCB2	SRCB3	SRCB4
ACI 318 (2014) Node A	436	438	467	423
ACI 318 (2014) Node B	<b>407</b>	<b>408</b>	<b>423</b>	<b>400</b>
AASHTO LRFD (2012) Node A	<b>322</b>	<b>304</b>	<b>356</b>	<b>415</b>
AASHTO LRFD (2012) Node B	407	408	423	504



## **CHAPTER 4**

### **FINITE ELEMENT ANALYSIS**

This chapter demonstrates how to implement finite element method using commercial software to investigate behavior and capacity of RC beam with and without embedded steel trusses. Finite element models (ANSYS 18.2) was employed to model, simulate and predict shear strength of such beams, which the experimental study was done by Zhang et al. (2016). The assumption, modeling and analysis procedure are described as follows.

#### **4.1 Modeling assumptions**

Modeling assumptions made in this study described as follow:

1. Concrete and steel were modeled as isotropic materials.
2. Poisson's ratio was assumed to be constant throughout the loading history.
4. Concrete was assumed to be multilinear isotropic hardening material
5. Steel was assumed to be an elastic-perfectly plastic material and identical in tension and compression.
6. Perfect bond exists between concrete and steel reinforcement.
7. Perfect bond exists between concrete and steel truss members
8. Time-dependent nonlinearities such as creep, shrinkage, and temperature change were excluded in this study.

#### **4.2 Element-type selection in ANSYS 18.2**

This section described the element types that used in ANSYS models to represent all materials. Elements that used in this studies are extensively used and recommended by ANSYS and previous researchers. These materials are: concrete, steel reinforcement, steel truss member, steel plate at loading point and support plates.

##### **4.2.1 Concrete**

SOLID65 is used to model the concrete (ANSYS, 2018) . The solid is capable of cracking in tension and crushing in compression. In concrete applications, capability of

the element may be used to model concrete while rebar capability is available for modeling reinforcement behavior. The element is specified by eight nodes having three degrees of freedom at each node translation in the nodal x, y, and z directions. Geometry and node locations for this element type are shown in Figure 4.1.

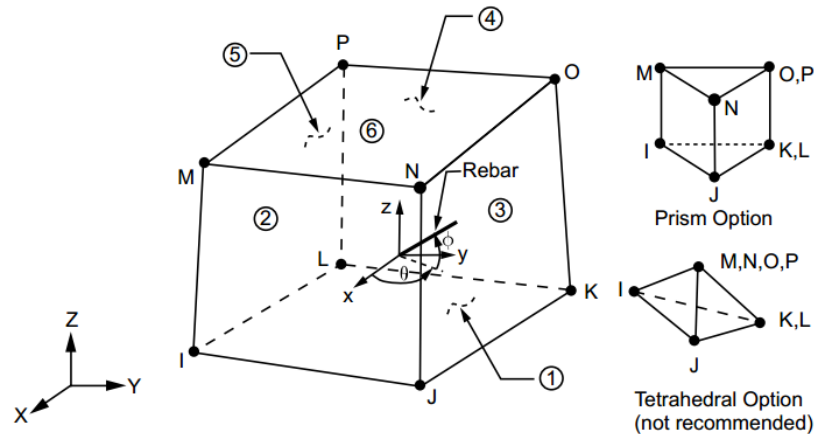


Figure 4.1 Solid65 3-D reinforced concrete solid (ANSYS, 2018)

#### 4.2.2 Steel reinforcement

LINK180 element is used to model steel reinforcement (ANSYS, 2018). The element is a uniaxial tension-compression element with three degrees of freedom at each node: translations in the nodal x, y and z directions. Geometry and node locations for this element is shown in Figure 4.2.

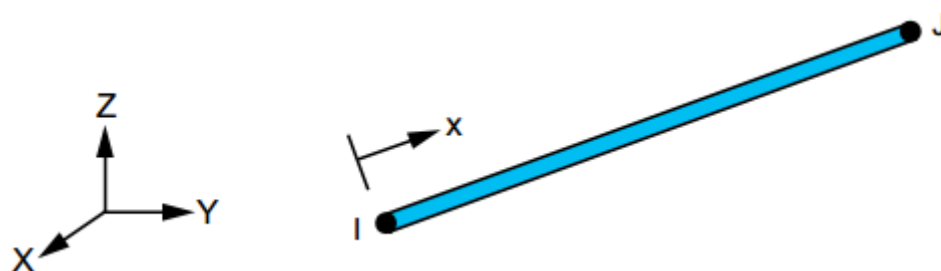


Figure 4.2 Link180 3-D spar element (ANSYS, 2018)

#### 4.2.3 Steel plate

The SOLID185 element is used to model steel plates at supports and loading location in the model (ANSYS, 2018). Solid185 is used for 3-D modeling of solid structures. It is defined by eight nodes having three degrees of freedom at each node:

translations in nodal x, y, and z directions. The element has plasticity, hyperelasticity, stress, stiffening, creep, large deflection, and large strain capabilities. Geometry and node location for this element is shown in Figure 4.3.

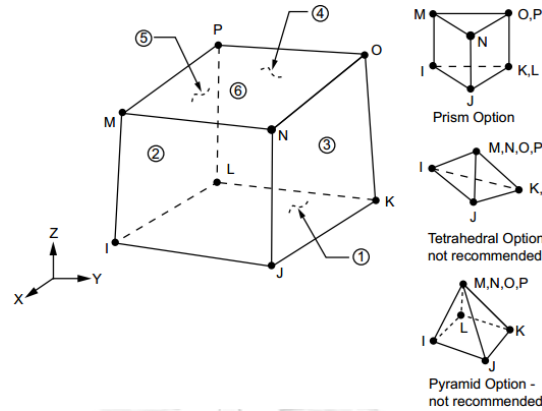


Figure 4.3 Solid185 3-D solid element (ANSYS, 2018)

The element type that used in FE models in this study was summarized in. Table 4-1

Table 4-1 Summary of element types for ANSYS models

Material type	Element Type
Concrete	Solid65
Steel reinforcement, angle steel, and flat steel	Link180
Steel plate	Solid185

### 4.3 Material models

In this part, the mechanical behavior of concrete and steel plates, steel reinforcement, and steel section are described in following sections.

#### 4.3.1 Concrete

Development of a model for behavior of concrete is a challenging task. Concrete has different behavior in compression and tension, and it is a quasi-brittle material. Tensile strength of concrete is usually 8-15% of compressive strength (Shah et al., 1995). Typical stress-strain curve for normal weight concrete (Bangash, 1989) is shown in Figure 4.4

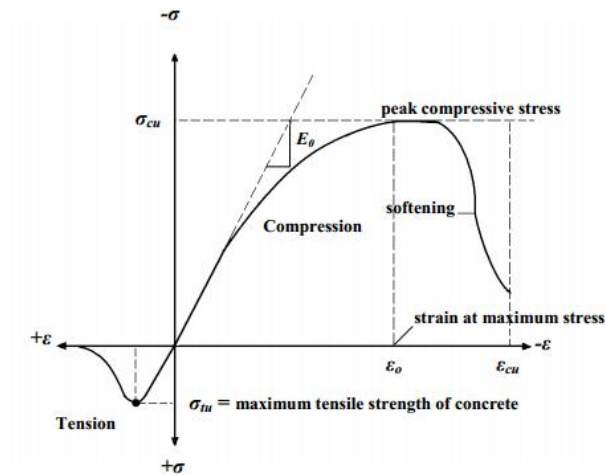


Figure 4.4 Typical uniaxial compressive and tensile stress-strain curve for concrete (Bangash, 1989)

In compression, the stress-strain curve is linearly elastic up to approximately 30% of the maximum compressive strength of concrete. The stress increases slowly up to the maximum compressive strength above this point (Bangash, 1989).

#### 4.3.1.1 Finite element input data

For concrete, ANSYS requires input data for material properties as follow:

- Elastic modulus  $E_c$  (MPa)
- Ultimate uniaxial compressive strength  $f'_c$  (MPa)
- Ultimate uniaxial tensile strength (modulus of rupture,  $f_r$ ) (MPa)
- Poisson's ratio ( $\nu$ )
- Shear strength transfer coefficient ( $\beta_t$ )
- Compressive uniaxial stress-strain relationship for concrete

The ultimate concrete compressive and tensile strength of each beam model was calculated by Eq. (4.1) and Eq. (4.2), respectively ACI 318 (2014).

$$f'_c = \left( \frac{E_c}{4700} \right)^2 \quad (4.1)$$

$$f_r = 0.62\lambda\sqrt{f'_c} \quad (4.2)$$

where:  $E_c$ ,  $f_c'$ , and  $f_r$  are in SI unit; Poisson's ratio was assumed to be 0.2 for concrete (Bangash, 1989); the shear transfer coefficient ( $\beta_t$ ) represents condition of crack-face value, which is 0.0 to 1.0.

In this study, the values of such parameters which used in the models restaged in Table 4-2.

Table 4-2 Summary of material properties and parameters of concrete models

Test specimen	SRCB1	SRCB2	SRCB3	SRCB4
Compressive strength, $f_c'$ (MPa)	41.54	41.73	44.11	40.41
Modulus of elasticity, $E_c$ (MPa)	34,110	34,100	34,560	33,720
Tensile strength, $f_r$ (MPa)	4.02	4.02	4.14	3.96
Open Shear transfer coefficient, $\beta_t$	0.3	0.3	0.3	0.3
Closed Shear transfer coefficient, $\beta_t$	0.8	0.8	0.8	0.8
Poisson's ratio of concrete, $\nu$	0.2	0.2	0.2	0.2

#### 4.3.1.2 Compressive uniaxial stress-strain relationship

ANSYS program requires the uniaxial stress-strain relation for concrete in compression. Numerical expressions (Desayi and Krishnan, 1964) Eq. (4.3) and Eq. (4.4) were used along with Eq. (4.5) by Gere and Timoshenko (1997) to construct the uniaxial compressive stress-strain curve for concrete in this study. The simplified compressive uniaxial stress-strain relationship is shown in Figure 4.5.

$$f = \frac{E_c \varepsilon}{1 + \left(\frac{\varepsilon}{\varepsilon_o}\right)^2} \quad (4.3)$$

$$\varepsilon_o = \frac{2f_c'}{E_c} \quad (4.4)$$



$$E_c = \frac{f}{\varepsilon} \quad (4.5)$$

where

$f$  = stress at any strain  $\varepsilon$  SI unit

$\varepsilon$  = strain at stress  $f$

$\varepsilon_0$  = strain at the ultimate compressive strength  $f'_c$

$E_c$  = young modulus of concrete (MPa)

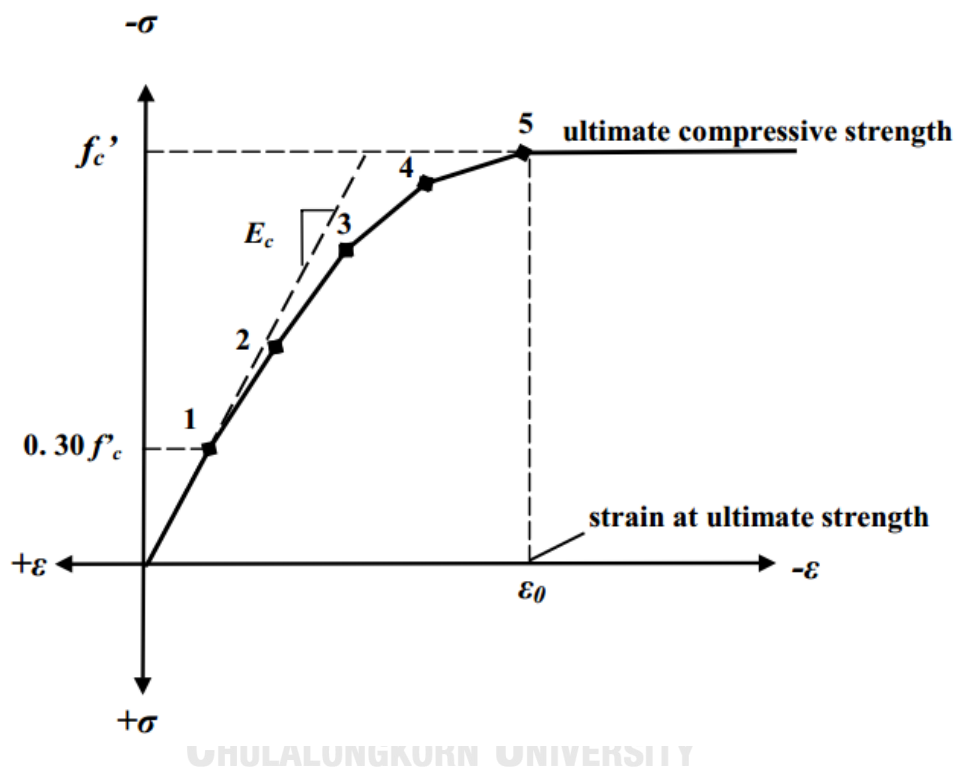


Figure 4.5 Simplified compressive uniaxial stress-strain curve for concrete

(Kachlakev et al., 2001)

The compressive uniaxial stress-strain curve for concrete for the studied beams in ANSYS models (Figure 4.6) was constructed from Eqs. (4.3), (4.4), and (4.5).

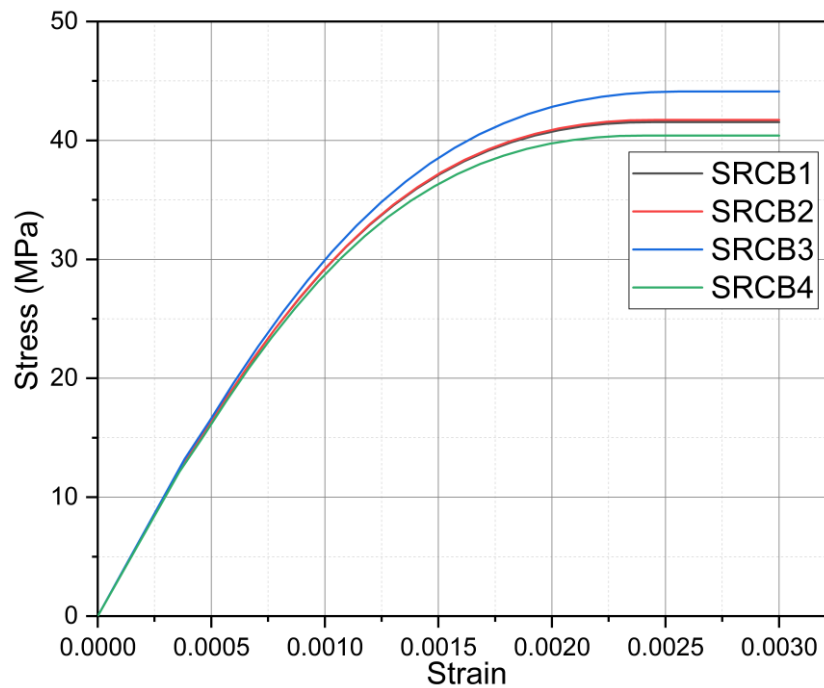


Figure 4.6 Compressive uniaxial stress-strain curve for ANSYS models

#### 4.3.1.3 Criterion of failure

A three-dimensional failure surface for concrete is shown in Figure 4.7. The most significant nonzero principal stress is in x and y-directions represented by  $\sigma_{xp}$  and  $\sigma_{yp}$ , respectively. Three failure surfaces are shown as projections on the  $\sigma_{xp} - \sigma_{yp}$  plane. Mode of failure depends on a function of the sign of  $\sigma_{zp}$  (principal stress in the z-direction). For example, if  $\sigma_{xp}$  and  $\sigma_{yp}$  are both negative (compressive) and  $\sigma_{zp}$  is slightly positive (tensile), cracking would be predicted in a direction perpendicular to  $\sigma_{xp}$ . However, if  $\sigma_{zp}$  is zero or slightly negative, the material is assumed to crush (ANSYS, 2018).

In concrete element, cracking occurred when principal tensile stress in any direction lies outside the failure surface. The elastic modulus of the concrete element is set to zero in the direction parallel to the principal tensile stress direction, after cracking. Crushing occurs when all principal stresses are compressive and lie outside the failure surface; afterward, the elastic modulus was set to zero in all direction (ANSYS, 2018), and the element effectively disappears.

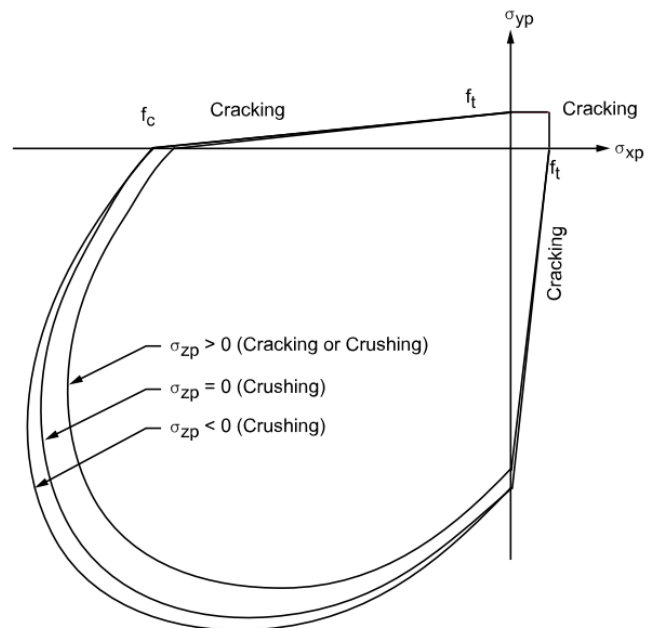


Figure 4.7 Three dimension failure surface for concrete (ANSYS, 2018)

#### 4.3.2 Steel reinforcement, steel section, and steel plate

The steel for the finite element models was assumed to be an elastic-perfectly plastic material and identical in tension and compression. Poisson's ratio of 0.3 is used for steel reinforcement (Gere and Timoshenko, 1997). The stress-strain relationship and material properties of the steel reinforcement are shown in

Figure 4.8. The steel section and steel plates were assumed to be linear elastic materials.

- $E_s$  = young modulus of elasticity (MPa)
- $f_y$  = yield stress (MPa)
- $\nu$  = poisson's ratio (equal = 0.3)
- $E_t$  = Tangent modulus, use  $0.02E_s$  (MPa)

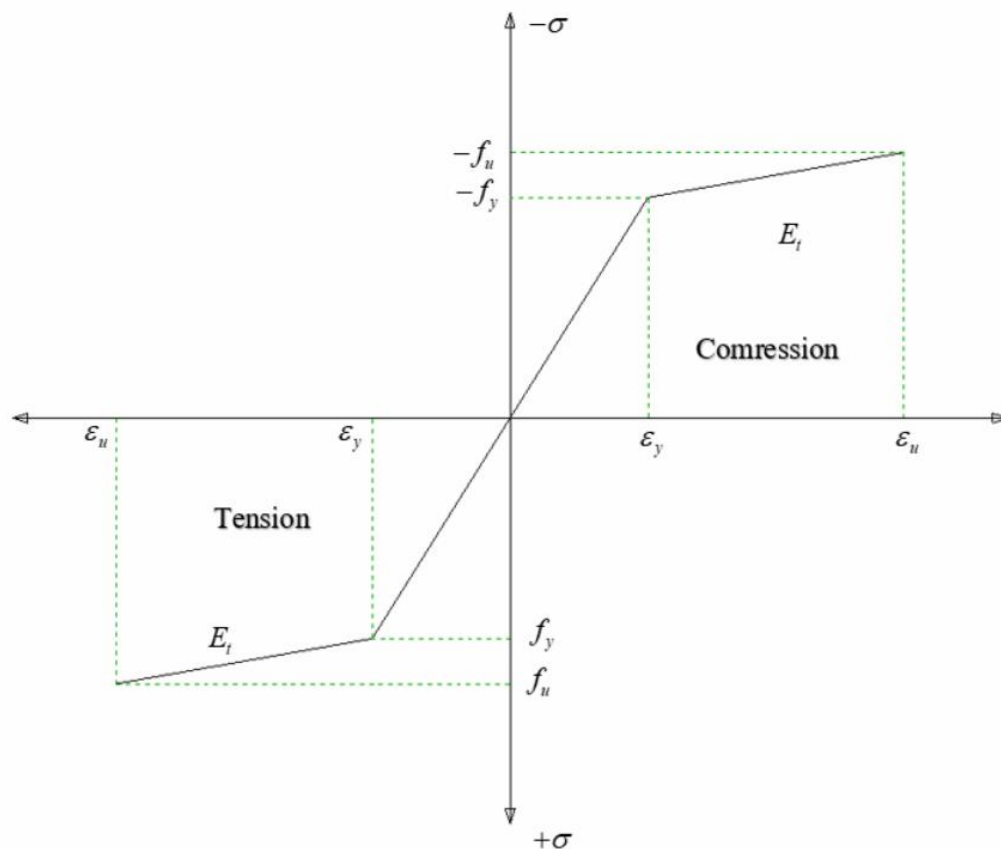


Figure 4.8 Stress-strain curve for steel reinforcement

Steel properties used in ANSYS models are summarized in Table 4-3 as follow:

Table 4-3 Summary of material properties and parameters of steel for models

Type of steel	Diameter or dimensions	Yield strength $f_y$	Ultimate strength $f_u$	Elasticity Modulus $E_s$	Cross sectional (Area)	Poisson ratio
	mm	MPa	MPa	GPa	mm <sup>2</sup>	
Rebar	8	363	465	210	25.13	0.3
Rebar	12	405	522	200	37.70	0.3
Rebar	16	378	472	200	50.27	0.3
Rebar	22	393	557	200	69.12	0.3
Flat steel	30 x 4	266	363	200	120	0.3

Angle steel	40 x 40 x 4	345	519	200	308	0.3
Angle steel	30 x 30 x 3	348	522	200	173	0.3
Loading plate	200x125x20	350	363	200		0.3
Support plate	200x125x20	350	363	200		0.3

## 4.4 Finite element models of the studied beams

### 4.4.1 Configuration and dimensions

The studied beams from Table 3-1 and the Detail configurations of each beam (Figure 2.30 to Figure 2.32) were modeled as follows:

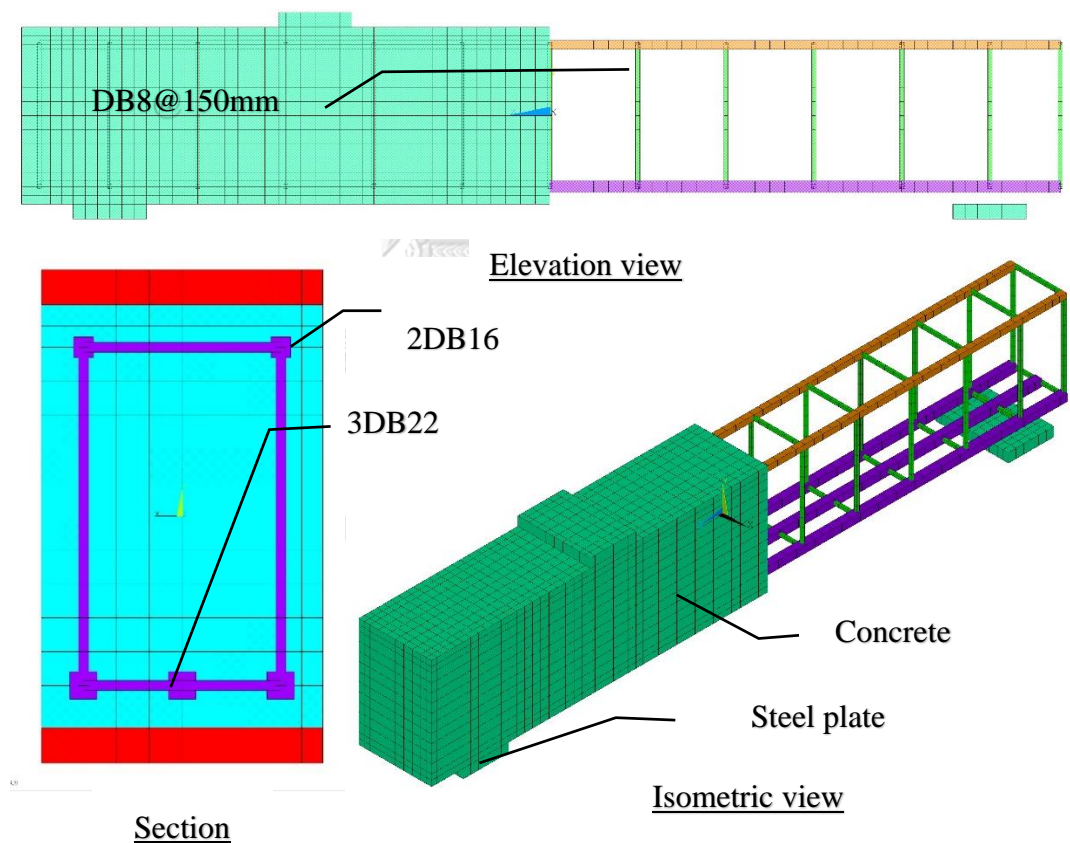


Figure 4.9 FE model-detail configuration of SRCB1

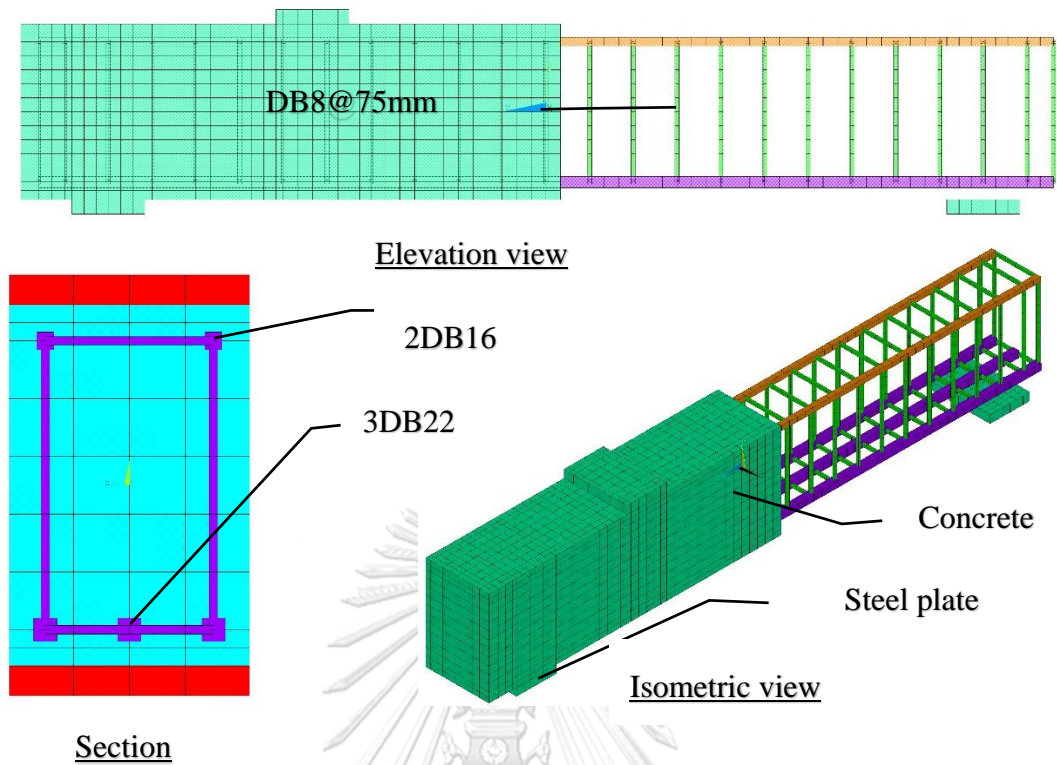


Figure 4.10 FE model-detail configuration of SRCB2

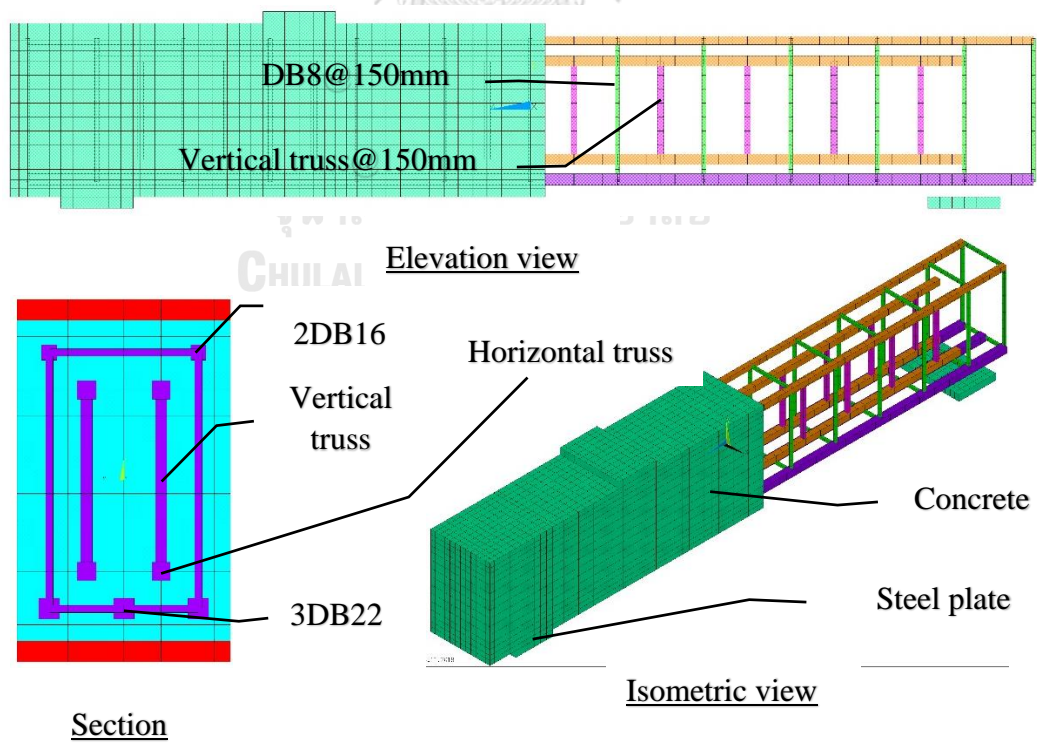


Figure 4.11 FE model-detail configuration of SRCB3

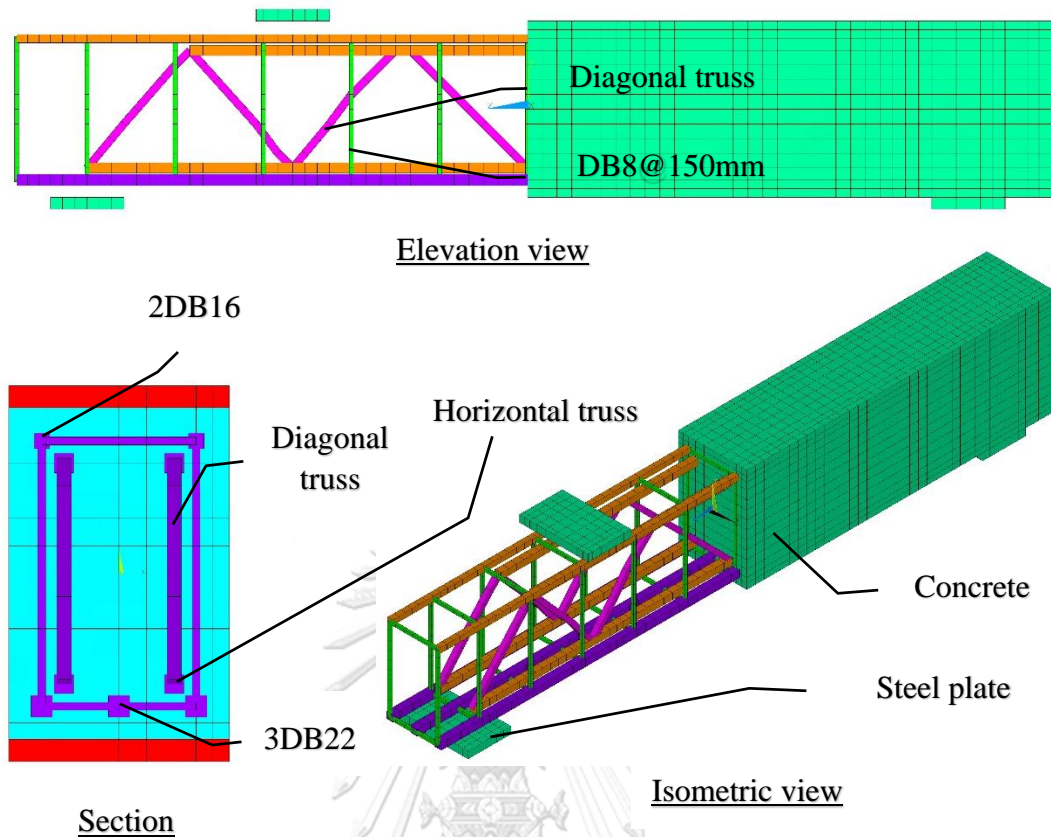


Figure 4.12 FE model-detail configuration of SRCB4

Finite element model-configurations presented in Figure 4.9 to Figure 4.12 for SRCB1 to SRCB4, respectively. The steel plate dimensions at support and loading point referred to Table 4-3

#### 4.4.2 Discretization

Meshing of concrete, steel reinforcement, flat plate and angle models described as follows.

##### 4.4.2.1 Concrete

To get better results from the Solid65 element, the use of a rectangular mesh is recommended (Kachlakev et al., 2001; Wolanski, 2004). Hence, the mesh is set such that square or rectangular elements are created. Overall mesh of the concrete for the studied beam models showed in Figure 4.9 to Figure 4.12.

#### 4.4.2.2 Steel reinforcement

Ideally, bonding behavior between the concrete and steel reinforcement should be considered. Although in this study, the perfect bond of concrete and steel rebar, flat steel, steel angle were assumed.

To provide the bonding performance, link180 element for steel reinforcing, flat steel or angle was connected between of each adjacent concrete Solid element; two materials shared the same node (Kachlakev et al., 2001; Wolanski, 2004). The meshing of the rebar was a distinct case compared to concrete volumes. No mesh of reinforcement, flat steel, angles are required because of the individual element was created in the modeling through the nodes generated by the mesh of the concrete volumes Figure 4.9 to Figure 4.12.

#### 4.5 Loads and boundary conditions

After primary models have been made, geometry, material properties, and meshed were built appropriately, the boundary condition and loads need to be defined.

Displacement boundary condition is required to restrain the model to obtain a unique solution and to ensure the model behave the same way as the experiment. Boundary condition need to be applied at points where the supports and loadings exist.

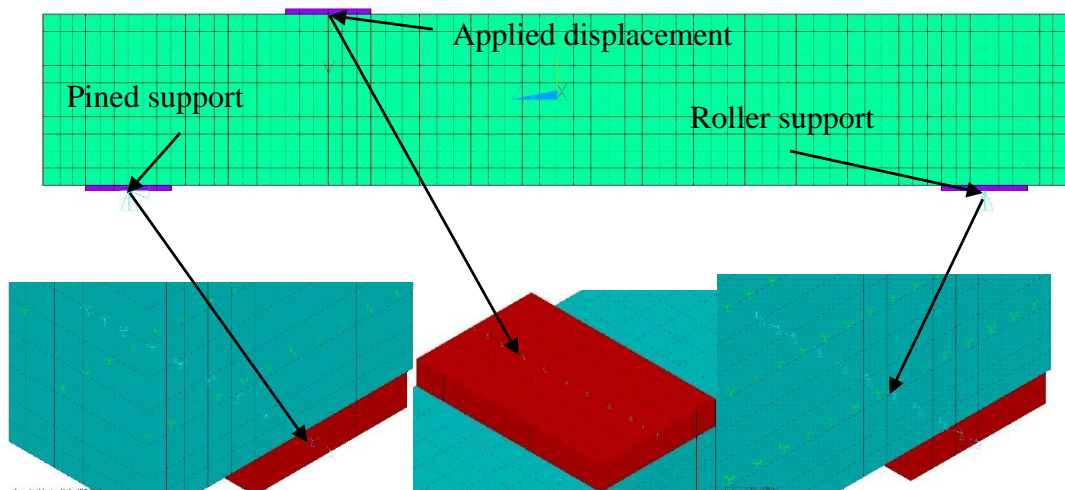


Figure 4.13 Loading and Boundary conditions

In Figure 4.13, supports were modeled as pined, and roller. A single line of nodes on the plate were given restraint in the UX and UY directions applied as constant value



of zero for roller support. Pinned support, the given restraint in UX, UY, and UZ directions, applied as constant value of zero.

Displacement, UY applied across the entire centerline of the steel plate Figure 4.13. The displacement applied equally at each node on the plate as displacement load control analysis.

#### 4.6 Analysis types

The Static analysis type was employed to simulate FE models under vertical displacement loading.

ANSYS employed “Newton-Raphson” approach to be solving nonlinear problem (ANSYS, 2018) . In this approach, the load was subdivided into a series of load increment. The load increment can be applied over several load steps. The use of Newton-Raphson equilibrium iterations in a single DOF nonlinear analysis is illustrated in Figure 4.14.

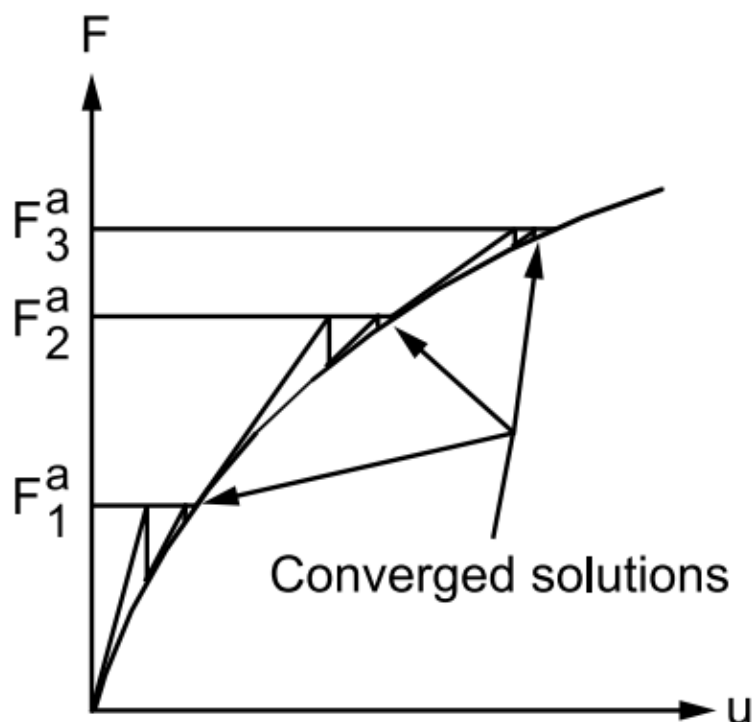


Figure 4.14 Newton-Raphson iterative solution(ANSYS 18.2 Inc., 2018)

Before each solution, Newton-Raphson method evaluates the out-of-balance load vector, which is the difference between the restoring force (the load corresponding to

the element stresses) and the applied load; program then performs a linear solution using the out-of-balance load and check for convergence. If convergence criteria are not satisfied, the out-of-balance load vector is re-evaluated. Stiffness matrix is updated, and a new solution obtained. This iterative procedure continues until the problem converges (ANSYS, 2018) .

Nonlinear static type is utilized for studied beam models. Typical commands utilize in this analysis are shown in the following tables:

Table 4-4 Nonlinear analysis control commands in ANSYS

Analysis options	Large Displacement Static
Calculate pre-stress effects	No
Time at End of load step	3
Automatic time stepping	On
Number of sub steps	600
Max no. sub steps	1000
Min no. of sub steps	100
Write items to results file	All Solution Items
Frequency	Write Every Sub Step

Table 4-5 Output control commands

Equation solvers	Sparse Direct
Restart control	1
Frequency	Write Every Sub Step

Table 4-6 Nonlinear algorithm and convergence criteria parameters

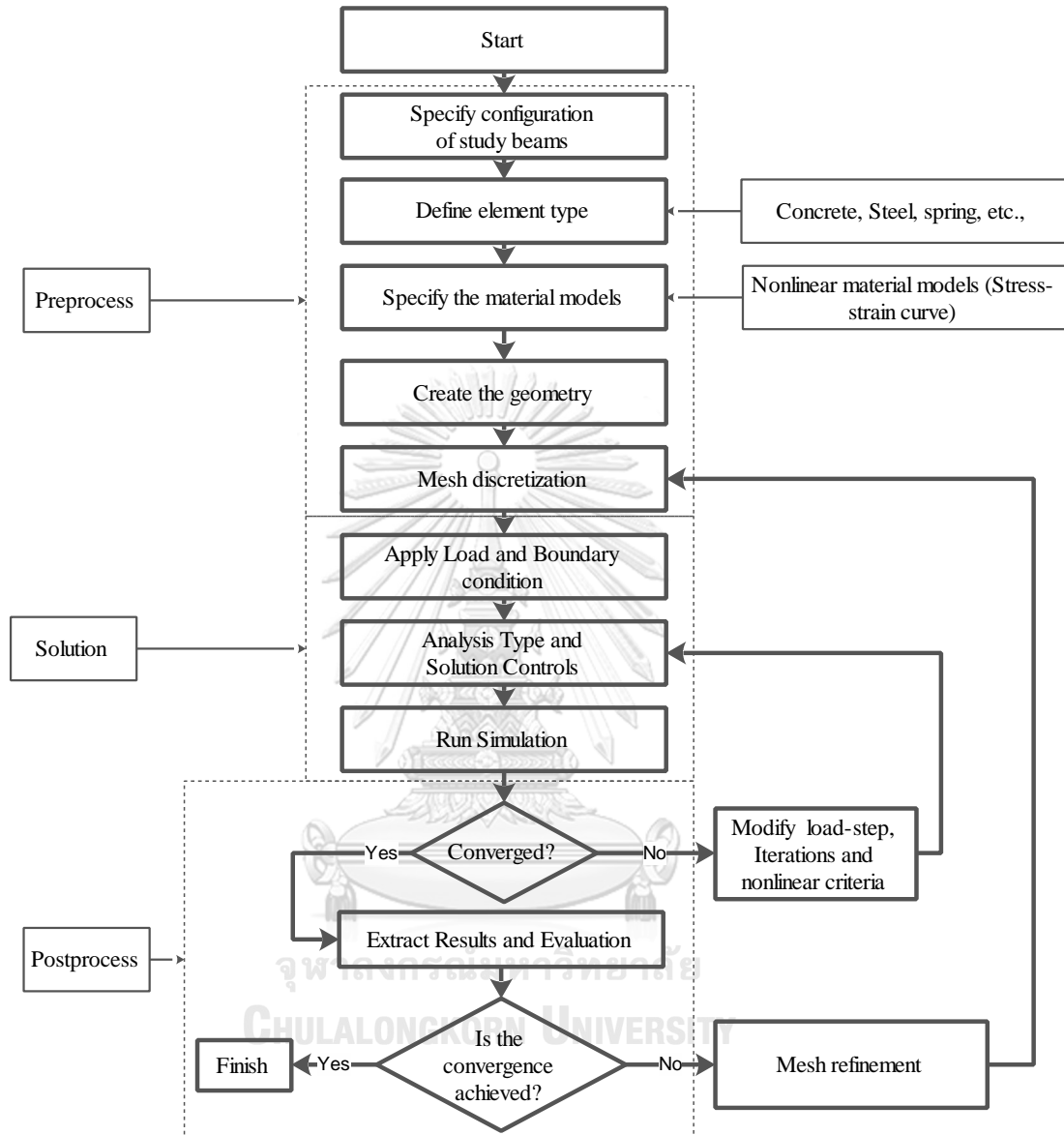
Line search	On
DOF solution predictor	Program Chosen
Maximum number of interactions	
Cutback control	Cutback according to predicted number of iter.

Equiv.Plastic strain	0.15	
Explicit creep ratio	0.1	
Implicit creep ratio	0	
Incremental displacement	10000000	
Point per cycle	13	
Set convergence criteria		
Label	F	U
Ref.Value	Calculated	Calculated
Tolerance	0.01	0.1
Norm	L2	L2
Min.Ref.	Not applicable	Not applicable

Table 4-7 Advance nonlinear control settings

Program behavior Upon Non-convergence	0
Nodal DOF Sol's	0
Cumulative Iterations	0
Elapsed time	0
CUP time	0

## 4.7 Finite element analysis procedure



+

Figure 4.15 Finite element analysis flowchart

## CHAPTER 5

### RESULTS AND DISCUSSIONS

In this chapter, the results of finite element models were presented. Comparison of shear strength of FE analysis with physical test result by Zhang et al. (2016) and also with analytical method following code provisions were discussed.

#### 5.1 Finite element analysis results

##### 5.1.1 Cracking and crushing of concrete

Figure 5.1 to Figure 5.4 showed first crack of the studied beams SRCB1 to 4 respectively. The concrete of SRCB1 in Figure 5.1 stated cracking when the applied load exceeded 70 kN, and SRCB2, SRCB3, SRCB4 were 68.2 kN, 81.6 kN, 76.3 kN respectively.

Cracks started to propagate at tension of the beam near loading point. The cracks spread out when the applied load has increased as shown in Figure 5.5 to Figure 5.8 of SRCB1 to SRCB 4 respectively.

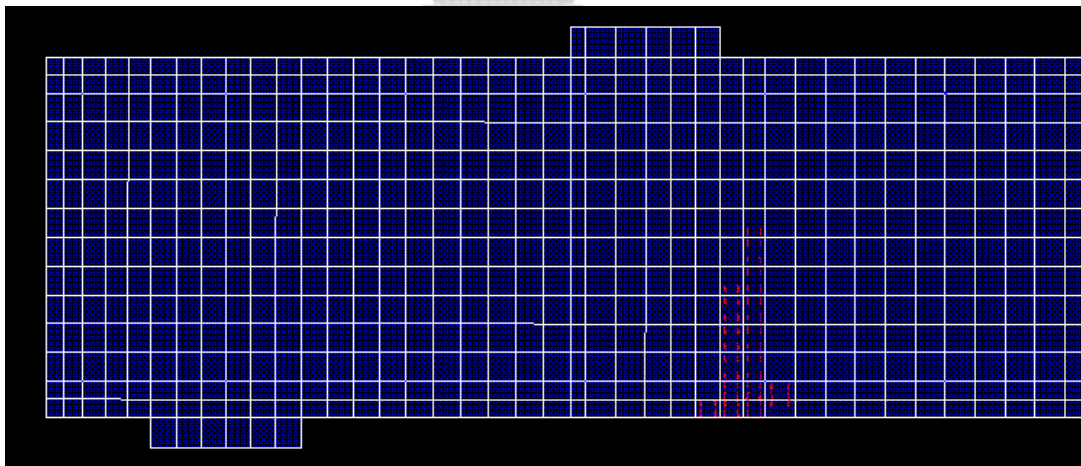


Figure 5.1 First crack of concrete SRCB1

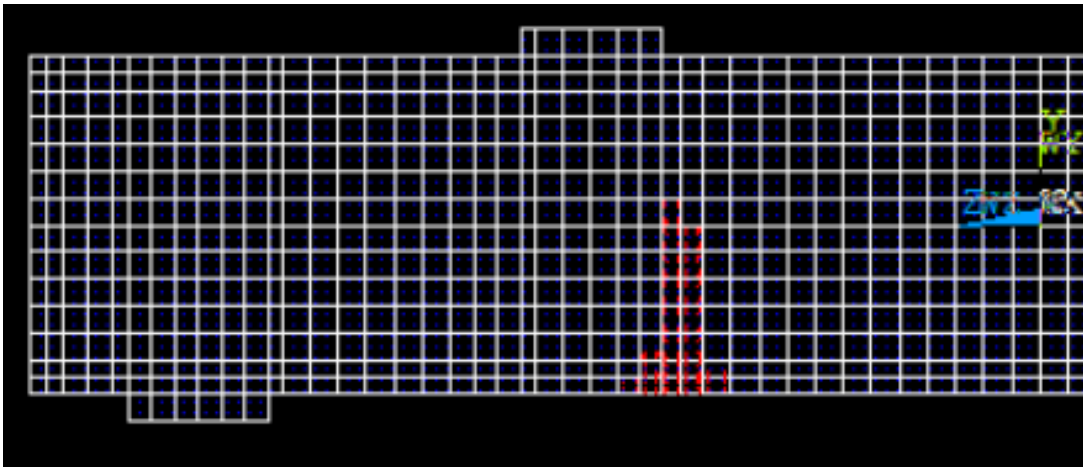


Figure 5.2 First crack of concrete SRCB2

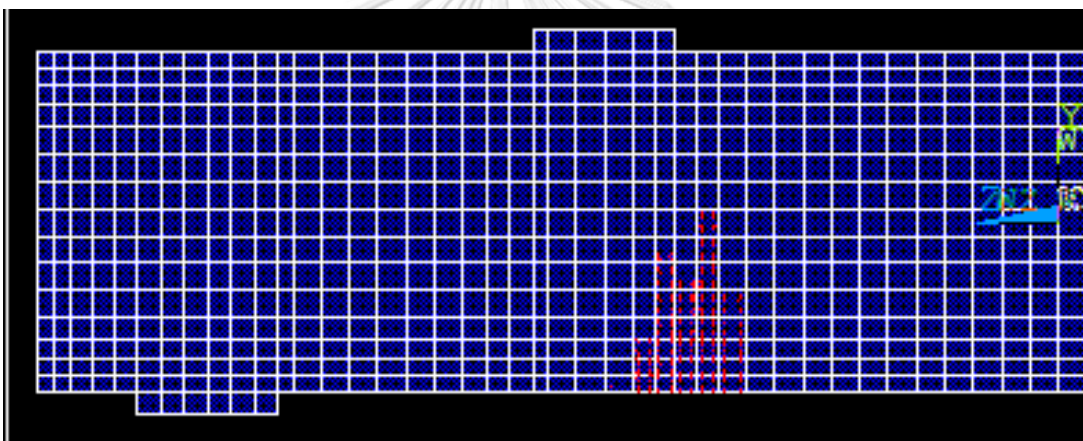


Figure 5.3 First crack of concrete SRCB3

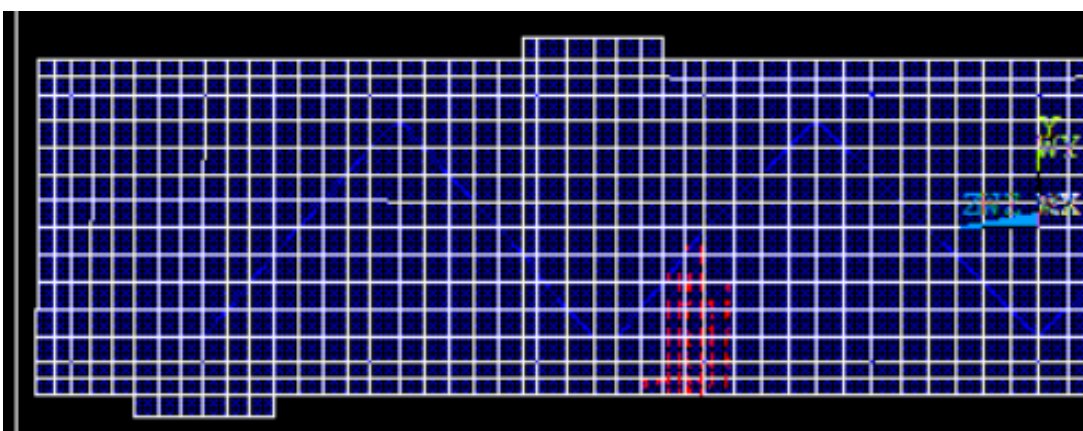


Figure 5.4 First crack of concrete SRCB4

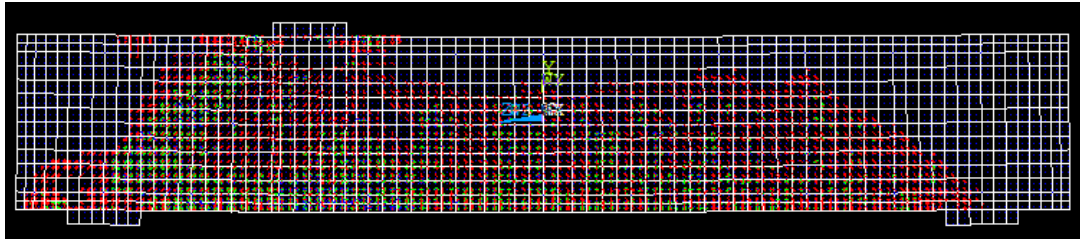


Figure 5.5 Multiple crack patterns of concrete SRCB1

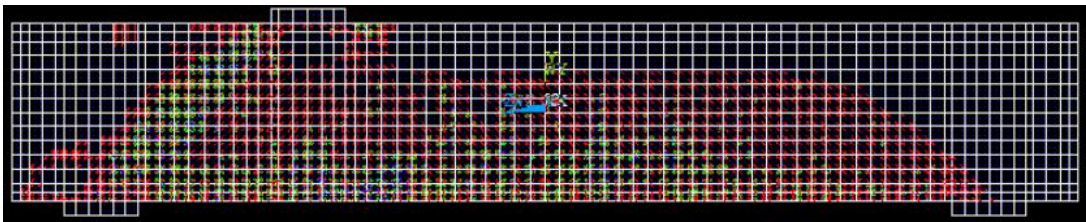


Figure 5.6 Multiple crack patterns of concrete SRCB2

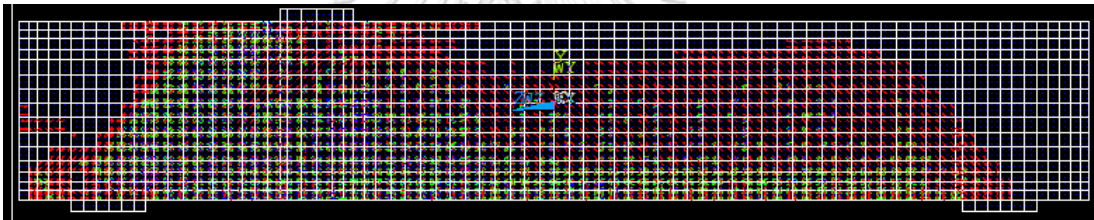


Figure 5.7 Multiple crack patterns of concrete SRCB3

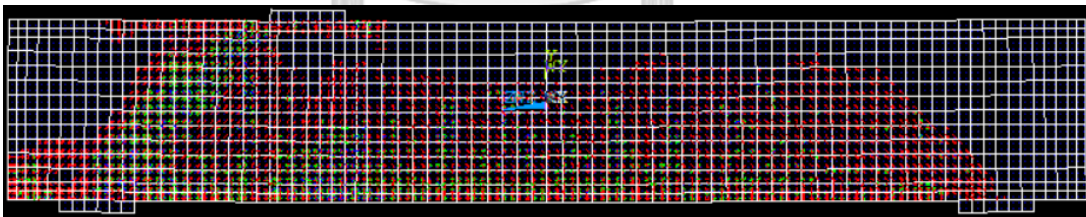


Figure 5.8 Multiple crack patterns of concrete SRCB4

At this point, the cracks of beams separated into several state as more loads were applied. The crack-patterns Figure 5.5 to Figure 5.8 have divided into first crack as red color, second crack as green color and third crack as blue color. The secondary and third cracks concentrated at the diagonal strut between loading point and support which represented shear transfer from applied to support reaction Figure 5.5 to Figure 5.8. Moreover, the diagonal first cracks near the far end-support represented a small amount of shear transfer to the far end-support.

### 5.1.2 Maximum stress of concrete and steel

Figure 5.9 displayed the maximum von mises stress of concrete SRCB1 which is 40.5 MPa, this equivalent to specified concrete compressive strength in Table 4-2 for SRCB1. At the time concrete crushing failure occurred the longitudinal bottom reinforcement and stirrups between diagonal compressive strut had yielded Figure 5.10. The studied beams: SRCB2, SRCB3, SRCB4 were the same manner Figure 5.11 to Figure 5.16 respectively.

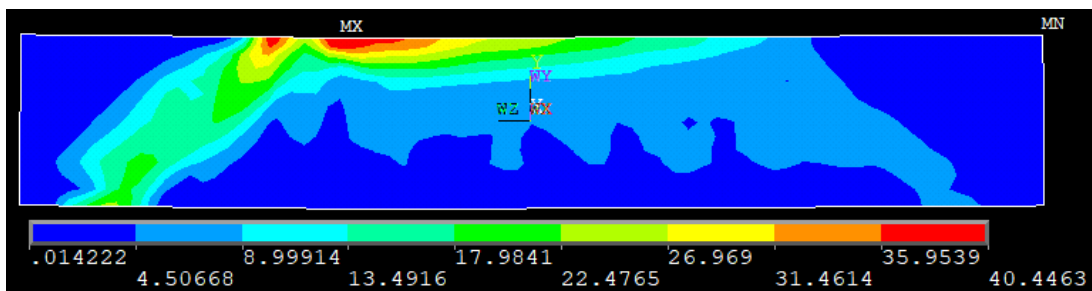


Figure 5.9 The maximum von mises stress of concrete SRCB1

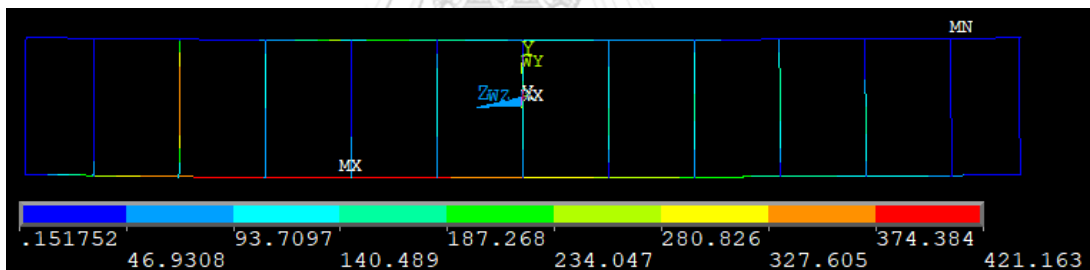


Figure 5.10 The maximum von mises stress of steel reinforcement SRCB1

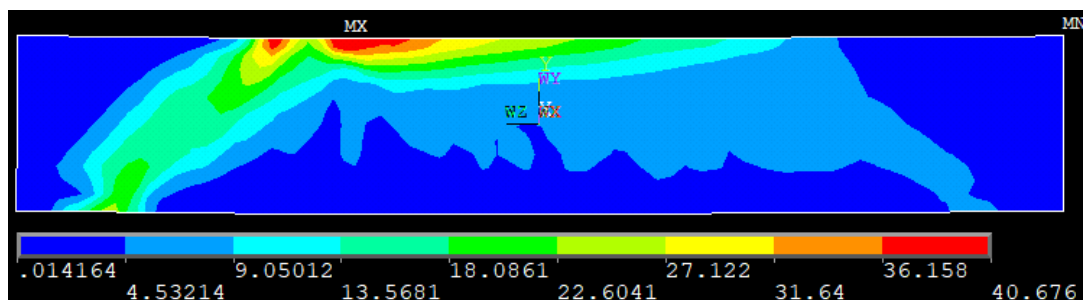


Figure 5.11 The maximum von mises stress of concrete SRCB2



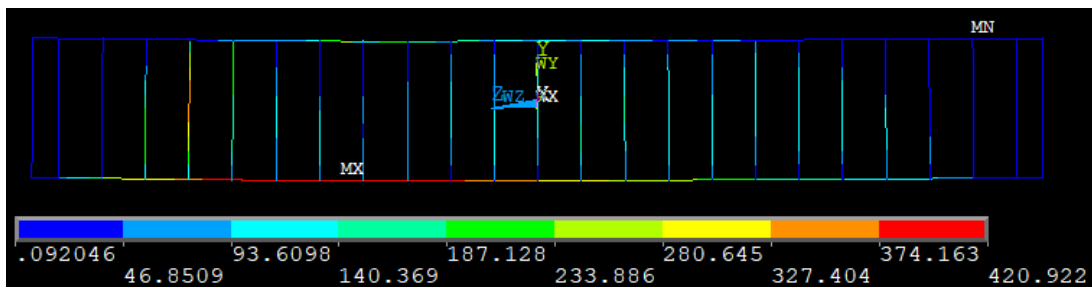


Figure 5.12 The maximum von mises stress of steel reinforcement SRCB2

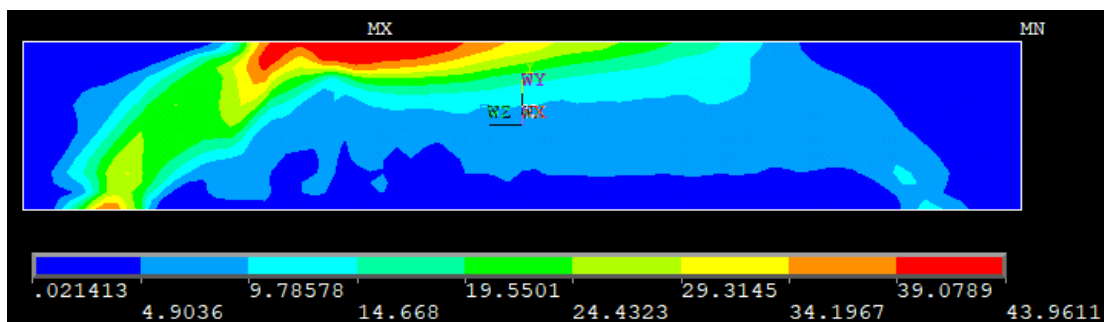


Figure 5.13 The maximum von mises stress of concrete SRCB3

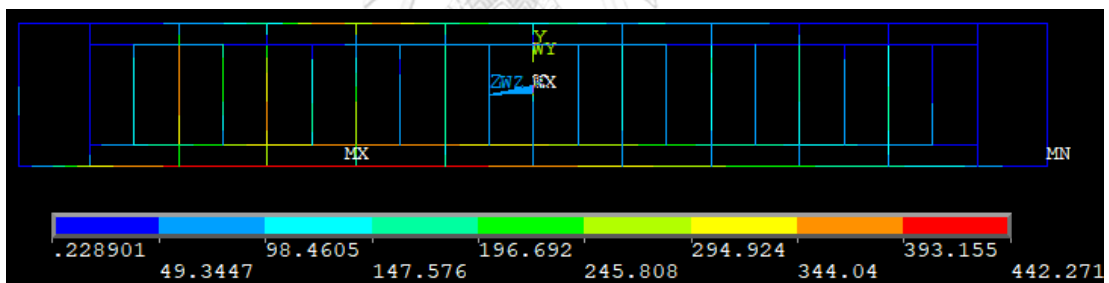


Figure 5.14 The maximum von mises stress of steel reinforcement SRCB3

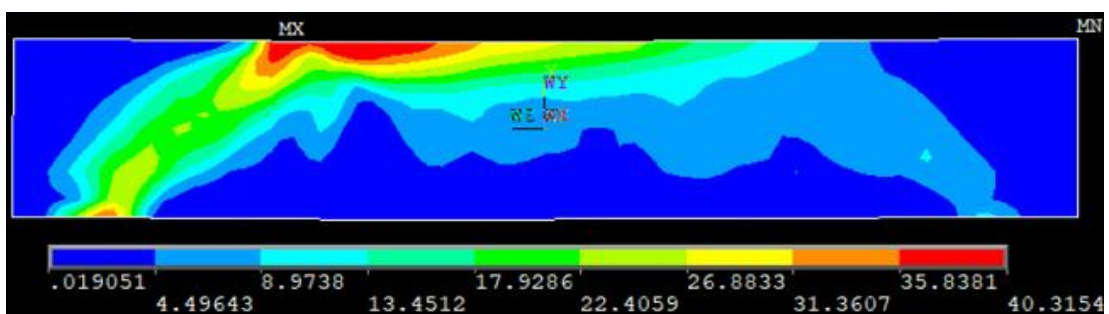


Figure 5.15 The maximum von mises stress of concrete SRCB4

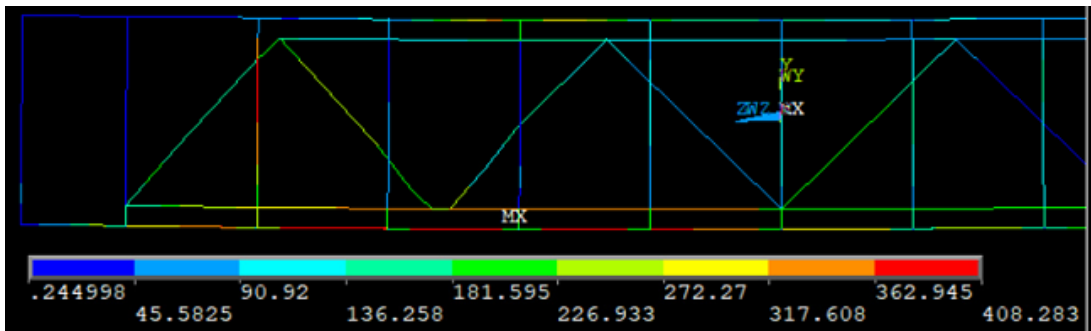


Figure 5.16 The maximum von mises stress of steel reinforcement SRCB4

### 5.1.3 Load-deflection curves

The FE analysis results of the studied beams as shown in load-deflection curve Figure 5.17 demonstrated that, at point A concrete started cracking, B steel started yielding and C was failure of concrete of beams.

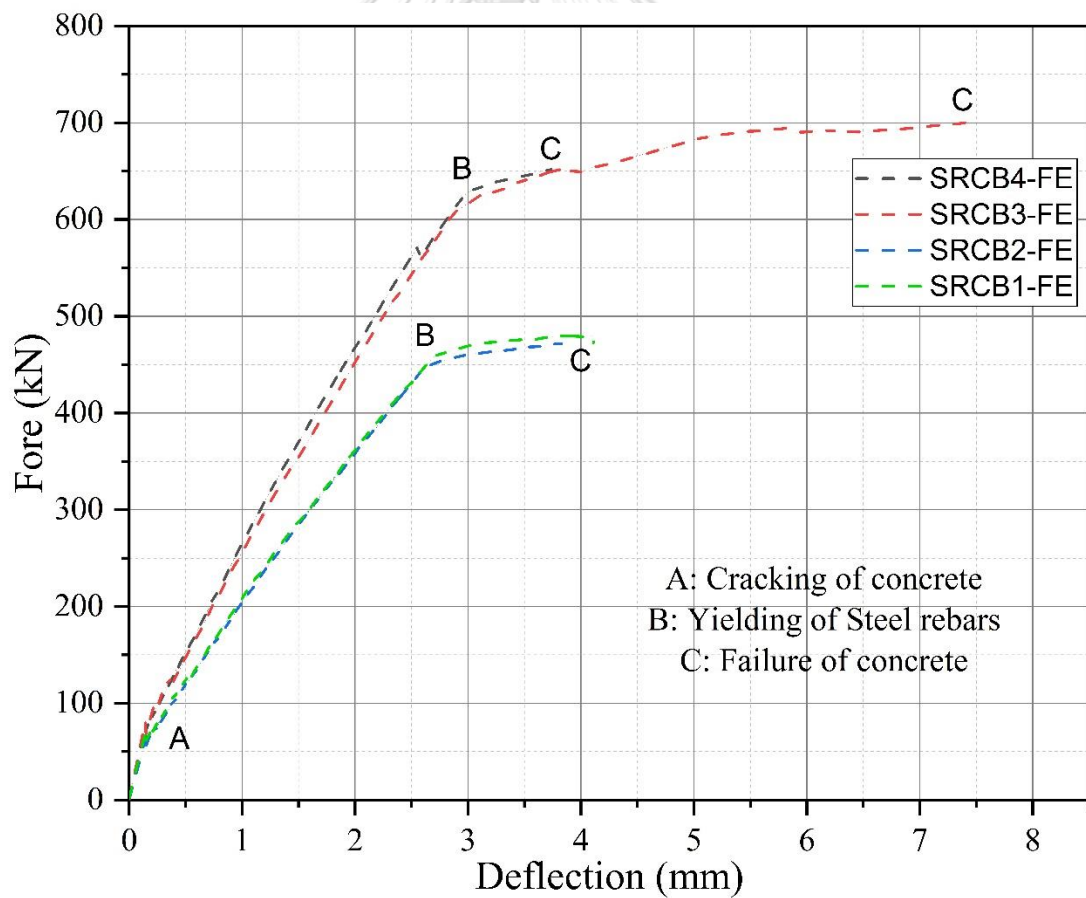


Figure 5.17 Load-deflection of FEM result of the studied beams

The load-deflection of SRCB1-FE and SRCB2-FE as indicated in Figure 5.17, it can be seen that vertical stirrups in FE models have not provided the improvement of shear strength of beams. Moreover SRCB3-FE and SRCB4-FE results (Figure 5.17) have not clearly indicated the difference in term strength and stiffness between vertical truss member and diagonal truss member inside the studied beams SRCB3-FE and SRCB4-FE respectively. However, SRCB3-FE AND SRCB4-FE have given higher shear-strength compare with SRCB1-FE AND SRCB2-FE.

## 5.2 FE results and physical test by Zhang et al. (2016)

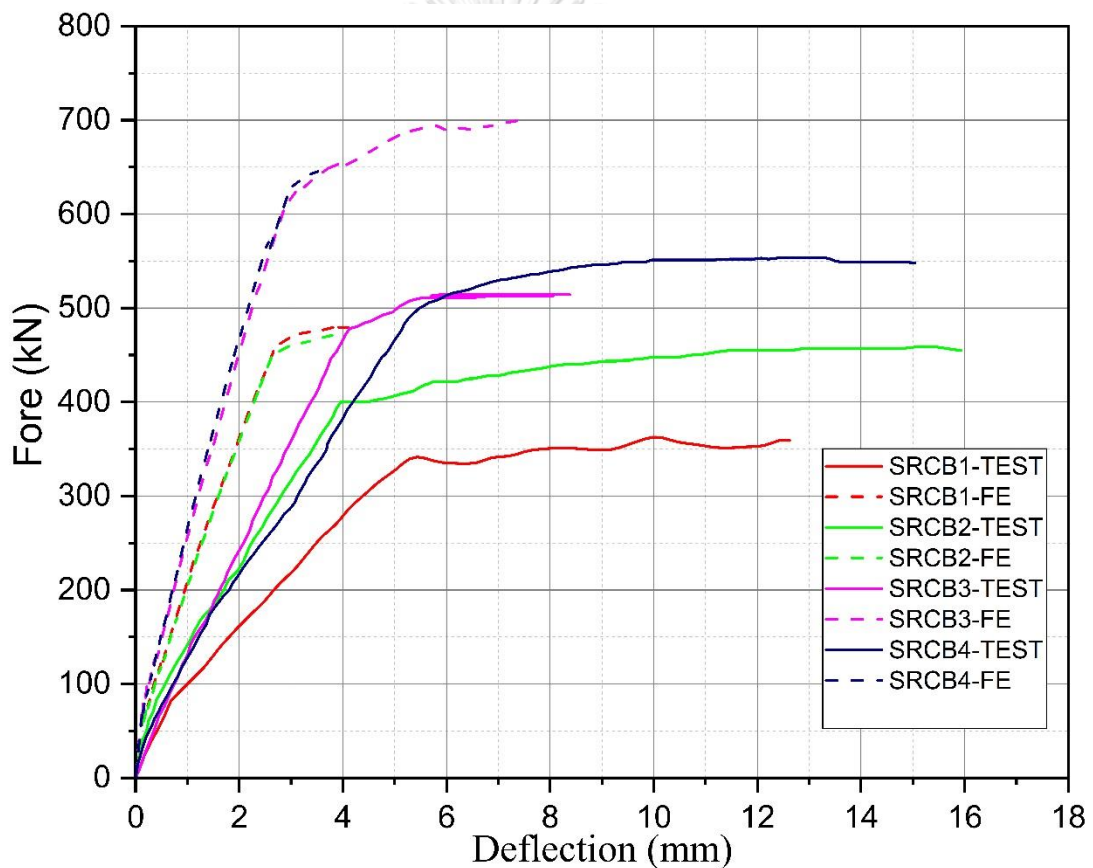


Figure 5.18 Load-deflection of FEM of the studied beams and test results by Zhang et al. (2016)

Figure 5.18 presented the load deflection of FE element result of the studied beams and physical test results by Zhang et al. (2016). It can be observed that FE models gave overpredicted the loads and stiffness of all beams.

- The stiffness of RC beams before yielding of steel, such as SRCB1-FE was higher about 2 times compare with SRCB1.
- After yeilding of steel, SRCB1-FE and SRCB2-FE captured small ductility compare with SRCB1 and SRCB2.
- The beams embadded steel trusses, stiffness at the linear of steel of SRCB4-FE was about 1.7 times compare with SRCB4. However, ductility of the SRCB4-FE was small.

### 5.3 Discussion of results of shear strength in current study

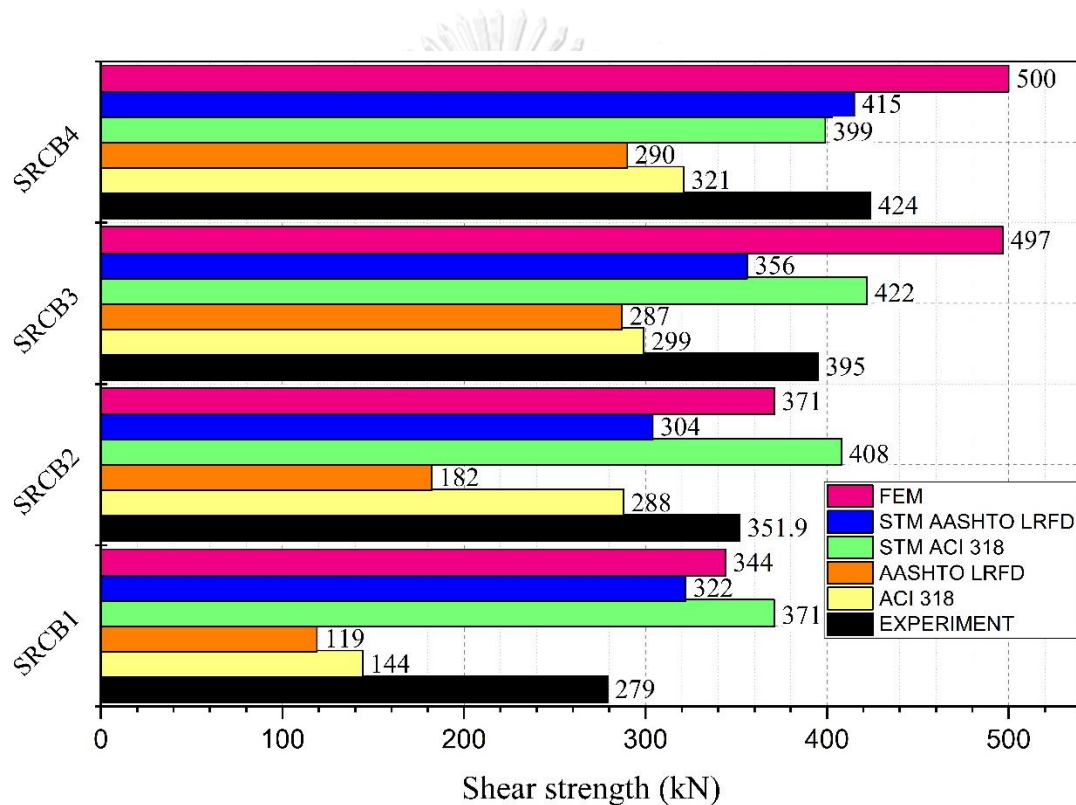


Figure 5.19 Summary of shear strength of the studied beams

Figure 5.19 illustrated summary of shear strength which included the conventional method and Strut-and-Tie Model STM following ACI 318 (2014) and AASHTO LRFD (2012), FE analysis and physical test from previous research. The comparison of shear strength Figure 5.20 found that

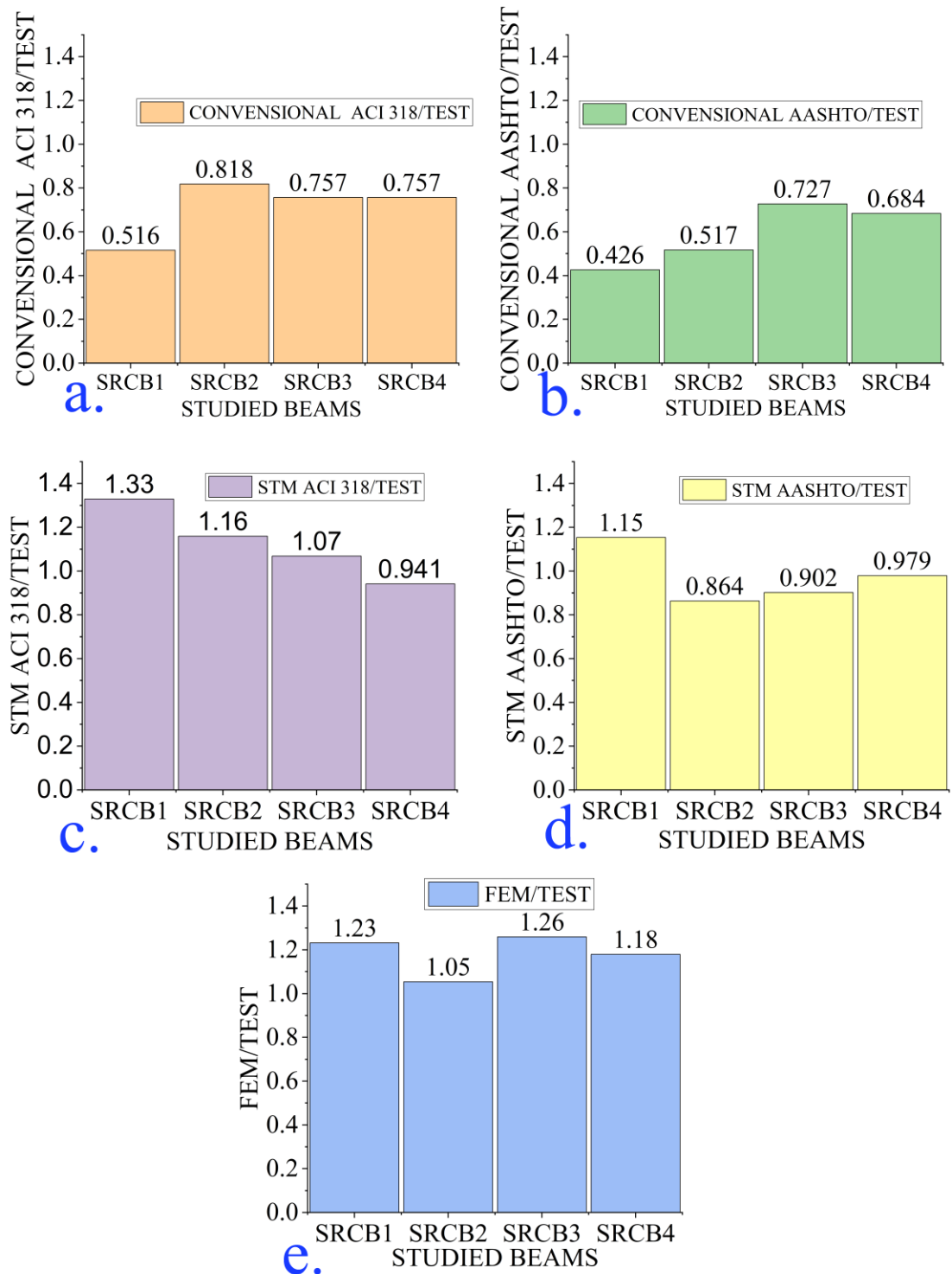


Figure 5.20 Shear strength ratio of proposed FEM, conventional shear strength formula, and STM to physical test beams by Zhang et al. (2016)

- The conventional method following ACI 318 (2014) Figure 5.20a underestimated shear capacity by comparing with the test of studied beams subjected to a point load near support by Zhang et al. (2016). It can be seen that shear strength of SRCB1, SRCB2, SRCB3, SRCB4 were underestimated by 48.4%, 18.2%, 24.3%, 24.3% by ACI 318 (2014) and 57.4%, 48.3%, 27.3%, 31.6% by AASHTO LRFD (2012) Figure 5.20b respectively.
- STM ACI 318 (2014) Figure 5.20c showed a closed prediction for SRCB3 and SRCB B4; however, it overestimates shear strength of SRCB1 and SRCB2 by approximately 52% against test results.
- STM AASHTO (2012) Figure 5.20d gave shear strength of SRCB2 to SRCB4 that were in good agreement with test results of Zhang et al. (2016). On the other hand, SRCB1 overpredicted shear strength by 15%.
- The perfect bond interaction FE results Figure 5.20 provided overestimation of shear strength of SRCB1, SRCB2, and SRCB3, SRCB4 by 23.2%, 5.4%, 25.9% and 17.9%, respectively .

## CHAPTER 6

### CONCLUSIONS AND RECOMMENDATIONS

#### 6.1 Conclusions

This study presented various approaches to predict the shear strength of two conventional RC beams and two RC beams with embedded steel trusses. The methods used to estimate shear capacity in this research are Analytical method following ACI 318 (2014) and AASHTO LRFD (2012), finite element method. In the previous chapters, the model description, the results obtained in current study along with a discussion were presented. Based on the results obtained from the proposed methods, the following conclusions could be drawn:

1. The conventional shear design formula following ACI 318 (2014) as well as AASHTO LRFD (2012) under-estimated shear capacity of RC beam and RC beam with embedded steel trusses at small shear to depth ratio.
2. Shear capacity of beams computed from STM ACI 318 (2014) were based on maximum effective compressive strut which depended on compressive strength and angle between diagonal strut and tension tie of STM. ACI 318 gave a little over-estimated shear strength of RC beams with and without embedded steel trusses.
3. Shear capacity of beams computed from STM AASHTO LRFD (2012) were based on the limiting compressive stress of strut which depended on the principal tensile strain of concrete, ultimate compressive strength and angle between diagonal strut and tensile tie of STM. AASHTO LRFD provided a good prediction of shear strength of such beams with embedded steel trusses.
4. FEM over-estimated the shear strength of RC beam with and without embedded steel trusses in comparison to experimental test. More investigation should be conducted to obtain a better estimation of shear strength by FEM before it can be used in practice.

## 6.2 Recommendations

1. For STM method, more configurations of struts and ties should be investigated as the results predicted from different configuration maybe different.
2. When applying STM method, the influence of each member of the embedded steel truss needs more investigation.
3. In this study, the analysis process of FE models used the commercial software (ANSYS). Using other available FE analysis software to conduct comparative studies are also interesting to determine which software that can give more accurate results comparing with experimental test data.
4. In this study, the bonding between concrete and steel interface was assumed to be perfect. Further investigation of bond slip characteristics between concrete and steel rebar, angle steel and flat plate are needed. Moreover, bond slip model between concrete and those steels need further investigation in FE analysis studies.
5. In this study, concrete and steel was assumed to have no separation under tension. Further investigation of surface separation characteristics between concrete and steel truss are needed.
6. More studies using different beam sizes and material properties should be carried out.



## REFERENCES

- Ahmad, S., Shah, A., Zaman, N., and Salimullah, K., (2011). "Design and Evaluation of the Shear Strength of Deep Beams by Strut-and-Tie Model (STM)", *Iranian Journal of Science and Technology, Transactions of Civil Engineering*, 35(1), 1-13.
- American Association of State Highway and Transportation Officials, (2012). *LRFD Bridge Design Specifications*, Washington, DC.
- American Concrete Institute, (2005). *Building Code Requirements for Structural Concrete (ACI 318M-05)*, Farmington Hills, MI.
- American Concrete Institute, (2011). *Building Code Requirements for Structural Concrete (ACI 318M-11)*, Farmington Hills, MI.
- American Concrete Institute, (2014). *Building Code Requirements for Structural Concrete (ACI 318M-14)*, Farmington Hills, MI.
- ANSYS 18.2 Inc., (2018). *Ansys Mechanical APDL Element Reference*, Canonsburg, PA.
- Bangash, M., (1989). *Concrete and Concrete Structures: Numerical Modelling and Applications*, Elsevier Applied Science, UK.
- Baskar, K., Shanmugam, N., and Thevendran, V., (2002). "Finite Element Analysis of Steel–Concrete Composite Plate Girder", *Journal of Structural Engineering*, 128(9), 1158-1168.
- Bentz, E. C., Vecchio, F. J., and Collins, M. P., (2006). "Simplified Modified Compression Field Theory for Calculating Shear Strength of Reinforced Concrete Elements", *ACI Structural Journal*, 103(4), 614-624.
- Bircher, D., Tuchscherer, R., Huizinga, M., Bayrak, O., Wood, S. L., and Jirsa, J. O., (2009). *Strength and Serviceability Design of Reinforced Concrete Deep Beams*, (FHWA/TX-09/0-5253-1), Texas Department of Transportation, Austin, TX.
- Collins, M. P., Mitchell, D., Adebar, P., and Vecchio, F. J., (1996). "A General Shear Design Method", *ACI Structural Journal*, 93(1), 36-45.
- Dahmani, L., Khennane, A., and Kaci, S., (2010). "Crack Identification in Reinforced Concrete Beams using ANSYS Software", *Strength of Materials*, 42(2), 232-240.
- Dassault Systèmes Simulia Corporation, (2010). *Analysis User's Manual, Version 6.10*, ABAQUS Inc., Providence, RI.

- Desayi, P., and Krishnan, S., (1964). "Equation for the Stress-Strain Curve of Concrete", *ACI Journal Proceedings*, 61(3), 345-350.
- European Committee for Standardization, (2004). *Eurocode 2: Design of Concrete Structures - Part 1-1: General Rules and Rules for Buildings*, Brussels, Belgium.
- Gere, J., and Timoshenko, S., (1997). *Mechanics of Materials*, (Vol. 534), PWS Pub Co., Boston, MA.
- Ibrahim, A. M., and Mahmood, M. S., (2009). "Finite Element Modeling of Reinforced Concrete Beams Strengthened with FRP Laminates", *European Journal of Scientific Research*, 30(4), 526-541.
- Ismail, K. S., Guadagnini, M., and Pilakoutas, K., (2016). "Numerical Investigation of the Shear Strength of RC Deep Beams Using the Microplane Model", *Journal of Structural Engineering*, 142(10), 1-13.
- Kachlakev, D. I., Miller, T. H., Potisuk, T., Yim, S. C., and Chansawat, K., (2001). *Finite Element Modeling of Reinforced Concrete Structures Strengthened with FRP Laminates*, (FHWA-OR-RD-01-XX), Oregon Department of Transportation, Washington, DC.
- Leng, Y. B., Song, X. B., and Wang, H. L., (2015). "Failure Mechanism and Shear Strength of Steel-Concrete-Steel Sandwich Deep Beams", *Journal of Constructional Steel Research*, 106, 89-98.
- Londhe, R. S., (2011). "Shear Strength Analysis and Prediction of Reinforced Concrete Transfer Beams in High-Rise Buildings", *Structural Engineering and Mechanics*, 37(1), 39-59.
- MacGregor, J. G., Wight, J. K., Teng, S., and Irawan, P., (1997). *Reinforced Concrete: Mechanics and Design*, (Vol. 3), Prentice Hall, Upper Saddle River, NJ.
- Machacek, J., and Cudejko, M., (2009). "Longitudinal Shear in Composite Steel and Concrete Trusses", *Engineering Structures*, 31(6), 1313-1320.
- Mahmoud, A. M., (2016). "Finite Element Modeling of Steel Concrete Beam Considering Double Composite Action", *Ain Shams Engineering Journal*, 7(1), 73-88.
- Martin, A. M., and Kuriakose, M., (2016). "Finite Element Modeling and Analysis of Reinforced Concrete Beam Retrofitted with Fibre Reinforced Polymer

- Composite", *International Journal of Engineering Trends and Technology*, 38(4). doi:10.14445/22315381/IJETT-V38P234, 190-197.
- Mitchell, D., and Collins, M. P., (1974). "Diagonal Compression Field Theory-a Rational Model for Structural Concrete in Pure Torsion", *ACI Journal Proceedings*, 71(8), 396-408.
- Mörsch, E., (1902). *Der Eisenbetonbau, Seine Anwendung und Theorie*, K. Wittwer, Stuttgart
- Nie, J. G., Pan, W. H., Tao, M. X., and Zhu, Y. Z., (2017). "Experimental and Numerical Investigations of Composite Frames with Innovative Composite Transfer Beams", *Journal of Structural Engineering*, 143(7). doi:10.1061/(ASCE)ST.1943-541X.0001776, 04017041.
- Nilson, A., H, David, D., and Dolan Charles, W., (2004). *Design of Concrete Structures*, McGraw-Hill Higher Education, Inc., 1221 Avenue of the Americas, New York, NY.
- Özcan, D. M., Bayraktar, A., Şahin, A., Haktanir, T., and Türker, T., (2009). "Experimental and Finite Element Analysis on the Steel Fiber-Reinforced Concrete (SFRC) Beams Ultimate Behavior", *Construction and Building Materials*, 23(2), 1064-1077.
- Panjehpour, M., Chai, H. K., and Voo, Y. L., (2015). "Refinement of Strut-and-Tie Model for Reinforced Concrete Deep Beams", *PloS one*, 10(6). doi:10.1371/journal.pone.0130734, 1-17.
- Rahal, K. N., and Collins, M. P., (1999). "Background to the General Method of Shear Design in the 1994 CSA-A23. 3 Standard", *Canadian Journal of Civil Engineering*, 26(6), 827-839.
- Ritter, W., (1899). "Die Bauweise Hennebique (Hennebiques Construction Method)", *Schweizerische Bauzeitung*, 33(7), 41-61.
- Sabuwala, T., Linnell, D., and Krauthammer, T., (2005). "Finite Element Analysis of Steel Beam to Column Connections Subjected to Blast Loads", *International Journal of Impact Engineering*, 31(7), 861-876.

- Shah, S. P., Swartz, S. E., and Ouyang, C., (1995). *Fracture Mechanics of Concrete: Applications of Fracture Mechanics to Concrete, Rock and other Quasi-brittle Materials*, John Wiley & Sons.
- Shrivastava, P., Bajpai, Y., and Rai, A., (2015). "Finite Element Analysis and Comparative Study of Reinforced Concrete Beams Laminated with and without FRP", *International Journal of Engineering & Science Research*, 5(1), 12-18.
- Subarao, L. R., (2006). *Studies in Transfer Beams for High-Rise Buildings*. (Ph.D. Thesis), Indian Institute of Technology Roorkee. Uttarakhand, India.
- Vasudevan, G., and Kothandaraman, S., (2014). "Finite Element Analysis of Bearing Capacity of RC Beams Retrofitted with External Bars", *Strength of Materials*, 46(6), 831-842.
- Vecchio, F. J., and Collins, M. P., (1986). "The Modified Compression Field Theory for Reinforced Concrete Elements Subjected to Shear", *ACI Journal Proceedings*, 83(2), 219-231.
- Vecchio, F. J., and Collins, M. P., (1988). "Predicting the Response of Reinforced Concrete Beams Subjected to Shear using Modified Compression Field Theory", *ACI Structural Journal*, 85(3), 258-268.
- Weng, C., Yen, S., and Chen, C., (2001). "Shear Strength of Concrete-Encased Composite Structural Members", *Journal of Structural Engineering*, 127(10), 1190-1197.
- Weng, C., Yen, S., and Jiang, M., (2002). "Experimental Study on Shear Splitting Failure of Full-scale Composite Concrete Encased Steel Beams", *Journal of Structural Engineering*, 128(9), 1186-1194.
- Wolanski, A. J., (2004). *Flexural Behavior of Reinforced and Prestressed Concrete Beams using Finite Element Analysis*. (Master Thesis), Marquette University.
- Wu, Y., Cai, J., Yang, C., Zhou, Y., and Zhang, C., (2011). "Mechanical Behaviours and Engineering Application of Steel Truss Reinforced Concrete Transfer Beam in Tall Buildings", *Structural Design of Tall and Special Buildings*, 20(6), 735-746.
- Zhang, F., and Yamada, M., (1993). "Composite Columns Subjected to Bending and Shear", *Composite Construction in Steel and Concrete II*, Potosi, Missouri. June 14-19, 1992.

Zhang, N., Fu, C. C., Chen, L., and He, L., (2016). "Experimental Studies of Reinforced Concrete Beams Using Embedded Steel Trusses", *ACI Structural Journal*, 113(4), 701-710.



## APPENDIX

### Finite element analysis batch script in ANSYS of SRCB1

```
/CLEAR
/COM,REINFORCED CONCRETE BEAM
/FILENAME,SRCB1_DISPLACEMENT_CONTROL,ON      !FILE NAME
/TITLE,SRCB1_DISPLACEMENT_CONTROL  !DISPLACEMENT CONTROL
/PREP7                                !MODEL CREATION PREPROCESSOR.
!!!!!!=====!ELEMENT TYPES=====
ET,1,SOLID65                          !CONCRETE ELEMENT
KEYOPT,1,1,0                          !INCLUDE EXTRA DISPLACEMENT
KEYOPT,1,3,2                          !FEATURES OF 1 AND APPLY !CONSISTENT
                                       !NEWTON-RAPHSON LOAD VECTOR
KEYOPT,1,5,0                          !PRINT CONCRETE LINEAR SOLUTION ONLY AT
                                       !CENTRIOD
KEYOPT,1,6,0                          !PRINT CONCRETE NONLINEAR SOLUTION
                                       !ONLY AT CENTRIOD
KEYOPT,1,7,1                          !INCLUDE TENSILE STRESS RELAXATION
                                       !AFTER CRACKING
KEYOPT,1,8,0                          !PRINT THE WARINING
ET,2,LINK180                          !STEEL REBAR ELEMENT
ET,3,SOLID185                          !STEEL PLATE ELEMENT
ET,5,COMBIN39                          !BOND-SLIP ELEMENT
KEYOPT,5,1,0                          !UNLOAD ALONG SAME LOADING CURVE
KEYOPT,5,2,0                          !COMPRESSIVE LOADING FOLLOWS !DEFINED
                                       COMPRESSIVE CURVE
KEYOPT,5,3,0                          !KEYOPT(4) OVERRIDES KEYOT(3)
KEYOPT,5,4,1                          !3-D LONGITUDINAL ELEMENT
                                       !(UX,UY, AND !UZ)
KEYOPT,5,6,0                          !BASIC ELEMENT PRINTOUT
R,1                                    ! SET OF THE ELEMENT REAL CONSTANTS
!:=BOND SLIP FORCE DB22 (MODEL CODE 2010 ) NORMAL BOND
```

R,2,0,0,0.3,7126.172,0.6,9403.041 !CONSTANT VALUE OF FORCE AND SLIP  
 RMORE,0.9,11058.719,1.2,12407.387,1.6,13920.532 !OF SPRING ELEMENT  
 RMORE,3.6,13920.532,4,13592.99,4.4,13265.448 !  
 RMORE,4.8,12937.906,5.2,12610.364,5.6,12282.822 !  
 RMORE,7,11136.425,7.5,11136.425,8,11136.425 !  
 RMORE,8.5,11136.425,9,11136.425,9.5,11136.425 !  
 RMORE,12,11136.425 !  
 !=BOND SLIP FORCE DB22 (MODEL CODE 2010 ) GOOD BOND  
 R,3,0,0,0.2,14625.065,0.4,19297.889!CONSTANT VALUE OF FORCE AND SLIP  
 RMORE,0.6,22695.843,0.8,25463.718,1,27841.063 !OF SPRING ELEMENT  
 RMORE,2,27841.063,2.5,25056.957,3,22272.851 !  
 RMORE,3.5,19488.744,4,16704.638,4.5,13920.532 !  
 RMORE,5,11136.425,6.5,11136.425,7,11136.425 !  
 RMORE,7.5,11136.425,8,11136.425,8.5,11136.425 !  
 RMORE,12,11136.425 !  
 !!!!!=====MATERIAL PROPERTIES=====  
 !!!!!=====Concrete material=====  
 MP,EX,11,34110 !LINEAR CONSTANT OF YOUNG MODULUS OF  
 !ELASTICITY  
 MP,PRXY,11,0.2 !LINEAR CONSTANT OF POISSON RATIO  
 TB,MISO,11,1,23,0 !DEFINED MULTILINEAR ISOTROPIC STRESS-  
 !STRAIN CURVE  
 TBPT,DEFI,0.000365347405452946,12.462!  
 TBPT,DEFI,0.00047,15.45617 !  
 TBPT,DEFI,0.000574,18.548958 !  
 TBPT,DEFI,0.000678,21.463439 !  
 TBPT,DEFI,0.000782,24.181351 !  
 TBPT,DEFI,0.000886,26.689769 !  
 TBPT,DEFI,0.00099,28.980913 !  
 TBPT,DEFI,0.001094,31.051768 !  
 TBPT,DEFI,0.001198,32.903532 !  
 TBPT,DEFI,0.001302,34.540991 !

TBPT,DEFI,0.001406,35.971845 !  
 TBPT,DEFI,0.00151,37.206041 !  
 TBPT,DEFI,0.001614,38.255156 !  
 TBPT,DEFI,0.001718,39.131832 !  
 TBPT,DEFI,0.001822,39.849294 !  
 TBPT,DEFI,0.001926,40.420953 !  
 TBPT,DEFI,0.00203,40.860077 !  
 TBPT,DEFI,0.002134,41.179548 !  
 TBPT,DEFI,0.002238,41.39168 !  
 TBPT,DEFI,0.002342,41.508091 !  
 TBPT,DEFI,0.00243564936968631,41.54 !  
 TBPT,DEFI,0.003,41.54 !  
 TBPT,DEFI,0.01,41.54 !  
 !=====CONCRETE MATERIAL PARAMETER=====

TB,CONC,11,1,9,0 !MAT 11, CONSTANT C1 TO C9  
 TB,DATA,1,0.3,0.8,4.04,-1,, !OPEN CRACK, CLOSED CRACK COEFFICIENT  
 !OF CONCRTE CRACKING AND CRUSHING OF  
 !CONCRETE  
 TB,DATA,9,0.6,,,,, !TENSILE CRACK FACTOR "DEFAULT"  
 !!=====STEEL REBAR MATERIAL=====

!!=====DB22=====

MP,EX,222,200000 !LINEAR CONSTANT OF YOUNG MODULUS OF  
 !ELASTICITY  
 MP,PRXY,222,0.3 !LINEAR CONSTANT OF POISSON RATIO  
 TB,BISO,222,1,2 !DEFINED BILINEAR ISOTROPIC STRESS-  
 !STRAIN CURVE  
 TB,DATE,1,393,4000 !SPECIFIED YIELD STRENGTH ANG TANGENT  
 !MUDULAS  
 !!!=====RB8=====

MP,EX,28,210000 !LINEAR CONSTANT OF YOUNG MODULUS OF  
 !ELASTICITY  
 MP,PRXY,28,0.3 !LINEAR CONSTANT OF POISSON RATIO



```

TB,BISO,28,1,2      !DEFINED BILINEAR ISOTROPIC STRESS-
                    !STRAIN CURVE
TBDATE,1,363,4200  !SPECIFIED YIELD STRENGTH ANG TANGENT
                    !MUDULAS
                    !!!=====DB16=====
MP,EX,216,200000    !LINEAR CONSTANT OF YOUNG !MODULUS OF
                    ELASTICITY
MP,PRXY,216,0.3     !LINEAR CONSTANT OF POISSON RATIO
TB,BISO,216,1,2     !DEFINED BILINEAR ISOTROPIC STRESS-
                    !STRAIN CURVE
TBDATE,1,378,4000  !SPECIFIED YIELD STRENGTH ANG TANGENT
                    MUDULAS
                    !!!=====STEEL PLATE AT SUPPORT AND LOADING PLATE=====
MP,EX,2233,200000   !LINEAR CONSTANT OF YOUNG MODULUS OF
                    !ELASTICITY
MP,PRXY,2233,0.3    !DEFINED BILINEAR ISOTROPIC STRESS-
                    !STRAIN CURVE
TB,BISO,2233,1,2    !BILINEAR ISOTROPIC
TBDATE,1,350,4000  !SPECIFIED YIELD STRENGTH ANG TANGENT
                    !MUDULAS
                    !!=====SECTION TYPE AND SECTION DATA=====
SECTYPE,8,LINK,,RB8, !DEFINED SECTION NUMBER "RB8"
SECDATA,50.27,       !CROSS SECTIONAL AREA OF "RB8"
SECTYPE,12,LINK,,DB12, !DEFINED SECTION NUMBER "DB12"
SECDATA,113.10,     !CROSS SECTIONAL AREA OF "DB12"
SECTYPE,16,LINK,,DB16, !DEFINED SECTION NUMBER "DB16"
SECDATA,210.06,     !CROSS SECTIONAL AREA OF "DB16"
SECTYPE,22,LINK,,DB22, !DEFINED SECTION NUMBER "DB22"
SECDATA,380.13,     !CROSS SECTIONAL AREA OF "DB22"
                    !!!=====MODELING=====
*SET,H,300          !mm (HEIGHT OF THE BEAM)
*SET,L,1800         !mm (LENGTH OF THE BEAM)

```

```

*SET,W,200          !mm (WIDTH OF THE BEAM)
*SET,TP,25         !mm (THICKNESS OF PLATE)
*SET,WP,200       !mm (WIDTH OF PLATE)
*SET,LP,125       !mm (LENGTH OF PLATE)
*SET,LDP,400      !mm (FROM CENTER OF THE BEAM)
*SET,LSP,750      !mm (FROM CENTER OF THE BEAM)
*SET,COVER,30     !mm (CONCRETE COVER)
*SET,SP,150       !mm (SPACING OF STIRRUPS)
!*SET,TTE,45      !mm (COVER FROM HORIZONTAL TRUSS ELEMENT TO
                  !EDGE)

*SET,TOLER_X,0.001 !mm (TOLERANCE OFFSET
*SET,TOLER_Z,0.005 !mm (TOLERANCE OFFSET
!!!=====CONCRETE=====
BLOCK,-W/2,W/2,-H/2,H/2,-L/2,L/2          !BEAM
BLOCK,-WP/2,WP/2,H/2,H/2+TP,LDP+LP/2,LDP-LP/2 !LOADING PLATE
BLOCK,-WP/2,WP/2,-H/2,-H/2-TP,LSP+LP/2,LSP-LP/2 !LEFT      SUPPORT
                  !PLATE
BLOCK,-WP/2,WP/2,-H/2,-H/2-TP,-LSP+LP/2,-LSP-LP/2 !LEFT      SUPPORT
                  !PLATE

!=====SUB DIVIDE THE CONCRETE VOLUME=====
*DO,ii,-L/2,L/2,SP          !DIVIDE VOLUME USING DO COMMAND
WPAVE,0,0,ii                !MOVE WORKING PLANE TO SPECIFIED
                              !LOCATION
VSBW,ALL,,                  !DIVIDE VOLUME
*ENDDO                       !
                              !=====
*DO,ii,LSP-LP/2,LSP+LP/2,LP/2 !
WPAVE,0,0,ii                !
VSBW,ALL,,                  !
*ENDDO                       !
                              !=====
*DO,jj,-LSP-LP/2,-LSP+LP/2,LP/2 !

```

```

WPAVE,0,0,jj          !
VSBW,ALL,,           !
*ENDDO               !
                    !=====
*DO,jj,LDP-LP/2,LDP+LP/2,LP/2 !
WPAVE,0,0,jj          !
VSBW,ALL,,           !
*ENDDO               !
                    !=====
WPAVE,0,0,-L/2+COVER !
VSBW,ALL,,           !
WPAVE,0,0,L/2-COVER  !
VSBW,ALL,,           !
                    !-----
WPSTYL,DEFA          !
WPROTA,0,0,90        !
*DO,ii,-W/2+COVER,W/2-COVER,W/2-COVER !
WPAVE,ii,0,0         !
VSBW,ALL,,           !
*ENDDO               !
                    !-----
                    จุฬาลงกรณ์มหาวิทยาลัย
                    CHULALONGKORN UNIVERSITY
WPSTYL,DEFA          !
WPROTA,0,90,0        !
*DO,ii,-H/2+COVER,H/2-COVER,H-2*COVER !
WPAVE,0,II,0         !
VSBW,ALL,,           !
*ENDDO               !
WPSTYL,DEFA          !
ALLSEL               !
/VIEW,1,1,1,1       !ISOMETRIC VIEW

VPLOT                 !PLOT VOLUME

```

```

!!!=====GROUPING COMPONENTS=====
          !!=====TOP BAR=====
LSEL,S,LOC,Z,-L/2+COVER,L/2-COVER !GROUPING   LINE   COMPONENT
                                          !FOR
LSEL,R,LOC,Y,H/2-COVER                !GENERATE TOP REBAR
LSEL,R,LOC,X,-W/2+COVER                !
LSEL,A,LOC,X,W/2-COVER                 !
LSEL,R,LOC,Z,-L/2+COVER,L/2-COVER !
LSEL,R,LOC,Y,H/2-COVER                !
CM, TOP_BAR, LINE                       !
          !!!=====BOT BAR=====
LSEL,S,LOC,Z,-L/2+COVER,L/2-COVER !
LSEL,R,LOC,Y,-H/2+COVER              !
LSEL,R,LOC,X,-W/2+COVER              !
LSEL,A,LOC,X,W/2-COVER               !
LSEL,R,LOC,Z,-L/2+COVER,L/2-COVER !
LSEL,R,LOC,Y,-H/2+COVER              !
LSEL,A,LOC,X,0                        !
LSEL,R,LOC,Z,-L/2+COVER,L/2-COVER !
LSEL,R,LOC,Y,-H/2+COVER              !
CM, BOT_BAR, LINE                      !
!=====GENERATE BOTTOM REINFORCEMENT LINE      !
CMSEL,S,BOT_BAR                        !GROUPING LINE COMPONENT
LGEN,2,ALL,,TOLER_X,0,TOLER_Z,,0 !TO MAKE A SET OF STEEL NODE
CMSEL,S,BOT_BAR                        ! FOR CONSIDERING BOND SLEEP
LSEL,INVE                               !BETWEEN CONCRETE AND STEEL
LSEL,R,LOC,Z,L/2-COVER-TOLER_Z,-L/2+COVER-TOLER_Z      !
LSEL,R,LOC,Y,-H/2+COVER                !
LSEL,R,LOC,X,-W/2+COVER+TOLER_X,W/2-COVER+TOLER_X      !
LSEL,U,LOC,X,-W/2+COVER+2*TOLER_X,0-TOLER_X*2          !
LSEL,U,LOC,X,0+2*TOLER_X,W/2-COVER-TOLER_X*2          !
CM, BOT_BARS_BOND, LINE                 !

```

## !!!=====STIRRUPS=====

```

*SET,TOLER,0.005                !GROUPING LINE COMPONENT
LSEL,S,LOC,Y,-H/2+COVER+TOLER,H/2-COVER-TOLER  !FOR STIRRUP
LSEL,A,LOC,X,-W/2+COVER+TOLER,W/2-COVER-TOLER  !
LSEL,U,LOC,Y,-H/2-TP-TOLER,-H/2                !
LSEL,U,LOC,Y,H/2,H/2+TP                        !
LSEL,R,LOC,X,-W/2+COVER,W/2-COVER              !
LSEL,U,LOC,X,0-TOLER,0+TOLER                   !
LSEL,R,LOC,Z,-L/2+COVER,L/2-COVER              !
LSEL,U,LOC,Z,LSP+LP/2-TOLER,LSP+LP/2+TOLER    !
LSEL,U,LOC,Z,LSP-LP/2-TOLER,LSP-LP/2+TOLER    !
LSEL,U,LOC,Z,-LSP+LP/2-TOLER,-LSP+LP/2+TOLER  !
LSEL,U,LOC,Z,-LSP-LP/2-TOLER,-LSP-LP/2+TOLER  !
LSEL,U,LOC,Z,LDP-LP/2-TOLER,LDP-LP/2+TOLER    !
LSEL,U,LOC,Z,LDP+LP/2-TOLER,LDP+LP/2+TOLER    !
LSEL,U,LOC,Z,LDP-TOLER,LDP+TOLER              !
CM,STIRRUPS,LINE                               !

```

## !!!=====VOLUME OF BEAM=====

```

VSEL,S,LOC,Y,-H/2,H/2                !GROUPING OFVOLUME COMPONENT
VSEL,R,LOC,Z,-L/2,L/2                !FOR GENERATING CONCRETE BEAM
VSEL,R,LOC,X,-W/2,W/2                !
CM,BEAM,VOLU                           !

```

## !!!=====VOLUME OF LOADING PLATE=====

```

VSEL,S,LOC,Y,H/2,H/2+TP              !GROUPING OFVOLUME COMPONENT
VSEL,R,LOC,X,-WP/2,WP/2              !FOR GENERATING STEEL LOADING
                                       !PLATE
VSEL,R,LOC,Z,LDP+LP/2,LDP-LP/2      !
CM,LOADING,VOLU                       !

```

## !!!=====VOLUME OF SUPPORT PLATE=====

```

VSEL,A,LOC,Y,-H/2-TP,-H/2           !GROUPING OFVOLUME COMPONENT
VSEL,R,LOC,Z,-L/2,L/2               !FOR GENERATING STEEL SUPPORT PLATE
VSEL,R,LOC,X,-W/2,W/2                !

```

```

CM,SUPPORT,VOLU      !
                    !!!=====MESHING=====
ALLSEL                !
VCLEAR,ALL           !
LCLEAR,ALL           !
MSHAPE,0,3D         !
MSHKEY,2             !MAP MESH THE MODEL
!ESIZE,25            !ELEMENT SIZE CONTROL
LESIZE,ALL,25, , , , ,1  !ELEMENT SIZE CONTROL
CMSEL,S,BEAM,ALL     !SELECTING BEAM
VATT,11,1,1,,,,     !VATT, MAT, REAL, TYPE, ESYS, SECNUM
VMESH,ALL            !MESHING
CMSEL,S,LOADING,VOLU !SELECTING STEEL LOADING PLATE
CMSEL,A,SUPPORT,VOLU !SELECTING STEEL SUPPORT PLATE
VATT,2233,1,3,,,,   !!VATT, MAT, REAL, TYPE, ESYS, SECNUM
VMESH,ALL            !MESHING
NUMMRG,NODE          !MERGING NODE
NUMMRG,KP            !MERGING NODE
CMSEL,S,TOP_BAR      !SELECTING TOP REBAR
LATT,216,1,2,,,,,16  !LATT, MAT, REAL, TYPE, --, KB, KE, SECNUM
LMESH,ALL            !SELECTING STEEL LOADING PLATE
CMSEL,S,BOT_BARS_BOND !SELECTING BOTTOM REBAR
LATT,222,1,2,,,,,22  !LATT, MAT, REAL, TYPE, --, KB, KE, SECNUM
LMESH,ALL            !MESHING
CMSEL,S,STIRRUPS,LINE !SELECTING STIRRUP
LATT,28,1,2,,,,,8    !LATT, MAT, REAL, TYPE, --, KB, KE, SECNUM
LMESH,ALL            !MESHING
ALLSEL                !SELECT EVERY THING
EPLOT                !PLOTING ELEMENTS
/ESHAPE,1            !SHOWING ELEMENT SHAPE
/TRLCY,ELEM,1        !SHOWING TRANSPARENCY
CPDELE,ALL           !DELETE COUPLING SET

```

```

!====NODES=====
NSEL,S,LOC,Z,LDP          !CREATE GROUP OF NODE
NSEL,R,LOC,Y,H/2+TP      !FOR APPLYING DISPLACEMENT
!NSEL,R,LOC,X,0          !
CM,DISPLACEMENT-N2,NODE  !
!====COUPLING CONSTRAINT NODE=====
!=====
ESEL,S,MAT,,222          !GROUPING NODE COMPONENT
NSLE,S                   !OF BOTTOM STEEL REBAR
CM,ST_NODES,NODE        !GROUPING NODE COMPONENT
ESEL,S,MAT,,11          !OF CONCRETE COINCIDE WITH
NSLE,S                   !STEEL NODE
NSEL,R,LOC,Y,-H/2+COVER  !
NSEL,R,LOC,Z,L/2-COVER,-L/2+COVER  !
NSEL,R,LOC,X,-W/2+COVER,W/2-COVER  !
CM,CON_NODES,NODE      !
CMGRP,COUPLE_NODE,ST_NODES,CON_NODES !GROUPING STEEL
                                !AND CONCRETE
                                !COMPONENT
!=====CREATE COINCIDENT NODE TO REPRESENT BOND SLIP OF THE
!BEAM
CMSEL,S,COUPLE_NODE      !CREATE COUPLING SET OF EACH NODE
CPCYC,UX,0.0001,,TOLER_X,0,TOLER_Z,1  !
CPCYC,UY,0.0001,,TOLER_X,0,TOLER_Z,1  !
CPCYC,UZ,0.0001,,TOLER_X,0,TOLER_Z,1  !
!!!====GROUPING NODE TO APPLY BOUNDARY CONDITION==
NSEL,S,LOC,X,-W/2,W/2    !GROUPING NODE FOR PINE
NSEL,R,LOC,Y,-H/2-TP    !SUPPORT CONDITION
NSEL,R,LOC,Z,LSP        !
CM,L-SUPPORT,NODE       !
NSEL,S,LOC,X,-W/2,W/2    !GROUPING NODE FOR ROLLER
NSEL,R,LOC,Y,-H/2-TP    !SUPPORT CONDITION

```

```

NSEL,R,LOC,Z,-LSP      !
CM,R-SUPPORT,NODE      !
!!!=====LOADING TO BE APPLIED=====
          !DISPLACEMENT LOAD SET
*SET,U1,2              !mm
*SET,U2,3              !mm
*SET,U3,6              !mm
FINISH                 !END
!=====SOLUTION=====
!==APPLY BOUNDARY CONDITION
/SOLU                  !THE SOLUTION PROCESSOR
LSCLEAR,ALL           !CLEAR ALL LOAD BEFORE APPLY LOAD SET
ANTYPE,STATIC         !STATIC ANALYSIS
SOLCONTROL,ON        !SOLUTION CONTROL
NROPT,FULL,,ON       !NEWTON-RAPHSON OPTION IN A STATIC
LNSRCH,ON             !ACTIVATES A LINE SEARCH WITH
NLGEOM,ON            !NEWTON-RAPHSON
AUTOTS,ON            !AUTOMATIC TIME STEPPING
CNVTOL,U,0,0.1,2,1  !CONVERGENCE CRITERIA
OUTRES,ALL,ALL       !CONTROL THE SOLUTION DATA WRITTEN
                    !TO THE DATABASE
NCNV,2               !TERMINATES THE ANALYSIS
                    !IF THE SOLUTION FAILS TO CONVERGE
!!!=====SUPPORT BOUNDARY CONDITION=====
CMSEL,S,L-SUPPORT    !BOUNDARY CONDITION AT THE LEFT
                    !HANDSIDE
D,ALL,UY,0           !PINE SUPPORT
D,ALL,UX,0           !
D,ALL,UZ,0           !
CMSEL,S,R-SUPPORT    !BOUNDARY CONDITION AT THE LEFT
                    !HANDSIDE
D,ALL,UY,0           !ROLLER SUPPORT

```



```

D,ALL,UX,0          !
!!!=====APPLY SET OF LOAD=====
CMSEL,S,DISPLACEMENT-N2  !DISPLACEMENT
D,ALL,UY,-U1        !LOAD STEP1
TIME,U1             !TIME AT THE END LOAD STEP
NSUBST,1000,1000,100,ON  !SET NUMBER OF SUBSTEP
KBC,0               !SPECIFIED RAMPED LOADING WITHIN
                    !LOAD STEP
NEQIT,500          !MAXIMUM NUMBER OF EQUILIBRIUM
!STABILIZE, REDUCE,DAMPING,1,NO,0.2  !STABILIZATION
ALLSEL              !WRITES LOAD AND LOAD STEP OPTION
LSWRITE,1          !TO FILE
!=====
CMSEL,S,DISPLACEMENT-N2  !DISPLACEMENT
D,ALL,UY,-U2        !LOAD STEP2
TIME,U2             !
NSUBST,500,1000,100,ON  !
KBC,0               !
NEQIT,500          !
!STABILIZE, REDUCE,DAMPING,1,NO,0.2  !
ALLSEL              !
LSWRITE,2          !
!=====
CMSEL,S,DISPLACEMENT-N2  !DISPLACEMENT
D,ALL,UY,-U3        !LOAD STEP3
TIME,U3             !
NSUBST,500,1000,100,ON  !
KBC,0               !
NEQIT,500          !
!STABILIZE, REDUCE,DAMPING,1,NO,0.2  !
ALLSEL              !
LSWRITE,3          !

```

```

LSSOLVE,1,3,1      !
FINISH             !
!=====
/POST1             !THE DATABASE RESULTS POSTPROCESSOR
CMSEL,S,DISPLACEMENT-N2  !SELECT NODE FOR REACTION FORCE
PRRSOL,FY          !PLOT REACTION FORCE
!=====
/POST26            !THE TIME-HISTORY RESULTS POSPROCESSOR
LINES,2000         !MAXIMUM ROW OF TIME-HISTORY RESULTS
NSOL,5,NODE(-W/2,-H/2,LDP),U,Y,DEFLEC_Y1      !VERTICAL
                                                    !DEFLECETION
NSOL,6,NODE(W/2,-H/2,LDP),U,Y,DEFLEC_Y2 !VERTICAL DEFLECETION
NSOL,8,NODE(0,-H/2,LDP),U,Y,DEFLEC_Y3  !VERTICAL DEFLECETION
!=====
RFORCE,4,NODE(-W/2,H/2+TP,LDP),F,Y,REACT_Y1  !VERTICAL REACTION
RFORCE,9,NODE(W/2,H/2+TP,LDP),F,Y,REACT_Y2  !VERTICAL REACTION
RFORCE,3,NODE(0,H/2+TP,LDP),F,Y,REACT_Y3    !VERTICAL REACTION
FINISH

```

## VITA

**NAME** Khonesavanh Pormeuangpieng

**DATE OF BIRTH** I was born on December 24, 1990

**PLACE OF BIRTH** I was born in a small village which is located in countryside of Pek District, Xiengkhoung Province, Laos.

**INSTITUTIONS ATTENDED** I went to Lat buak primary and middle school, Xiengkhoung Province, then I completed high school in Hua phan Province, after that I attended higher studies in Civil Engineering Faculty of Engineering National University of Laos (NUOL) in Vientiane capital. After I achieved my bachelor's degree in 2012, I worked as Civil Engineer. At beginning of January 2017, I started my master's degree in civil engineering, major Structural Engineering at Chulalongkorn University, Bangkok Thailand.

**HOME ADDRESS** I live in Peub village, Pek district, Xiengkhoung province Laos PDR